Enhanced Multicarrier Techniques for Professional Ad-Hoc and Cell-Based Communications

(EMPhAtiC)

Document Number D7.2

Resource allocation and energy efficient design

Contractual date of delivery to the CEC:	31/10/2014
Actual date of delivery to the CEC:	19/11/2014
Project Number and Acronym:	318362 EMPhAtiC
Editor:	Jérôme Louveaux (UCL)
Authors:	Yao Cheng (ITU), Jianshu Zhang (ITU), Kristina Naskovska (ITU), Ahmad Nimr (ITU), Martin Haardt (ITU), David Gregoratti (CTTC), Stephan Pfletschinger (CTTC), Dorin Panaitopol (TCS), Antonio Cipriano (TCS), Yahia Medjahdi (UCL), Jérôme Louveaux (UCL).
Participants:	CTTC,UCL,ITU,THALES
Workpackage:	WP7
Security:	Public (PU) / Restricted (RE)
Nature:	Report
Version:	1.1
Total Number of Pages:	95

Abstract:

This deliverable summarizes the final contributions on relaying and coverage extension. In the first part, several results of D7.1 are extended. In particular, the channel frequency selectivity is taken into account and solutions are investigated to cope with it in multi-hop relaying networks as well as in two-way relaying schemes. In the latter case, joint channel and physical layer network decoding is also included in the analysis. Performance evaluations of multi-hop relaying and two-way relaying are then presented in a few specific scenarios using the SONIR simulation tool in the first case, and using a physical layer abstraction method in the second case. Finally, the issue of resource allocation is investigated in an asynchronous decode-and-forward relaying scheme using OFDM or FBMC. A joint subcarrier and power allocation algorithm is proposed to maximize the sum-rate taking into account the potential interference resulting from the asynchronism.

Document Revision History

Version	Date	Author	Summary of main changes
0.1	20/10/2014	All involved partners	Initial draft of the document with all draft contributions
1.1	09/11/2014	All involved partners	First proposal with updates of all section

Keywords: Relaying, coverage extension, two-way relaying, FBMC, OFDM, resource allocation.

Table of Contents

1. **Introduction**

This deliverable presents the final part of the work performed in WP7 on “Relay and coverage extension”. Several sections present additional contributions with respect to tasks T7.1 and T7.2, coming in the continuity of the work presented in deliverable D7.1. In addition, the results of task T7.3 are also reported.

Section 2 investigates the issue of channel frequency selectivity for multi-hop relaying networks using FBMC (Filter-bank based multicarrier modulation). The numerical results shown in D7.1 imply that, when the channel can no longer be approximated as flat on the width of the subcarriers, the FBMC/OQAM based multi-hop relaying networks suffer from performance degradation due to the residual intrinsic interference and the resulting error propagation. In order to solve this issue, section 2 studies the possible application of multi-tap equalization in the context of multi-hop relaying networks with DF (decode-and-forward) strategy. Both pre- and post-equalizers are considered for each hop. The numerical results provide insights into the impact of the number of hops on the performance and the choice of appropriate transmit as well as receive processing for each hop.

Section 3 investigates the application of two-way relaying using non-binary network coding in the case of frequency-selective channels. Network coding has been shown to provide a solution for two users to use a relay simultaneously, thereby increasing the available throughput at the expense of a small performance (BER) loss. It has been studied however almost exclusively for a simple AWGN channel. In section 3, the case of frequency selective channel is investigated by using FBMC transmission. Both complete and functional decoding are presented and compared, as well as combined with joint non-binary LDPC decoding. Finally, the advantage of adaptive modulation is also presented.

Section 4 extends some of the work presented in deliverable D7.1 where the fundamental limits of a FBMC based two-way DF system was studied taking into account the power allocation but assuming that a perfect PLNC (Physical layer network coding) scheme is available. In this section, a practical XOR based PLNC scheme is investigated. Multi-tap pre-equalization at the source and equalization at the destination are derived in order to cope with the channel frequency selectivity, then joint detection with the channel code is developed. Simulation results compare the performance of this technique for OFDM and FBMC based systems, in different channel situations.

Section 5 and 6 are devoted to more practical (system-level) performance evaluations of some of the proposed strategies for relaying networks.

Section 5 focuses on multi-hop relaying networks using FBMC, and presents in detail how the SONIR (Self-Organizing Network with Intelligent Relaying) simulation tool has been adapted to take into account frequency selective channel and handle the case of FBMC transmission. Various simulation results are then presented.

Section 6 proposes a PHY abstraction method to evaluate and compare the performance of two possible relaying schemes, DF relaying and two-way relaying, with SC-FDMA (single carrier Frequency division multiple access) transmission. Packet-level considerations are taken into account to adapt these relaying schemes in various scenarios. The proposed PHY abstraction method is validated and then used in MAC-level simulations. Extensive

simulation results are presented for the considered scenarios. While these results clearly show that the PER (packet error rate) of DF scheme is better than the PER of two-way relaying scheme for many scenarios, adaptive two-way relaying provides a higher achievable throughput and is therefore a convenient relaying scheme in terms of total transmitted packets.

Section 7 investigates the issue of resource allocation for FBMC-based DF relaying. These issues have received a lot of attention for OFDM-based relaying, and many of the existing techniques could be applied almost directly in a synchronized FBMC scenario as long as the interference between nodes remains low. One of the advantages of FBMC however is the possibility to remove the need of synchronization by using the better spectral selectivity. Section 7 therefore considers a non-synchronized scenario and investigates the optimization of the sum rate in an OFDM or FBMC based DF-relay transmission system under sum power constraint, taking into account the potential interference between adjacent subcarriers. The impact of interference and the efficiency of the proposed algorithm are investigated through simulation results.

Section 8 draws the main conclusions of the deliverable.

2. Investigation of FBMC based multi-hop relaying networks with multi-tap equalization

2.1 *Description and motivation*

One of the focuses of WP7 is to investigate the application of FBMC/OQAM in multi-hop relaying networks. In deliverable D7.1, we have presented results with respect to the range extension in FBMC/OQAM based multi-hop relaying networks. Different transmission schemes for point-to-point multiple-stream MIMO FBMC/OQAM systems [1] that can be employed in each hop of the multi-hop relaying network have been investigated. Then we have discussed several possible relaying strategies at the relay nodes by taking into account the existence of the intrinsic interference inherited from the FBMC/OQAM modulation. Note that it is assumed that the channel on each subcarrier is flat fading in the aforementioned investigations. The numerical results shown in D7.1 imply that when this assumption is violated, the FBMC/OQAM based multi-hop relaying networks suffer from a performance degradation due to the residual intrinsic interference and the resulting error propagation. To alleviate the restriction on the frequency selectivity of the channel, we conduct an investigation on the application of multi-tap equalization in FBMC/OQAM based multi-hop relaying networks. Decode-and-forward is chosen as the relaying strategy. Assuming that each node of the multi-hop relaying network is equipped with a single antenna, we propose to employ multi-tap equalization [2] at each hop to mitigate both the inter-symbol interference and the inter-carrier interference. In the sequel, the design of the pre-equalizer and the equalizer for each hop is first reviewed. Then, we introduce the linear model of a multi-hop relaying network that is considered in this report and present the numerical results, before conclusions are drawn in the end.

2.2 *Multi-tap equalization at the nodes of FBMC/OQAM-based multi-hop relaying networks*

In FBMC/OQAM systems, the real and imaginary parts of each complex-valued data symbol are staggered by half of the symbol period [3], [4] such that the desired signal and the intrinsic interference are separated in the real domain and in the pure imaginary domain, respectively. In [5] and [6] where receive processing techniques have been developed for MIMO FBMC/OQAM systems, it is assumed that the channel frequency responses of adjacent subcarriers do not vary. Consequently, the intrinsic interference is cancelled by taking the real part of the resulting signal after the equalization. To alleviate the constraint on the frequency selectivity of the channel, a zero forcing (ZF) based approach and a coordinated beamforming based transmission strategy have been proposed in [8], [7], and [1] to enable multi-stream transmissions in a MIMO FBMC/OQAM system where the channel is not restricted to flat fading. Nevertheless, these schemes still suffer from a performance degradation especially at the high SNR regime as long as the assumption that the channel on each subcarrier is flat fading is violated. It should be noted that for multi-hop relaying networks it is especially important to ensure satisfactory reliability of the transmission at each hop due to the error propagation phenomenon. Hence, to avoid a performance degradation in case of highly frequency selective channels, one has to resort to

multi-tap equalization techniques that have been developed for point-to-point FBMC/OQAM systems. Here we propose to employ the design of the pre-equalizer and the equalizer in [2] for each hop of the FBMC/OQAM based multi-hop transmission. Note that there also exist other multi-tap equalization techniques for single-antenna FBMC/OQAM systems that target highly frequency selective propagation conditions, such as [9], [10].

In the following, we review the data model of a point-to-point FBMC/OQAM system and then briefly describe the aforementioned design of the pre-equalizer and the equalizer in [2].

Assuming that the total number of subcarriers is M, the transmitted FBMC/OQAM signal can be written as [2]

$$s(k) = \sum_{m=0}^{M-1} \sum_{n=-\infty}^{-\infty} x_m(n) f_m(k - \frac{M}{2} n), \quad f_m(k) = p(k) e^{j\frac{2\pi}{M} m\left(k - \frac{L-1}{2}\right)}, \tag{2-1}$$

where $f_m(n)$ represents the synthesis filter of the m-th subcarrier, $p(k)$ is the prototype shaping pulse of the odd length L, and $x_m(n)$ denotes the symbol transmitted on the m-th frequency at the n-th time instant. The symbols are drawn from OQAM schemes such that $x_m(n) = d_m(n)\theta_m(n)$, where $d_m(n)$ is real PAM symbol and $\theta_m(n)$ is a phase term described as

$$\theta_m(n) = \begin{cases} 1 & m+n \text{ even} \\ j & m+n \text{ odd} \end{cases}.$$

The signal received at the relay can be written as

$$r(k) = s(k) * h(k) + w(k), \tag{2-2}$$

where $h(k)$ is the propagation channel, and $w(k)$ is the additive white noise. The demodulated signal $y_q(n)$ of the q-th subcarrier can be formulated as [2]

$$y_q(n) = \theta_q^*(n) \sum_{m=q-1}^{q+1} x_m(n) * g_{qm}(n) + \theta_q^*(n) w_q(n), \tag{2-3}$$

where g_{qm} is obtained by downsampling $h(n) * f_m(n) * f_q^*(-n)$ given by

$$g_{qm}(n) = \left(h(n) * f_m(n) * f_q^*(-n)\right)_{\downarrow \frac{M}{2}}, \qquad n = -L_{g_1}, \dots, L_{g_2}$$

and

$$w_q(n) = \big(w(n) * f_q^*(-n)\big)_{\downarrow M/2}.$$

An equalizer $a_q(n)$ and/or a pre-equalizer $b_q(k)$ at the transmitter side can be applied for the q-th subcarrier to mitigate the inter-carrier interference and the inter-symbol interference. First, we consider the case where the transmitter has perfect channel state information and the pre-equalizer takes care of the suppression of the interference, while the equalizer at the receiver is single-tap and real-valued. Consequently, the signal for the q-th subcarrier signal after equalization is defined as

$$z_q(n) = \mathrm{Re}\left\{\theta_q^*(n) \sum_{m=q-1}^{q+1} a_q\, b_m^*(n) * x_m(n) * g_{qm}(n)\right\} + \mathrm{Re}\big\{a_q \theta^*(n) w_q(n)\big\}. \tag{2-4}$$

A matrix-vector form is given by

$$z_q(n) = \mathrm{Re}\left\{\theta_q^*(n) \sum_{m=q-1}^{q+1} a_q\, \boldsymbol{b}_m^H \boldsymbol{G}_{qm} \Theta_m(n) \boldsymbol{d}_m(n)\right\} + \mathrm{Re}\big\{a_q \theta^*(n) w_q(n)\big\}, \tag{2-5}$$

where

$$\begin{aligned} \boldsymbol{b}_m &= \big[b_m(-L_{b_2}), \cdots, b_m(L_{b_1})\big]^T, \\ \boldsymbol{d}_m(n) &= \big[d_m(n + L_{b_2} + L_{g_2}), \cdots, d_m(n - L_{b_1} - L_{g_1})\big]^T, \\ \Theta_m(n) &= \mathrm{diag}\big\{\theta_m(n + L_{b_2} + L_{g_2}), \cdots, \theta_m(n - L_{b_1} - L_{g_1})\big\}, \end{aligned}$$

and the $(L_{b1} + L_{b_2} + 1)$-by-$(L_{b_1} + L_{b_2} + L_{g_1} + L_{g_2} + 1)$ matrix $\boldsymbol{G}_{qm}$ is a circulant matrix with its first row equal to $[g_{qm}(-L_{g_2}), \cdots, g_{qm}(L_{g_1}), 0, \cdots, 0]$. The expression in (2-5) has the following more compact form

$$z_q(n) = \mathrm{Re}\left\{\sum_{m=q-1}^{q+1} a_q\, \boldsymbol{b}_m^H \bar{\boldsymbol{G}}_{qm}(n) \boldsymbol{d}_m(n)\right\} + \mathrm{Re}\big\{a_q \theta_q^*(n) w_q(n)\big\}. \tag{2-6}$$

where $\bar{\boldsymbol{G}}_{qm}(n) = \theta_q^*(n) \boldsymbol{G}_{qm} \Theta_q(n)$.

The pre-equalizer is designed to suppress the interference leaked to the adjacent subcarriers. Hence, an optimization problem is constructed to maximize the signal to leakage plus noise ratio (SLNR) [2]. The pre-equalizer is then given by

$$\widetilde{\boldsymbol{b}}_{q,e}^{(opt)} = \arg \max_{\widetilde{\boldsymbol{b}}_{q,e}} \left(\frac{\widetilde{\boldsymbol{b}}_{q,e}^T \boldsymbol{R}_q \widetilde{\boldsymbol{b}}_{q,e}}{\widetilde{\boldsymbol{b}}_{q,e}^T \boldsymbol{Q}_q \widetilde{\boldsymbol{b}}_{q,e}}\right), \tag{2-7}$$

where

$$\boldsymbol{R}_q = \bar{\boldsymbol{G}}_{qq,e}\boldsymbol{e}_l\boldsymbol{e}_l^T\bar{\boldsymbol{G}}_{qq,e}^T,$$

$$Q_{\boldsymbol{q}} = \bar{\boldsymbol{G}}_{q-1q,e}\bar{\boldsymbol{G}}_{q-1q,e}^T + \bar{\boldsymbol{G}}_{qq,e}(\boldsymbol{I} - \boldsymbol{e}_l\boldsymbol{e}_l^T)\bar{\boldsymbol{G}}_{qq,e}^T + \bar{\boldsymbol{G}}_{q+1q,e}\bar{\boldsymbol{G}}_{q+1q,e}^T + \frac{N_0}{2P_T/M}\boldsymbol{I}.$$

And $\boldsymbol{b}_{q,e}$ and $\bar{\boldsymbol{G}}_{qq,e}$ are obtained by stacking the real part and imaginary part of $\boldsymbol{b}_q$ and $\bar{\boldsymbol{G}}_{qq}$, respectively. Here $\boldsymbol{e}_l$ denotes a unit vector of length $(L_{b_1} + L_{b_2} + L_{g_1} + L_{g_2} + 1)$ and has all zero elements but one at $l = L_{b_2} + L_{g_2} + 1$. The solution of (2-7), $\widetilde{\boldsymbol{b}}_{q,e}^{(opt)}$, is the normalized eigenvector corresponding to the largest eigenvalue of $\boldsymbol{Q}_q^{-1}\boldsymbol{R}_q$. For more details of the derivation, the readers are referred to [2].

Alternatively, a one-tap pre-equalizer can be used at the transmitter, while a multi-tap equalizer is designed to eliminate the inter-symbol interference and the inter-carrier interference. The corresponding signal for the q-th subcarrier signal after equalization takes the following form

$$z_q(n) = \mathrm{Re}\left\{\theta_q^*(n)\sum_{m=q-1}^{q+1} b_m\, a_q^*(n) * x_m(n) * g_{qm}(n)\right\} + \mathrm{Re}\{\theta_q^*(n)a_q^*(n) * w_q(n)\}, \quad (2\text{-}8)$$

where the pre-equalizer is real-valued, and $a_q(n)$ has non-zero values for $-L_{a_2} \le n \le L_{a_1}$. Similarly, the matrix-vector form of (2-8) is given by

$$z_q(n) = \mathrm{Re}\left\{\sum_{m=q-1}^{q+1} b_m\, \boldsymbol{a}_q^H\bar{\boldsymbol{G}}_{qm}(n)\boldsymbol{d}_m(n)\right\} + \mathrm{Re}\{\boldsymbol{a}_q^H(n)\boldsymbol{w}_q(n)\}. \quad (2\text{-}9)$$

where

$$\bar{\boldsymbol{G}}_{qm}(n) = \theta_q^*(n)\boldsymbol{G}_{qm}\Theta_m(n)$$
$$\boldsymbol{a}_q = \left[a_q(-L_{a_2}), \cdots, a_q(L_{a_1})\right]^T,$$
$$\boldsymbol{d}_m(n) = \left[d_m(n + L_{a_2} + L_{g_2}), \cdots, d_m(n - L_{a_1} - L_{g_1})\right]^T,$$
$$\Theta_m(n) = \mathrm{diag}\{\theta_m(n + L_{a_2} + L_{g_2}), \cdots, \theta_m(n - L_{a_1} - L_{g_1})\},$$
$$\boldsymbol{w}_q(n) = \theta_q^*(n)\left[w_q(n + L_{a_2}), \cdots, w_q(n - L_{a_1})\right]^T,$$

and the $(L_{a1} + L_{a_2} + 1)$-by-$(L_{a_1} + L_{a_2} + L_{g_1} + L_{g_2} + 1)$ $\boldsymbol{G}_{qm}$ is a circulant matrix with the first row equal to $[g_{qm}(-L_{g_2}), \cdots, g_{qm}(L_{g_1}), 0, \cdots, 0]$.

The multi-tap equalizer that maximizes the signal to noise and interference ratio (SINR) corresponds to the solution of the following optimization problem [2]

$$\boldsymbol{a}_{q,e}^{(opt)} = \arg\max_{\boldsymbol{a}_{q,e}}\left(\frac{\boldsymbol{a}_{q,e}^T \boldsymbol{R}_q \boldsymbol{a}_{q,e}}{\boldsymbol{a}_{q,e}^T \boldsymbol{Q}_q \boldsymbol{a}_{q,e}}\right), \tag{2-10}$$

where

$$\boldsymbol{R}_q = \bar{\boldsymbol{G}}_{qq,e}\boldsymbol{e}_l\boldsymbol{e}_l^T\bar{\boldsymbol{G}}_{qq,e}^T,$$

$$Q_{\boldsymbol{q}} = \bar{\boldsymbol{G}}_{qq-1,e}\bar{\boldsymbol{G}}_{qq-1,e}^T + \bar{\boldsymbol{G}}_{qq,e}(\boldsymbol{I} - \boldsymbol{e}_l\boldsymbol{e}_l^T)\bar{\boldsymbol{G}}_{qq,e}^T + \bar{\boldsymbol{G}}_{qq+1,e}\bar{\boldsymbol{G}}_{qq+1,e}^T + \frac{N_0}{2P_T/M}\boldsymbol{W}_q.$$

In this case $\boldsymbol{e}_l$ is a unit vector of length $(L_{a_1} + L_{a_2} + L_{g_1} + L_{g_2} + 1)$ and has all zero elements but one at $l = L_{a_2} + L_{g_2} + 1$. Finally, $\boldsymbol{a}_{q,e}^{(opt)}$ is obtained as the eigenvector with respect to the largest eigenvalue of $\boldsymbol{Q}_q^{-1}\boldsymbol{R}_q$.

2.3 *Linear model for FBMC-based multi-hop relaying networks*

Similarly as in the range extension analysis that we have presented in deliverable D7.1, we adopt a one-dimensional linear model for the broadband PMR multi-hop relay network. It is assumed that the relays are placed on a straight line between the base station and the mobile terminal. Frequency selective propagation conditions are considered for all links between the base station and the mobile terminal. We illustrate such a linear model in Figure 2-1.

Let us denote the number of relays that assist the communications between the base station and the mobile terminal as R_{relays}, which leads to $(R_{\text{relays}} + 1)$ links. We also assume that the R_{relays} relays are uniformly placed between the base station and the mobile terminal.

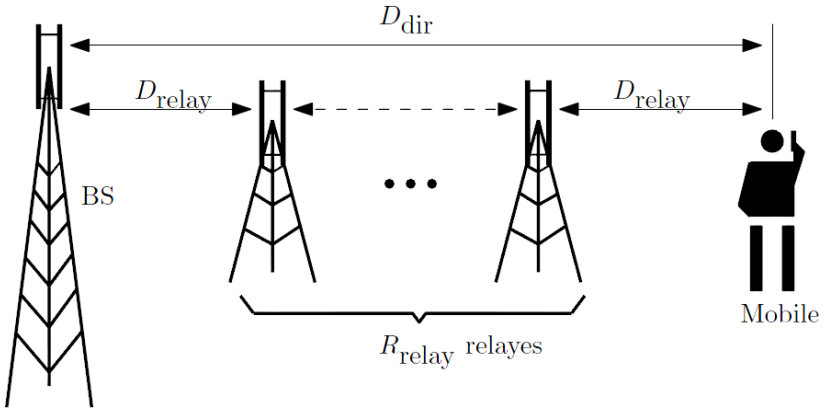

Figure 2-1 Linear relay model

It is worth noting that this one-dimensional model can be easily extended to a more realistic two-dimensional multi-hop relaying scenario. However, as adopted in several other

publications, such as [11], [12], and [15], this simple linear relay model based on a path-loss analysis is sufficient to provide insights into the potential of multi-hop relaying networks.

Assuming all the relays have the same transmit power as the base station, the received SNR in case of such a multi-hop relaying network can be written as [11]

$$\mathrm{SNR}_{\mathrm{relay}} = \mathrm{SNR}_{\mathrm{direct}} \left(\frac{D_{\mathrm{dir}}}{D_{\mathrm{relay}}} \right)^{\zeta} = \mathrm{SNR}_{\mathrm{direct}} \left(R_{\mathrm{relay}} + 1 \right)^{\zeta} \tag{2-11}$$

where $\mathrm{SNR}_{\mathrm{direct}}$ represents the receive SNR of the direct link between the base station and the mobile terminal. Here ζ denotes the path loss exponent. For free space and typical cellular configurations ζ takes the values of 2 and 3.5, respectively. It can be seen that the $\mathrm{SNR}_{\mathrm{relay}}$ increases as the path loss exponent ζ takes a larger value or the number of relays R_{relay} between base station and mobile terminal increases. Moreover, the increase in $\mathrm{SNR}_{\mathrm{relay}}$ is more pronounced when a larger ζ is considered which usually corresponds to a more realistic propagation path loss scenario. In addition, for high SNR values, the wireless link capacity increases logarithmically with a growing SNR, as verified by considering the Shannon capacity expression [11]. This analysis indicates benefits in terms of an improved receiver SNR thanks to the use of the multi-hop relaying technology and also justifies its potential of range extension. The received SNR at the destination terminal can be increased dramatically, and therefore the boost of the capacity is also expected.

As already pointed out in deliverable D7.1, although amplify-and-forward (AF) is a relatively simple relaying strategy that does not lead to heavy computational load at the relaying nodes, it would cause severe error propagation in FBMC/OQAM based multi-hop relaying networks. The reason is that the existence of the intrinsic interference at each hop. In deliverable D7.1, we have proposed and have investigated several relaying strategies that are able to mitigate the intrinsic interference induced at each link to some extent. Nevertheless, it still proves challenging to effectively avoid the performance degradation due to error propagation especially in case of highly frequency selective channels. Therefore, we propose to choose decode-and-forward (DF) as the relaying strategy. For each hop, either the SLNR maximizing multi-tap pre-equalizer reviewed in the previous subsection is employed at the transmitting node, or the SINR maximizing multi-tap equalizer is used at the receiving node. In the first case, the equalizer has a single tap, while a single-tap pre-equalizer is adopted in the second case.

2.4 *Simulation results*

In this subsection, we evaluate the uncoded bit error rate (BER) performance of the FBMC/OQAM based multi-hop relaying network. The linear model illustrated in Figure 2-1. The R_{relay} relays assist the transmission between the base station and the mobile terminal, resulting in $(R_{\mathrm{relay}} + 1)$ hops. The total number of subcarriers is 128, and the subcarrier spacing is 15 kHz. The PHYDYAS prototype filter [14] with overlapping factor *K* = 4 is employed. Perfect channel state information at the transmitter as well as at the receiver is assumed. In case of CP-OFDM, the length of the cyclic prefix (CP) is ¼ the symbol period. The

information symbols are drawn from a 16 QAM constellation. As mentioned in previous subsections, each node in the multi-hop relaying networks is equipped with a single antenna, and a single stream is transmitted. Here the path loss exponent ζ =3.5. For all the examples, the ITU Veh-A [13] channel model is considered. In Table 2-1, we present a summary of the simulation parameters used for the numerical results presented in this subsection.

Frame structure	
Bandwidth	1.4 MHz
Subcarriers number	128 subcarriers
Subcarrier spacing	15 kHz
OFDM CP	¼ Symbol period
FBMC filter	OFDM/OQAM PHYDYAS
Overlapping factor	4
Modulation and coding schemes	16-QAM, uncoded
Transmitter/Receiver	
Noise power spectral density	Various
MS/RS number of antenna	1
Transmission scheme	single stream
HH antenna model	Isotropic
Propagation	
Path-loss model	path loss exponent ζ = 3.5
Fast fading channel models	ITU-Vehicular A
Channel estimation	Ideal

Table 2-1 Overview of the simulation parameters

In the first example, we show the uncoded BER performance at each link of the FBMC/OQAM based multi-hop relaying network. Multi-tap equalization [2] is employed to mitigate the inter-symbol interference and the inter-carrier interference. Specifically, a multi-tap pre-equalizer and a single-tap equalizer are employed at the transmitting node and the receiving node, respectively. Or a single-tap pre-equalizer and a multi-tap equalizer are employed at the transmitting node and the receiving node, respectively. Figure 2-2 depicts the results. Note that in the legend of the figure, L_a and L_b denote the number of taps of the multi-tap equalizer and the number of taps of the multi-tap pre-equalizer, respectively. It is observed that these two cases lead to a similar performance. As the length of the multi-tap equalizer or the length of the multi-tap pre-equalizer increases, a

performance improvement is achieved, due to the enhanced capability of suppressing the inter-symbol and inter-carrier interference.

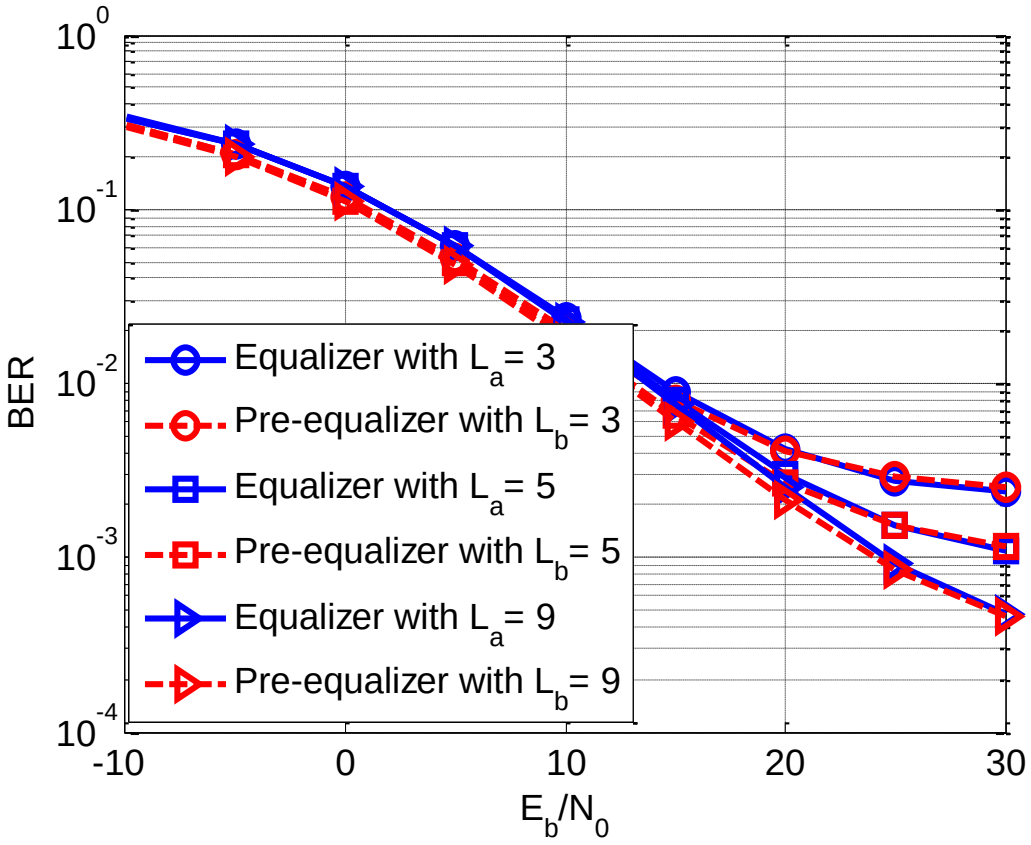

Figure 2-2 BER versus SNR for a single hop of the FBMC/OQAM based multi-hop relaying network where a multi-tap equalizer or a multi-tap pre-equalizer is employed; ITU Veh-A channel

We further investigate the impact of the number of hops on the BER performance at a relatively low SNR regime. In Figure 2-3, the BER performance versus the number of hops for the FBMC/OQAM based multi-hop relaying network is presented. For each hop either a multi-tap pre-equalizer at the transmitter or a multi-tap equalizer at the receiver is employed. We can see that except of the 3-tap case, a larger number of hops leads to a better BER performance due to an increased receive SNR. This advantage of the multi-hop relaying technology has been pointed out in the previous text. In case of 3-tap pre-equalizers or equalizers, the residual interference at each hop is still not low enough. Consequently, as the number of hops increases, the error propagation is more severe, leading to the degraded performance compared to the case of a smaller number of hops. Similar to the single-link case, adopting a larger number of taps contributes to performance improvement. The advantage of increasing the number of hops is thus more pronounced with a longer pre-equalizer or a longer equalizer.

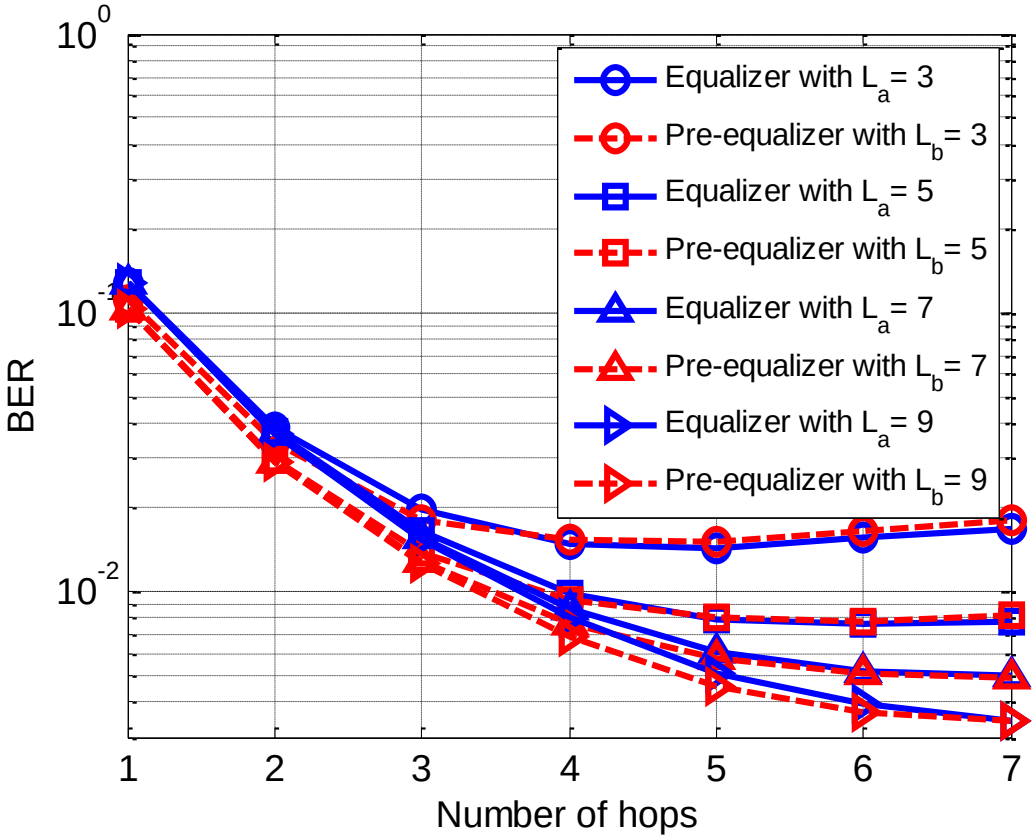

Figure 2-3 BER versus the number of hops with the SNR at 0 dB for the FBMC/OQAM based multi-hop relaying network where a multi-tap equalizer or a multi-tap pre-equalizer is employed; ITU Veh-A channel

Moreover, Figure 2-4 illustrates the impact of the number of hops on the BER performance of the FBMC/OQAM based multi-hop relaying network at a higher SNR, SNR = 10 dB. Similar to the previous examples, difference lengths of the pre-equalizer and the equalizer are considered. It can be seen that a 3-tap pre-equalizer or a 3-tap equalizer is not sufficient to deal with the error propagations in case that DF is employed. As the number of hops increases, it leads to a higher receive SNR. However, in such a relatively high SNR regime, the residual intrinsic interference becomes the dominant source of interference rather than the noise. Thus, the error propagation problem overweighs the increase of the receive SNR as the number of hops is larger. These results and observation imply a trade-off that the increased number of hops in an FBMC/OQAM based multi-hop relaying network contributes to enhanced receive SNR but more critical error propagation in the meanwhile. Note that this conclusion is consistent with those drawn in previous related publications on multi-hop relaying networks that a larger number of hops actually leads to the degradation of the BER performance at the high SNR regime [15]. In addition, the BER performance of the case where a multi-tap equalizer is employed is similar to that of the case where a multi-tap pre-equalizer is used. Therefore, to determine whether to perform the multi-tap pre-equalization or the multi-tap equalization for each hop, one should majorly consider other factors rather than the performance issue, such as the limit of computational load of each node, or the available knowledge of the channel state information.

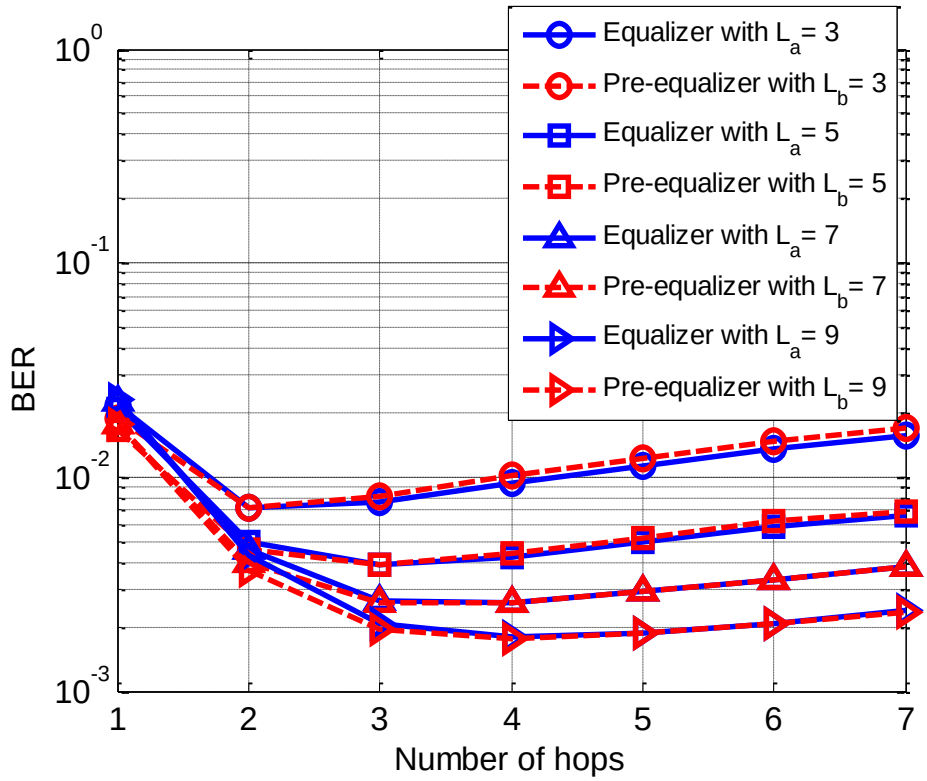

Figure 2-4 BER versus the number of hops with the SNR at 10 dB for the FBMC/OQAM based multi-hop relaying network where a multi-tap equalizer or a multi-tap pre-equalizer is employed; ITU Veh-A channel

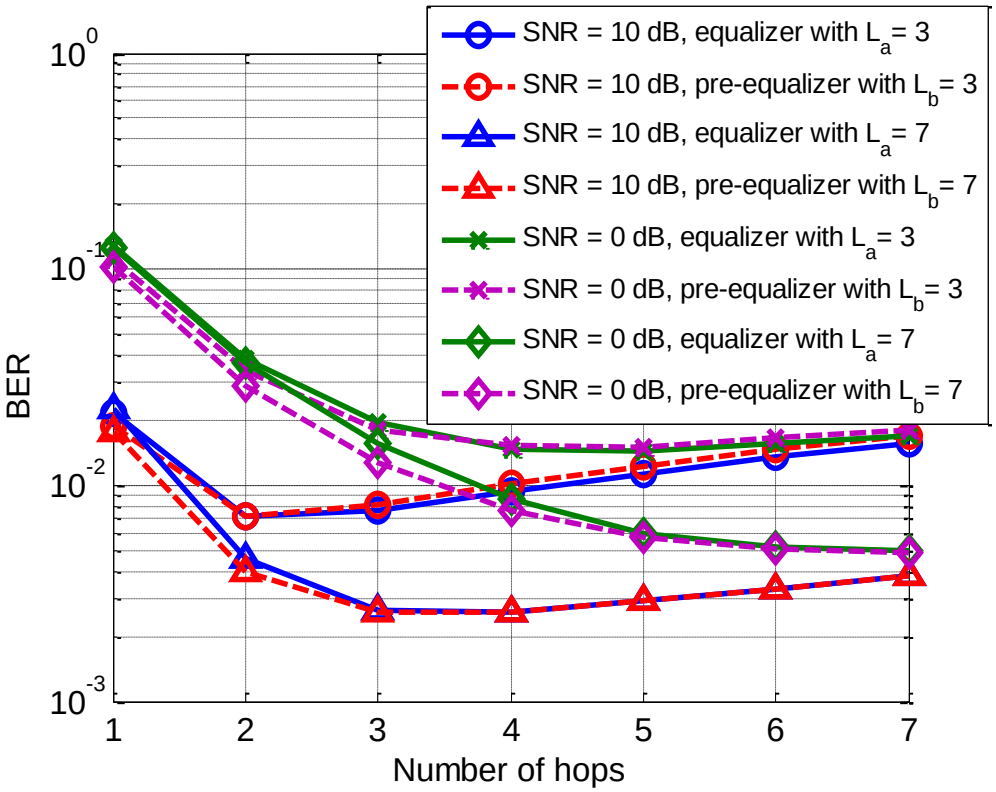

Figure 2-5 Comparison of the BER performance in case of SNR = 0 dB and SNR = 10 dB for the FBMC/OQAM based multi-hop relaying network where a multi-tap equalizer or a multi-tap pre-equalizer is employed; ITU Veh-A channel

To provide a clear view of the comparison between the BER performance at SNR = 0 dB and that at SNR = 10 dB, Figure 2-5 is also included in this document. Recall that a single antenna is equipped at each node in our investigations. It is worth noting that employing multiple antennas at the nodes will bring further benefits in terms of enhanced BER performance and range extension capability [15].

2.5 *Final remarks*

In this section, we have conducted an investigation of FBMC/OQAM based multi-hop relaying networks that employ multi-tap equalization. As the continuation of the range extension analysis for FBMC/OQAM based multi-hop relaying scenarios that has been presented in deliverable D7.1, the goal here is to alleviate the constraint on the channel frequency selectivity and to for the first time address the use of multi-tap equalization in broadband PMR multi-hop relaying networks. We have started with a brief introduction and motivation of our work and then have reviewed a state-of-the-art design of pre-equalizers and equalizers. What follows is a description of the linear model for multi-hop relaying networks that has been employed throughout our investigation. Moreover, we have briefly reviewed the relaying strategies that we have proposed in deliverable D7.1 for FBMC/OQAM based multi-hop relaying networks and have pointed out the need of employing DF to achieve a more effective mitigation of the inter-carrier and inter-symbol interference. In addition, it has been explained in detail how an FBCM/OQAM based multi-hop relaying network with DF and multi-tap equalization operates. Finally, we have assessed the performance of FBMC/OQAM based multi-hop relaying networks with multi-tap equalization. The extensive numerical results that have been shown provide insights into the impact of number of hops on the performance and the choice of appropriate transmit as well as receive processing for each hop.

3. **Multicarrier Two-Way Relaying with Nonbinary Coding**

In ad-hoc scenarios, relays can be introduced to widen communications range and/or improve the signal quality. However, relays typically introduce some delay since the user-to-user communication is not direct anymore but rather requires two or more hops. Things get worse when two users exchange information in both ways and are helped by the same relay: on a TDMA-based system, four slots are needed to cover all user-to-relay and relay-to-user links.

Recent advances in the field of network coding have shown how to reduce delays by introducing low-complexity operations at the users and at the relay. More specifically, the two-way relaying scheme divides the communication between two users into two slots only: in the first one, both users send their message to the relay. Then, in the second slot, the relay retransmits a function of both messages: since each user knows its own message, the other user's message can be recovered. It is worth noting that the relay does not need to separate and decode the two users' messages and can directly recover the combined message to transmit [23][24]. As we will see later, the binary (XOR) sum applied to linear channel codes allows us to carry out these operations in a simple, elegant way.

References [25]-[34] are examples of interesting results and achievable rates in the Additive White Gaussian Noise (AWGN) channel. When considering frequency selective channels, however, these results cannot be applied directly since the channels of the two users are characterized by different impulse responses and, hence, the linearity properties of the codes are not preserved. In this section, we propose an extension of the two-way relaying protocol to frequency selective channels based on multicarrier modulations. Indeed, for a sufficiently high number of subcarriers, the available spectrum can be divided into orthogonal subbands whose frequency response is approximately flat. Then, the two-way relaying strategy introduced above can be applied on each one of the subcarriers.

A typical assumption in multicarrier system is that the channel response varies slowly in time or, in other words, that several multicarrier symbols undergo the same channel response. Then, the channel offers some diversity only when considering all subcarriers. For this reason, codewords should be spread among multiple (all) subcarriers, as opposed to have separate per-subcarriers encoders, in order to exploit the said diversity.

We will consider two types of relays, namely

- Complete-Decode-Forward (CDF), that is the relay first decodes both messages and then forms the combined message and
- Functional-Decode-Forward (FDF), meaning that the relay directly decodes the combination, i.e. the XOR sum, of the users' messages.

As a final remark, it is worth mentioning that the two users require a high level of synchronism (same transmission rate and, especially, very low frequency offset and relative delay). For this reason, even if the proposed scheme can be applied to any multicarrier technology, we focus here on FBMC schemes, which are more robust than OFDM to those types of impairments.

3.1 *System Model*

We will now describe a multicarrier Two-Way Relay Channel (TWRC) based on FBMC. The focus will be mainly on the uplink (users-to-relay) channel, which is the bottleneck of the system since the two users have to transmit at the same time. The downlink (relay-to-users) phase is a simple broadcast transmission and does not present major difficulties.

3.1.1 **Preliminary considerations**

It is well known [3][25][26] that a well-designed FBMC link achieves a good separation among subcarriers. Indeed, inter-carrier interference and inter-symbol interference can be kept to negligible levels if the prototypes pulses (at transmitter and receiver sides) satisfy some reconstruction constraints and if the channel equalizer is properly tuned.

In order to create a multicarrier two-way relay channel based on FBMC, some precautions need to be taken. To start with, equalization should be carried out at the transmitter side, i.e. at the users, and not at the receiver side as usual. The reason is that the two users experience different channel conditions and, thus, a single equalizer at the relay will not serve its purpose. The channel-state information requirements should not be perceived as a strong limitation. Indeed, in the second transmission slot, the relay transmits its message to the users on the same channels and, hence, some sort of feedback can be implemented (or channel reciprocity can be exploited). Also, the users may take advantage of the channel knowledge for implementing a suitable power allocation strategy. Finally, releasing the relay from the equalization step reduces its complexity.

For simplicity, we will also assume that the subcarrier signals are real-valued. Again, this assumption is not unrealistic. For instance, with the EMPhAtiC FBMC/OQAM modulation scheme, one can consider the real and the imaginary parts of the complex OQAM symbols as two separate sets of real symbols. The entire transmission chain remains unaltered except for the staggering operation, which now looks as in Figure 3-1.

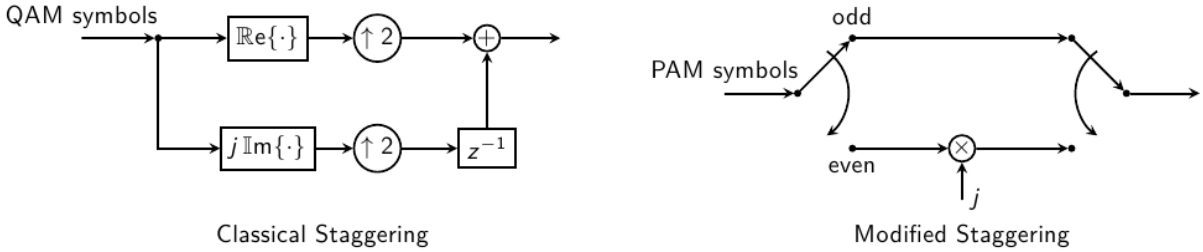

Figure 3-1: Staggering operation for QAM symbols (left) and PAM symbols (right).

3.1.2 **Uplink of the two-way relay channel**

The uplink of the two-way relay channel is actually a two-user multiple-access channel. For a system designed according to the considerations above, that is with M subcarriers that can be considered orthogonal, the signal model at the m-th subcarrier can be written as

$$y_m = h_{a,m}s_{a,m} + h_{b,m}s_{b,m} + w_m, \tag{3-1}$$

with user a (respectively b) transmitting symbol $s_{a,m}$ (respectively $s_{b,m}$) with power $h_{a,m}^2$ (respectively $h_{b,m}^2$, with $h_{\cdot,m} \in \mathbb{R}$). The Additive White Gaussian Noise (AWGN) is

represented by the random variable $w_m \sim \mathcal{N}(0,1)$. This signal model is illustrated in Figure 3-2.

Both symbols belong to a real Q-PAM constellation of unitary power so that the Signal-to-Noise Ratio (SNR) for user $x \in \{a, b\}$ is

$$\mathrm{SNR}_{x,m} = h_{x,m}^2. \tag{3-2}$$

Note that this is a high-level equivalent model, representing the signal at the output of the FBMC demodulator and hiding the effects of the channel impulse response, of the equalizer and of any other block in the transmission chain.

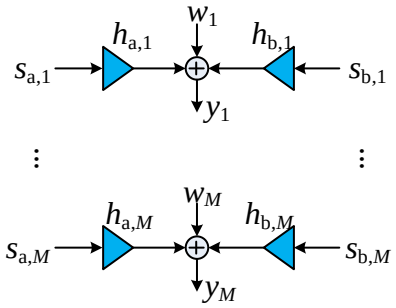

Figure 3-2: The uplink of the multi-carrier two-way relay channel

Figure 3-3 illustrates how the modulated symbols are mapped to the time-frequency grid of the FBMC system. As discussed in more detail below, we define vectorial modulated symbols $\mathbf{x}_a, \mathbf{x}_b \in \mathbb{R}^T$, with *T* a small integer, whose components are real-valued PAM constellation points. Let $\mathbf{x}_{a,n} = [x_{a,n,1}, \ldots, x_{a,n,T}]$ be the vector of PAM symbols which correspond to the *n*-th codeword symbol of user *a*. Then, we can write for the components of the multi-carrier symbols $s_{a,t,m} = x_{a,n,i}$ with $i \in \{1, \ldots, T\}$ and

$$m = \mathrm{mod}\big((n-1)T + i - 1, M\big) + 1 \in \{1,2, \ldots, M\}$$
$$t = \left\lfloor \frac{(n-1)T + i - 1}{M} \right\rfloor + 1$$

For user *b*, the same expressions hold.

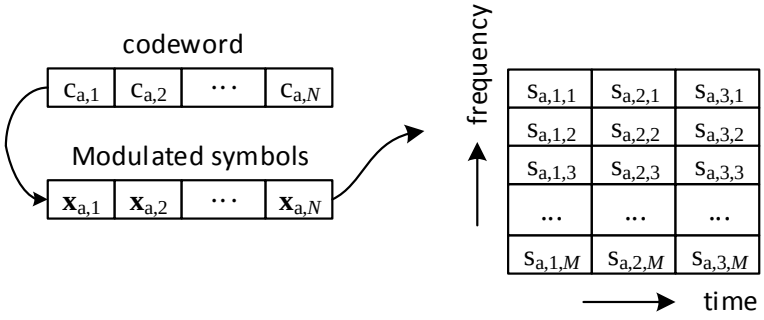

Figure 3-3: Mapping of codeword symbols to modulated symbols and to multi-carrier symbols for user *a*.

With this mapping from codeword to multi-carrier symbols, in the following we adopt a notation which is based on the indexing of the codeword symbols. This highlights the connection to the channel encoder and decoder and simplifies the discussion on the combination of symbols in the sense of network coding.

One codeword symbol then corresponds to a group of *T* subcarriers, for which we write

$$\mathbf{y}_n = \mathbf{H}_{a,n}\mathbf{x}_{a,n} + \mathbf{H}_{b,n}\mathbf{x}_{b,n} + w_n, \tag{3-3}$$

where $\mathbf{H}_{a,n}, \mathbf{H}_{b,n} \in \mathbb{R}^{T\times T}$ are diagonal matrices. The mapping between $h_{\cdot,m}$ and $\mathbf{H}_{\cdot,n}$ and the one between y_m and $\mathbf{y}_n$ follow straightforwardly from the mapping between $s_{\cdot,m}$ and $\mathbf{x}_{\cdot,n}$.

The reason for this seemingly more complicated notation is given by the non-binary coding scheme explained in the following subsection.

3.1.3 **Modulation with non-binary coding**

We represent the messages (i.e. the information packets) of both users as vectors in the Galois field $\Phi_q \triangleq GF(q)$, where the field order *q* is assumed to be a power of two, which is the case for virtually all channel coding schemes. These messages $\mathbf{u}_a \in \Phi_q^K$ and $\mathbf{u}_b \in \Phi_q^K$ are encoded into the codewords $\mathbf{c}_a = \left[c_{a,1}, c_{a,2}, \ldots, c_{a,N}\right] \in \Phi_q^N$ and $\mathbf{c}_b = \left[c_{b,1}, c_{b,2}, \ldots, c_{b,N}\right] \in \Phi_q^N$ by

$$\mathbf{c}_a = \mathbf{u}_a\mathbf{G}, \quad \mathbf{c}_b = \mathbf{u}_b\mathbf{G}, \tag{3-4}$$

where $\mathbf{G} \in \Phi_q^{K\times N}$ denotes the generator matrix. The codeword symbols $c_{a,n}, c_{b,n}$ are mapped to real-valued vectorial PAM symbols $\mathbf{x}_{a,n}, \mathbf{x}_{b,n}$ by

$$\mathbf{x}_{a,n} = \boldsymbol{\mu}(c_{a,n}), \qquad \mathbf{x}_{b,n} = \boldsymbol{\mu}(c_{b,n}) \tag{3-5}$$

where $\mu: \Phi_q \rightarrow \mathbb{R}^T$ denotes the mapping function. Each *q*-ary codeword symbol is mapped to *T* Q-PAM symbols, i.e. it holds $q = Q^T$ with $T = 1,2,\ldots$. Note that for $q > 2$ this is different to the usual QAM or PAM mappings for binary codes in which several coded bits are mapped to *one* QAM or PAM symbol. Here, instead, we map *one* coded symbol to several PAM symbols.

The average of including only one codeword symbol in the mapping is that in this way the equivalent channel between the encoder and the decoder remains memoryless, given that the physical channel does not introduce any memory. This property is implicitly assumed by a belief-propagation decoder which operates on a Tanner graph of the code. For binary codes, this assumption is only fulfilled exactly for BPSK while for higher-order modulations it does not hold. This difference can have a strong impact if the channel cannot be decomposed into equivalent binary-input channels, as is e.g. the case for MIMO. Performance gaps of several dBs can occur which are entirely due to this effect [35].

For $q = 16$, we can map one codeword symbol to four BPSK symbols, two 4-PAM simply to one 16-PAM symbol, as listed in Table 3-1. Although not used in the following, we note that it is possible for $T = 3$ to define a constellation of 16 constellation points in three complex dimensions by e.g. selecting 16 points from a 6-dimensional sphere packing [35][36].

T	1	2	3	4
Q	16	4	–	2

Table 3-1: Mappings for a field order $q = 16$.

As a basis for the two-way relay channel, we briefly describe the soft demapping of a *q*-ary channel code in the case of a single user. The received signal of a single-user channel with fading is given by

$$\boldsymbol{y}_n = \mathbf{H}_n \mathbf{x}_n + \mathbf{w}_n, \;\; \mathbf{w}_n \sim \mathcal{N}(0, \mathbf{I}_T), \; \mathbf{x}_n = \boldsymbol{\mu}(c_n) \; . \tag{3-6}$$

As input for the decoder, we need to compute the *a posteriori probabilities* (APP) for each codeword symbol, i.e.

$$p_n([\alpha]) \triangleq P[c_n = \alpha \mid \mathbf{y}_n], \; \alpha \in \Phi_q \tag{3-7}$$

where we denote by $[\alpha] \in \mathbb{Z}_q = \{0,1,\dots,q-1\}$ the integer value which corresponds to the GF element α. With Bayes' theorem we find

$$p_n([\alpha]) \propto p(\mathbf{y}_n \mid c_n = \alpha) \propto \exp(-\|\mathbf{y}_n - \mathbf{H}_n \boldsymbol{\mu}(c_n)\|^2) \; . \tag{3-8}$$

For binary codes, this can be reduced to a scalar value per coded bit, e.g. to the well-known L-values defined as $L_n \triangleq \frac{p_n(1)}{p_n(0)}$.

The benefit of preserving a memoryless channel between encoder and decoder is also reflected in the modulation-constrained capacity: while for the binary case, the achievable rate is limited by the BICM capacity, for $q > 2$ with the described mappings the achievable rate is limited by the coded modulation (CM) capacity, which is higher (or equal for some few special cases) than the BICM capacity [37][38].

Figure 3-4 shows the CM capacities for the modulations of Table 3-1 over the fast real-valued Rayleigh fading channel. An upper bound for the CM capacity is given by the ergodic capacity of the (real-valued) Rayleigh fading channel [39],

$$C_{Rayleigh} = \frac{1}{2 \ln 2} \exp\left(\frac{1}{SNR}\right) E_1\left(\frac{1}{SNR}\right), \tag{3-9}$$

where $E_1(x) \triangleq \int_x^\infty \frac{e^{-t}}{t} dt$ denotes the *exponential integral*. For the case of BPSK, a closed-form expression can be found in [40].

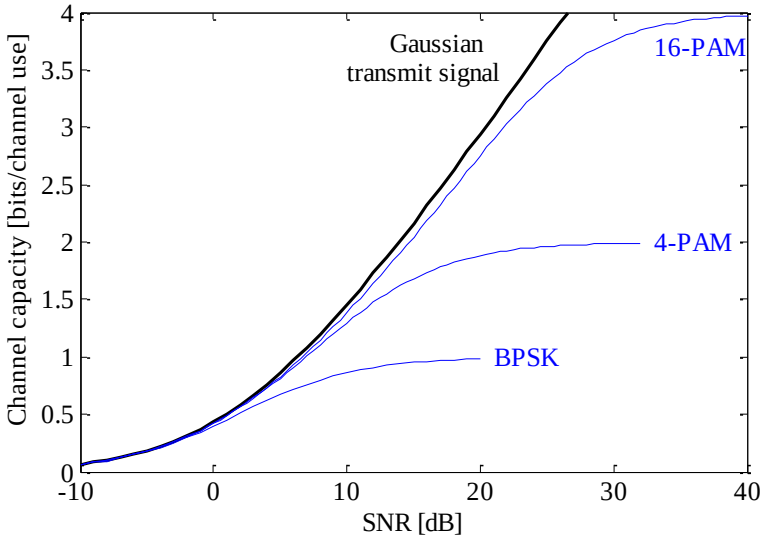

Figure 3-4: Channel capacities for the real-valued fast Rayleigh fading channel

3.1.4 **Demapping for complete and for functional decoding**

The conditional PDF (probability density function) of the TWRC according to (3-3) is given by

$$p(\mathbf{y}_n \mid c_a c_b) \propto \exp\left(-\left\|\mathbf{y}_n - \mathbf{H}_{a,n}\boldsymbol{\mu}(c_{a,n}) - \mathbf{H}_{b,n}\,\boldsymbol{\mu}(c_{b,n})\right\|^2\right), \tag{3-10}$$

For complete decoding, the relay tries to decode both messages $\mathbf{u}_a$ and $\mathbf{u}_b$. To this end, the APPs with respect to the coded symbols $c_{a,n}$ and $c_{b,n}$ have to the computed. In analogy to (3-7), this is given by

$$p_{a,n}([\alpha]) \triangleq P\left[c_{a,n} = \alpha \mid \mathbf{y}_n\right] = \sum_{\beta\in\Phi_q} P\left[c_{a,n} = \alpha, c_{b,n} = \beta \mid \mathbf{y}_n\right] \tag{3-11}$$

and

$$p_{b,n}([\beta]) \triangleq P\left[c_{b,n} = \beta \mid \mathbf{y}_n\right] = \sum_{\alpha\in\Phi_q} P\left[c_{a,n} = \alpha, c_{b,n} = \beta \mid \mathbf{y}_n\right]. \tag{3-12}$$

For functional decoding, the relay tries to decode directly for $\mathbf{u}_{ab} \triangleq \mathbf{u}_a + \mathbf{u}_b \in \Phi_q^K$. Here, we can exploit the linearity of the code and directly decode for the sum of both codewords, since this is also a codeword,

$$\mathbf{c}_{ab} \triangleq \mathbf{c}_a + \mathbf{c}_b = \mathbf{u}_a\mathbf{G} + \mathbf{u}_b\mathbf{G} = (\mathbf{u}_a + \mathbf{u}_b)\mathbf{G} = \mathbf{u}_{ab}\mathbf{G}\,. \tag{3-13}$$

Note that this arithmetic is defined in $\Phi_q \triangleq GF(q)$. Since we assume that q is a power of two, i.e. the field Φ_q is an extension field of $\Phi_2 = \{0,1\}$, the addition in Φ_q is the same as the vectorial addition in Φ_2 and hence the sum in the field Φ_q corresponds to the XOR operator on the binary representation of the codeword symbols. The APP with respect to the combined codeword symbol $c_{ab,n} = c_{a,n} + c_{b,n} \in \Phi_q$ is therefore given by

$$p_{ab,n}([\alpha]) \triangleq P\left[c_{ab,n} = \alpha \mid \mathbf{y}_n\right] = \sum_{\beta\in\Phi_q} P\left[c_{a,n} = \alpha + \beta, c_{b,n} = \beta \mid \mathbf{y}_n\right]. \tag{3-14}$$

Note that since Φ_q is an extension field of the binary field, it holds $\alpha + \beta = \alpha - \beta\ \forall \alpha, \beta \in \Phi_q$.

The simplest example for functional "decoding" is the AWGN TWRC, i.e. $h_a = h_b$ with uncoded BPSK. In this case, it is possible to recover the combined symbols c_{ab} but not the individual symbols c_a or c_b. However, for higher-order modulations, the situation is quite different. It has been shown that it is not possible to find a mapping $\mu: \Phi_q \to \mathbb{R}$ such that the sum of PAM symbols $x_a + x_b$ corresponds to a unique value of $c_a + c_b$ [41]. Figure 3-5 shows the superposition of two Gray-labeled 4-PAM constellations and the resulting bit labels for c_{ab}. We see that the values $x_a + x_b \in \{-2,2\}$ cannot be uniquely identified with a coded symbol c_{ab}. However, this is not necessarily a serious problem for a coded system with soft decoding: the APPs defined above automatically account for this peculiarity. Nevertheless, the search for multi-dimensional non-binary constellations which provide good performance for functional decoding remains an interesting research question.

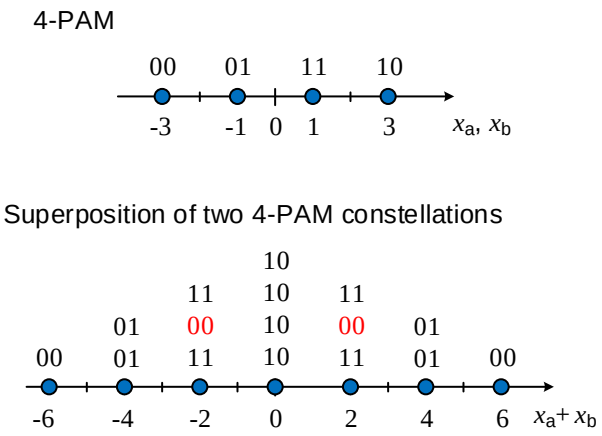

Figure 3-5: Superposition of two 4-PAM constellations. The bit labels for the combined symbols c_{ab} are not unique for some constellation points.

3.1.5 **Joint decoding of non-binary LDPC codes**

For the joint decoding of both codewords with a single decoder, we first define the joint codeword symbols by

$$d_n \triangleq q \cdot [c_{a,n}] + [c_{b,n}] \in \mathbb{Z}_{q^2} \tag{3-15}$$

and form the joint codeword $\mathbf{d} = [d_1, d_2, \dots, d_N] \in \mathbb{Z}_{q^2}^N$. The mapping from GF symbols to integers is necessary to define the symbols in the larger range $\mathbb{Z}_{q^2}$. Alternatively, we could define the joint codeword in Φ_q^2, i.e. each codeword symbol as a two-dimensional vector of Φ_q elements. It is, however, generally *not* possible to define the joint codeword symbols in the extension field Φ_{q^2}. For the definition of a joint belief-propagation decoder on the code's Tanner graph, the representation of the codeword symbols as integers according to (3-15) is sufficient to apply the transform-based check node processing, which reduces the complexity of a decoder in Φ_q from $O(q^2)$ to $O(q \log q)$. Analogously, the complexity of a joint decoder of two q-ary codewords scales with $O(q^2 \log q)$ [42]. For this joint decoder, the input is given by a vector of all APPs,

$$p_n(b) \triangleq P[d_n = b \mid \mathbf{y}_n] \propto \exp\left(-\left\|\mathbf{y}_n - \mathbf{H}_{a,n}\boldsymbol{\mu}\left(\left\lfloor\frac{d}{q}\right\rfloor\right) - \mathbf{H}_{b,n}\,\boldsymbol{\mu}(d \bmod q)\right\|^2\right), \quad (3\text{-}16)$$

for $b \in \mathbb{Z}_{q^2} = \{0,1,\ldots,q^2-1\}$.

From these APPs, we can obtain the APPs for the usual single-user decoder as

$$p_{a,n}(b_1) = \sum_{b_2=0}^{q-1} p_n(q \cdot b_1 + b_2)$$
$$p_{b,n}(b_2) = \sum_{b_1=0}^{q-1} p_n(q \cdot b_1 + b_2) \quad (3\text{-}17)$$
$$p_{ab,n}([\alpha]) = \textstyle\sum_{\beta \in \Phi_q} p_n(q \cdot [\alpha] + [\alpha + \beta])\,.$$

Here, we again have to carefully distinguish between the GF elements $\alpha \in \Phi_q$ and their associated integer values $[\alpha] \in \mathbb{Z}_q$.

3.2 *Mutual Information*

For a coded system with soft decoding, which is state-of-the-art in virtually all wireless systems, the uncoded BER is *not* a meaningful performance indicator. Instead, the mutual information of the equivalent channel between the encoder output and the decoder input can be used a precise performance metric [43][44]. From this mutual information, the word error rate (WER) of the coded system can be predicted with very good accuracy. In other words, the mutual information of the equivalent channel can also be used as a metric for physical-layer abstraction, which is often applied for system-level simulations [45].

3.2.1 **Mutual information for complete decoding**

For complete decoding, the uplink of the TWRC corresponds to the multiple-access channel, for which the rate regions in the single and multi-carrier case are well known [46][47]. Since here we focus on the symmetric case in which both users transmit at the same rate, the scalar channel capacity with equal rate for both users is the suitable performance bound. Taking into account the discrete transmit alphabet, we can write for the capacity of user *a*,

$$C_a \triangleq I(c_a;\mathbf{y}) = \textstyle\sum_{c_a=1}^{q-1} \int p(c_a,\mathbf{y}) \log_2 \frac{p(c_a,\mathbf{y})}{p(c_a)p(\mathbf{y})}\, d\mathbf{y},\,. \quad (3\text{-}18)$$

and analogously for user *b*. While there is no closed-form expression for C_a, for moderate values of *q*, it can be easily computed numerically.

3.2.2 **Mutual information for functional decoding**

Since the relay is only interested in the sum of both packets, it seems straightforward to compute the mutual information of the sum of the two symbols, $c_{ab} = c_a + c_b \in \Phi_q$. The mutual information $I(c_{ab};\mathbf{y})$ can be computed in a very similar way as C_a above, i.e.

$$C_{ab} \triangleq I(c_{ab};\mathbf{y}) = \textstyle\sum_{c_a=1}^{q-1} \int p(c_{ab},\mathbf{y}) \log_2 \frac{p(c_{ab},\mathbf{y})}{p(c_{ab})p(\mathbf{y})}\, d\mathbf{y},\,. \quad (3\text{-}19)$$

and the numerical computation can be carried out without problems, but we note that we encounter difficulties when we try to define an equivalent channel from c_a to $\mathbf{y}$. This difficulty is related to more fundamental problems in defining the "capacity" for the

transmission of the combined packet. Actually, there is evidence that the mutual information $C_{ab} = I(c_{ab}; \mathbf{y})$ does *not* constitute an upper bound for the rate of the combined packet [48] and, to the best of our knowledge, the capacity for functional decoding is not known.

The mutual informations C_a C_b and C_{ab} according to (3-18), (3-19) are plotted in Figure 3-6 for 2-PAM (BPSK), 4-PAM and 16-PAM over the real-valued fast Rayleigh TWRC. We note that for sufficient SNR, C_{ab} is higher than $C_a = C_b$. A noticeable difference to the single-user case is that modulations with higher rate do not always provide a higher mutual information.

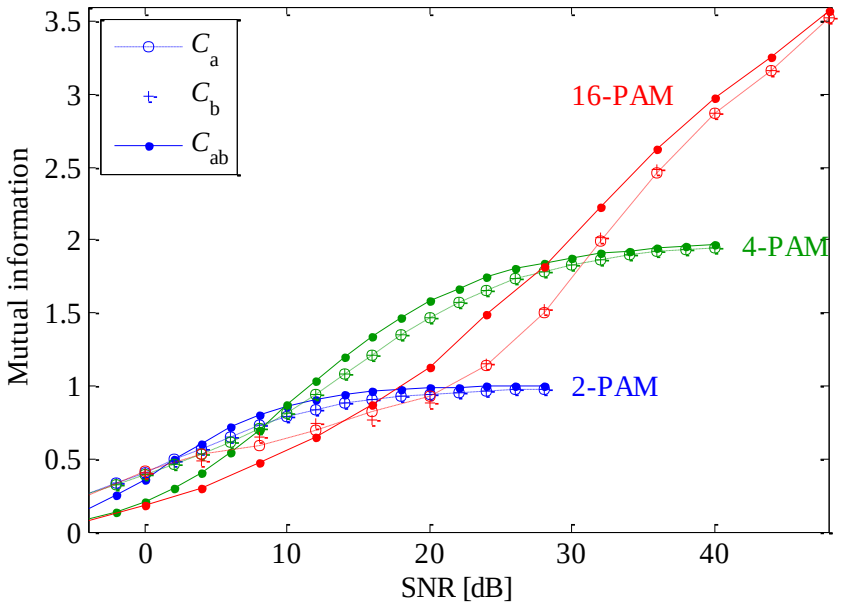

Figure 3-6: Mutual informations for complete and functional decoding

3.3 *Numerical Results*

The presented transmission scheme for the TWRC has been tested with a non-binary LDPC code in the Galois field of order $q = 16$ with rate $R_c = 1/2$. The message length is of $K = 180$ non-binary symbols (i.e., 720 bits), resulting in a codeword length of $N = 360$ symbols.

Figure 3-7 shows the word error rates for the three considered modulations for a fading channel, which may correspond to fast fading in time for a single-carrier system or to frequency-selective fading for a FBMC system with perfect equalization.

The following decoding methods have been applied,

- **Joint functional decoding**: a joint decoder as described in Section 3.1.5 is applied on the APPs given by (3-16) and from its output, the estimate $\hat{\mathbf{u}}_{ab}$ is derived.
- **Single-user functional decoding**: a single-user decoder is applied on the APPs given by (3-14) to recover directly $\mathbf{u}_{ab}$

- **Single-user complete decoding**: two single-user decoders are applied on the APPs (3-11), (3-12) to recover $\mathbf{u}_a$ and $\mathbf{u}_b$. Due to symmetry, the error rates are identical.

As predicted by the mutual informations in Figure 3-6, we can observe that single-user functional decoding is slightly superior to complete decoding, which has the double complexity since it has to decode two packets. Joint decoding achieves a remarkable gain for all modulations, albeit at the price of significantly more complexity.

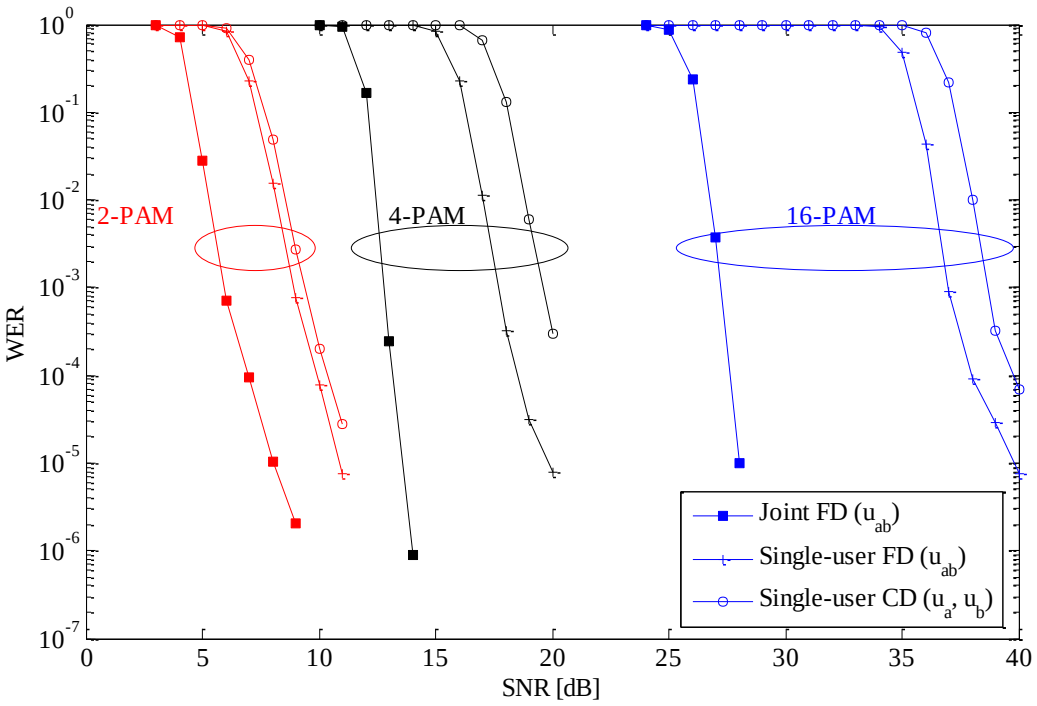

Figure 3-7: Word error rates for the TWRC with fast Rayleigh fading for $\{2,4,16\}$-PAM

3.3.1 **Adaptation in the multi-carrier TWRC**

The coding scheme above has also been tested with a FBMC/OQAM-based multicarrier TWRC. The FBMC/OQAM specifications are compliant with the directives of [58] (see Table 3-2 for a summary of the parameters). More specifically, we take $\mathrm{M} = 128$ subcarriers separated by 15 kHz, so that the sampling frequency is 1.920 MHz. The chosen prototype pulse (at both the transmitter and the receiver side) is the one proposed by the PHYDYAS project [59], with overlapping factor $\kappa = 4$.

Frame structure	
Subcarriers number	128 subcarriers
Subcarrier spacing	15 kHz
FBMC filter	OFDM/OQAM PHYDYAS
Overlapping factor	4

Modulation and coding schemes	2-PAM, 4-PAM, 16-PAM
Channel Coding	Non-binary LDPC code, field order $q = 16$, code rate $R_c = \frac{1}{2}$, message length $K = 180$ (720 bits), codeword length $N = 360$.
Propagation	
Fading channel models	ITU Extended Pedestrian A (EPA), Extended Vehicular A (EVA) and Extended Typical Urban (ETU)
Channel estimation	Ideal

Table 3-2: Summary of parameters.

Furthermore, the equalizer (based on ideal channel state information) consists of a single tap (channel inversion) and, as commented before, is implemented at the transmitter side, due to the impossibility for the relay to equalize both users' channels at the same time. We focus here on 2-PAM modulation only. This means that, for each codeword, we will need to transmit $4N = 1440$ 2-PAM symbols. In order to have a straightforward distribution of the symbols between the subcarriers, we will only use subcarriers 1–120, leaving the other 8 subcarriers off. This means that each codeword corresponds to $1440/120 = 12$ multicarrier symbols.

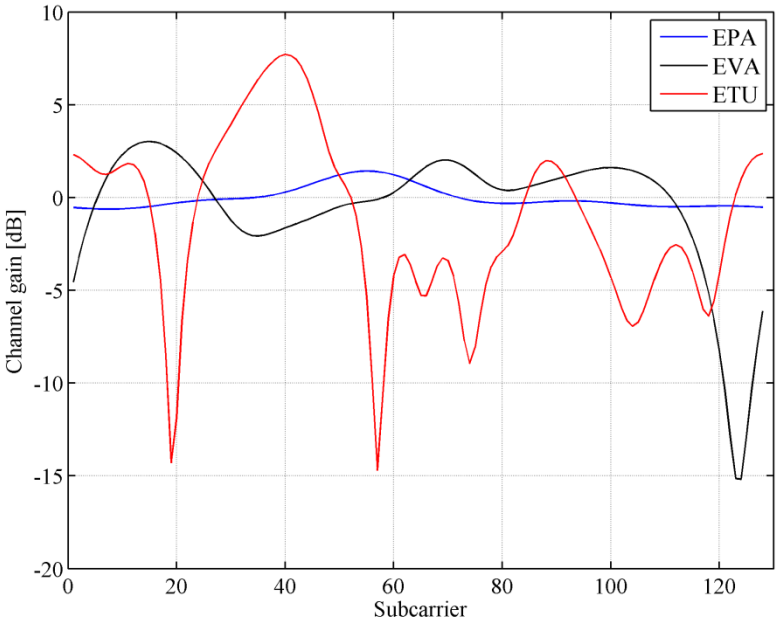

Figure 3-8: Channel gain examples for the three considered channel models.

Both user–relay channels are modelled as frequency selective, block fading channels, meaning that the channel response does not vary during the transmission of a codeword, but it is independently generated at each new codeword. Frequency selectivity behaves according to ITU Extended Pedestrian A (EPA), ITU Extended Vehicular A (EVA) or ITU Typical Urban (ETU) channel models (examples of the channel gain for the three models are depicted in Figure 3-8).

The WER corresponding to the three decoders described above (respectively, joint functional decoding, single-user functional decoding and single-user complete decoding) is reported in, respectively, Figure 3-9, Figure 3-10, and Figure 3-11. The performance obtained in the FBMC-based TWRC (red curves with label “MC-XXX”) with the three considered channel models are compared to those obtained in the single-carrier case (blue curves with label “SC-XXX”) under block fading or fast fading assumptions. The AWGN channel has been reported as a benchmark: as expected, with no fading, single-carrier TWRC and the multicarrier TWRC are equivalent. (There are no AWGN curves in Figure 3-11 since the complete decoding scheme cannot work when the two users are received with the same power.)

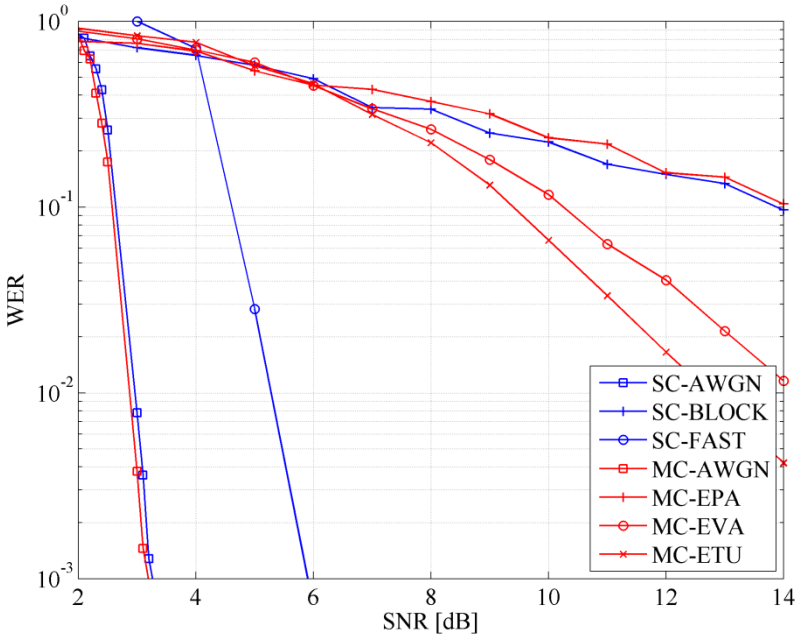

Figure 3-9: WER for joint functional decoding.

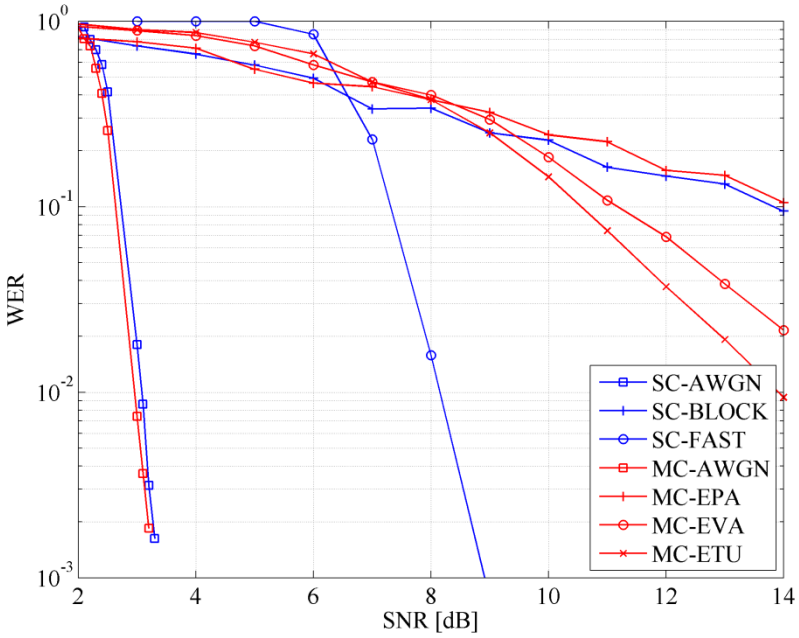

Figure 3-10: WER for single-user functional decoding.

Observing the three figures, the same trend can be recognized for the behaviour of the three decoding schemes as we increase the frequency selectivity of the channel. Specifically, we see that the lowly selective EPA channel behaves as block fading in the single-carrier case. As we increase frequency selectivity (first with EVA channel model and, further, with ETU channel model, see also Figure 3-8), the performance of the code improves, since frequency selectivity implies diversity among subcarriers. Unfortunately, the channel gains at the subcarriers are not independent and, thus, we cannot hope to achieve the WER obtained in the single-carrier fast-fading case.

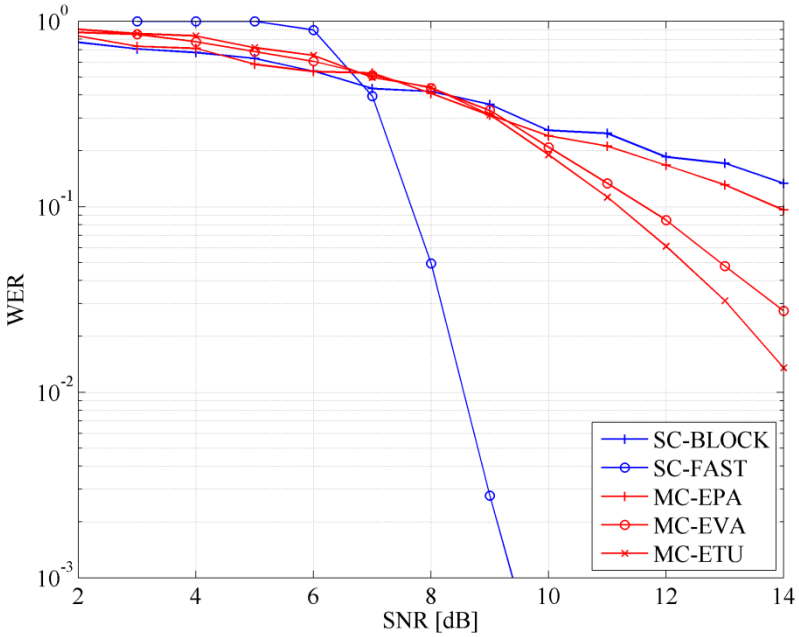

Figure 3-11: WER for single-user complete decoding.

3.4 *Comments on resource allocation*

The key aspect we consider in the multicarrier TWRC is the availability of channel state information at the transmitter. With this knowledge, the users can adapt their transmission parameters to the channel in order to increase their rate.

For complete decoding in the vector multiple-access channel, iterative waterfilling is known to be the optimum solution in the sense of sum capacity [47]. This solution, however, does not apply directly to the considered case, because of the discrete modulations employed (as opposed to Gaussian signalling). With arbitrary signalling, mercury/waterfilling power allocation is shown to be optimal in the single user case (see, e.g., [60]), but its extension to the multiple-access channel is still unknown.

The difficulties with finding an optimal power allocation suggest exploring other strategies. For instance, for practical purposes, rate selection and subchannel allocation are more suited than power allocation [49]. Figure 3-12 compares two simple examples in this direction. In one example, each user is assigned half of the available subchannels. With this orthogonal allocation, we obtain two single-user problems for the rate selection, which is trivially solved by observing from Figure 3-4 that the highest modulation achieves the highest capacity.

The second example consists in using functional decoding while adapting the modulation to the SNR according to Figure 3-6. Since the mutual information is computed per subchannel, we have to consider in addition that with the orthogonal allocation for complete decoding, the mutual information per multi-carrier symbol is divided by two for this case. Therefore, functional decoding is clearly superior for the entire SNR range.

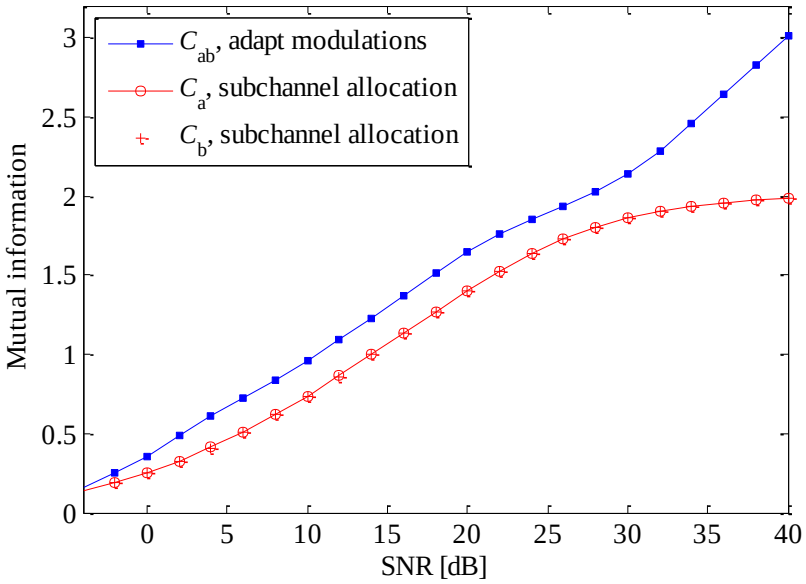

Figure 3-12: Achieved mutual informations with subchannel allocation for complete decoding and rate adaptation for functional decoding

3.5 *Conclusion*

In this section, we have combined non-binary channel coding with higher-order modulations for the single-carrier and multi-carrier symmetric two-way relay channel. For this combination, we investigated complete decoding as well as functional decoding for estimating the binary sum, a.k.a. the XOR, of both source packets at the relay. By investigating mutual information we demonstrated that functional decoding outperforms complete decoding for a sufficiently high SNR. The link-level simulation results indicate quite significant gains for joint decoding in all considered scenarios.

The proposed coding scheme has also been implemented in a more realistic scenario with actual FBMC modulators and frequency selective channel models following LTE specifications. The same considerations about functional decoding outperforming complete decoding hold true in this case. However, since the channel coefficients corresponding to the different subcarriers are not independent, some diversity gain is lost (especially for the lowly selective EPA model). A possible solution would be the introduction of a long interleaver that spreads codewords over a large number of multicarrier symbols, which undergo different instances of the channel. Obviously, this solution increases complexity and latency.

Finally, future research lines have been presented, which aim at improving performances by mean of smart resource (i.e., power, modulation order, subcarrier) allocation. In particular, a simple approach for adaptive modulation for the multi-carrier TWRC for functional decoding was presented and showed substantial gains compared to the corresponding complete decoding scheme with orthogonal subcarrier allocation.

4. Joint channel decoding and physical layer network coding for FBMC coded two-way relaying systems in highly frequency selective channel

In this section we develop practical network coding schemes such that the BER performance of the FBMC based decode-and-forward (DF) relaying systems can be evaluated in highly frequency selective channel. This work is an extension of our previous work in Section 3.1 of D7.1. Note that one major difference between this work and the work in Section 3 is that we have considered not only the network decoding design at the relay but also multi-tap pre-equalizers and equalizers at the users. Moreover, we have considered only binary decoding.

4.1 *Description and motivation*

Multicarrier communications systems have been proposed to be used for cognitive radio systems due to its flexibility in resource allocation among users. Orthogonal frequency division multiplexing (OFDM) has been widely applied in modern broadband systems to provide high data rate service. However, the large frequency sidelobes of OFDM signal result in inter-band interference to the adjacent primary users when synchronization is not guaranteed [2]. Moreover, the insertion of the cyclic prefix (CP) in each OFDM symbol decreases the system spectral efficiency. To overcome the limitations, the attention is drawn toward the filter bank multicarrier (FBMC) techniques. The FBMC technique does not require any CP and has reduced sidelobes and thus less inter-band interference. Therefore, the FBMC system is more spectrally efficient and thus might be more suitable for critical communications such as public safety applications.

Relaying techniques have been invented to extend the coverage of wireless networks. Compared to one-way relaying schemes, two-way relaying schemes provide better spectral efficiency since two nodes exchange information simultaneously through an intermediate relay node in two time slots. Nevertheless, due to the simultaneous access of the wireless medium in two-way relaying systems, the self-interference is inevitable. To mitigate the harmful effects of the self-interference, physical layer network coding (PLNC) schemes are deployed when decode-and-forward relaying strategy is used. In Section 3.1 of D7.1 we study the power allocation problem for a FBMC based two-way DF system in order to maximize the exchange rate assuming that a perfect PLNC scheme is available. In practice, perfect PLNC scheme is not known yet. Moreover, the practical XOR codes based PLNC is far from perfection. That is saying, the decoding and encoding method at the relay might significantly affect the achievable spectral efficiency. Inspired by [18] we develop a joint channel decoding and PLNC algorithm at the relay in this work.

4.2 *System description*

Let us briefly review the considered system model, which is also described in D7.1. We study a 3-node two-way DF relaying system, where two hand-held terminals (HHTs) HHT_1 and HHT_2 exchange information via an intermediate relay node. Each node is equipped with a single antenna and operates in half-duplex mode. FBMC/OQAM is chosen as the multi-carrier technique and the available bandwidth is divided into M subcarriers. Moreover, the channels are block fading and perfect synchronization is assumed. A complete communication takes two time slots. It is assumed that both HHTs apply the same signal

processing procedure during a complete transmission. In the first slot, as depicted in Figure 4-1, both HHTs transmit to the relay. We take HHT_1 as an example. After passing through a multi-tap pre-equalizer $a_{1,m}[k]$ on each subcarrier and a prototype low-pass filter $p[n]$, i.e., the synthesis filter bank (SFB) [2], the filtered transmitted FBMC/OQAM symbol at HHT_1 can be written as [3]

$$s_1[n] = \sum_{m=0}^{M-1} \sum_{k=-\infty}^{+\infty} \sqrt{P_{1,m}[k]} \left(\left(d_{1,m}[k] \beta_{1,m}[k] \right) * a_{1,m}^*[k] \right) \cdot p\left[n - k\frac{M}{2} \right] e^{j\frac{2\pi}{M} m \left(n - \frac{L-1}{2} \right)}, \tag{4-1}$$

where $d_{1,m}[k]$ denotes the real symbols drawn from a PAM constellation and $\beta_{1,m}[k] = \theta_{1,m}[k] e^{-j\pi km}$ is used for generating the OQAM symbols, where $\theta_{1,m}[k] = 1$ if $(m+k)$ is even and $\theta_{1,m}[k] = j$ if $(m+k)$ is odd. The energy of the prototype low-pass filter is normalized such that $\sum_{n=-\infty}^{+\infty} |p[n]|^2 = 1$ and L represents the pulse length [3]. The transmit power constraint at the HHT_1 has to be fulfilled such that $\sum_{m=1}^{M} P_{1,m}[k] \leq P_{1,max}$.

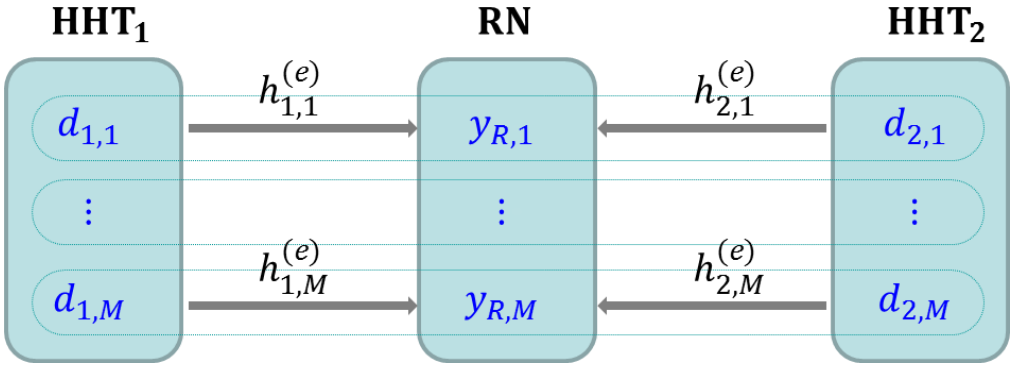

Figure 4-1: Multiple access channel phase. RN: relay node.

Let $h_{1,R}[n]$ and $h_{2,R}[n]$ denote the channel impulse response (CIR) from HHT_1 to the relay and the CIR from HHT_2 to the relay, respectively. The received signal at the relay is given by

$$r[n] = h_{1,R}[n] * s_1[n] + h_{2,R}[n] * s_2[n] + n_R[n], \tag{4-2}$$

where $s_2[n]$ is the transmitted signal from HHT_2 and has the same form as (4-1) by changing the index from 1 to 2. The term $n_R[n]$ denotes the zero-mean circularly symmetric complex Gaussian (ZMCSCG) noise. The relay uses a DF relaying strategy and thus it demodulates and decodes the received signal. We assume that the demodulation is performed by feeding the signal to the analysis filter bank (AFB) similarly as in [2], i.e., a bank of matched filters. The demodulated complex data on the q-th subcarrier at the k-th time instant at the relay is then expressed as [2]

$$\tilde{r}_q[k] = \sum_{m=q-1}^{q+1} \sum_{i=1}^{2} \sqrt{P_{i,m}[k]} \left(\left(d_{i,m}[k] \beta_{i,m}[k] \right) * a_{i,m}^*[k] \right) * g_{i,q,m}[k] + \tilde{n}_{R,q}[k], \tag{4-3}$$

where $g_{i,q,m}[k] = \left(f_m[k] * h_{i,R}[k] * f_q^*[-k]\right)_{\downarrow\frac{M}{2}}$ and $\tilde{n}_{R,q}[k] = \left(n_{R,q}[k] * f_q^*[-k]\right)_{\downarrow\frac{M}{2}}$, where $(\cdot)_{\downarrow\frac{M}{2}}$ represents the down sampling by a factor $\frac{M}{2}$ and $\tilde{n}_{R,q}[k]$ is the per-subcarrier ZMCSCG noise with zero mean and variance σ_R^2. Clearly, equation (4-3) implies only a single-tap real-valued equalizer is used at the relay, i.e., only power allocation is considered at the relay. This is similarly as in [2]. The estimated PAM symbols are then given by $\hat{r}_q[k] = \Re\{\theta_q^*[k]\tilde{r}_q[k]\}$. Following similar steps as in [2], $\tilde{r}_q[k]$ can be written in a matrix-vector form as

$$\hat{r}_q[k] = \sum_{m=q-1}^{q+1} \left(\sqrt{P_{1,m}[k]}\boldsymbol{a}_{1,m}^{\mathrm{T}}\boldsymbol{G}_{1,q,m}[k]\boldsymbol{d}_{1,m}[k] + \sqrt{P_{2,m}[k]}\boldsymbol{a}_{2,m}^{\mathrm{T}}\boldsymbol{G}_{2,q,m}[k]\boldsymbol{d}_{2,m}[k] \right) + \Re\{\theta_q^*[k]\tilde{n}_{R,q}[k]\}, \quad (4\text{-}4)$$

where $\boldsymbol{a}_{i,m} = \left[\Re\{\bar{\boldsymbol{a}}_{i,m}\}^{\mathrm{T}} \quad \Im\{\bar{\boldsymbol{a}}_{i,m}\}^{\mathrm{T}}\right]^{\mathrm{T}}$ and $\bar{\boldsymbol{a}}_{i,m} = [a_{i,m}[-L_{a_2}] \quad \cdots \quad a_{i,m}[L_{a_1}]]^{\mathrm{T}} \in \mathbb{C}^{1+L_{a_1}+L_{a_2}}$ for $i = 1,2$. Moreover, we assume that $L_{a_1} = L_{a_2} = L_a$. The matrix $\boldsymbol{G}_{i,q,m}[k]$ is defined in the same way as in [2]. The vector $\boldsymbol{d}_{i,m}[k]$ is defined as $\boldsymbol{d}_{i,m}[k] = [d_{i,m}[k + L_{a_2} + L_{g_2}] \quad \cdots \quad d_{i,m}[k - L_{a_1} - L_{g_1}]]^{\mathrm{T}}$, where L_{g_1} and L_{g_2} depend on the excess delay of the channel impulse response and the overlapping factor of the prototype filter [2] and $i = 1,2$. The pre-equalizer $\boldsymbol{a}_{i,m}$ is designed such that the signal to leakage plus noise ratio (SLNR) is maximized. Then the relay decodes the information from both HHTs and re-encodes and broadcasts it to both HHTs, as depicted in Figure 4-2. Again, the transmitted data is FBMC/OQAM modulated and is expressed as

$$r[n] = \sum_{m=0}^{M-1} \sum_{k=-\infty}^{+\infty} \sqrt{P_{R,m}[k]} d_{R,m}[k]\beta_{R,m}[k] \cdot p\left[n - k\frac{M}{2}\right] e^{j\frac{2\pi}{M}m\left(n-\frac{L-1}{2}\right)}, \quad (4\text{-}5)$$

where $d_{R,m}[k]$ denotes the real valued PAM symbols transmitted from the relay. Note that the relay applies only a single-tap pre-equalizer per subcarrier. The transmit power constraint at the relay has to be fulfilled such that $\sum_{m=1}^{M} P_{R,m}[k] \leq P_{R,max}$.

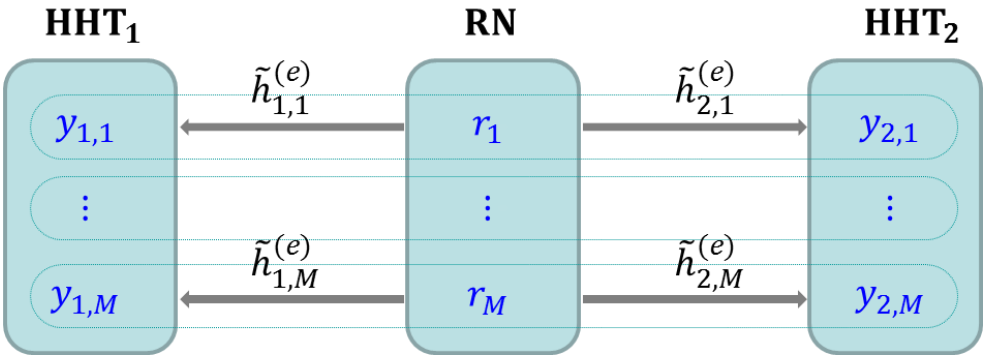

Figure 4-2: Broadcasting channel (BC) phase. RN: relay node.

Define the CIR from the relay to HHT_1 and to HHT_2 as $h_{R,1}[n]$ and $h_{R,2}[n]$, respectively. At the receiver side, each HHT performs a similar demodulation procedure as the relay. The difference is that multi-tap equalizer is applied to each subcarrier of each HHT. We take a

short cut by directly writing the estimated symbols in a matrix-vector form. The estimated PAM symbols can be expressed as

$$\hat{r}_{i,q}[k] = \sum_{m=q-1}^{q+1} \sqrt{P_{R,m}[k]}\boldsymbol{b}_{i,m}^{\mathrm{T}}\overline{\boldsymbol{G}}_{i,q,m}[k]\boldsymbol{d}_{R,m}[k] + \Re\{\tilde{n}_{i,q}[k]\}, \tag{4-6}$$

where $\tilde{n}_{i,q}[k] = \left(n_{i,q}[k] * b_q^*[k] * f_q^*[-k]\right)_{\downarrow\frac{M}{2}}$ with $\tilde{n}_{i,q}[k]$ represents the ZMCSCG noise with zero mean and variance σ_i^2, and where $\boldsymbol{b}_{i,m} = \left[\Re\{\overline{\boldsymbol{b}}_{i,m}\}^{\mathrm{T}} \quad \Im\{\overline{\boldsymbol{b}}_{i,m}\}^{\mathrm{T}}\right]^{\mathrm{T}}$ and $\overline{\boldsymbol{b}}_{i,m} = [b_{i,m}[-L_{b_2}] \quad \cdots \quad b_{i,m}[L_{b_1}]]^{\mathrm{T}} \in \mathbb{C}^{1+L_{b_1}+L_{b_2}}$ for $i = 1,2$. Moreover, we assume that $L_{b_1} = L_{b_2} = L_b$. The matrix $\overline{\boldsymbol{G}}_{i,q,m}[k]$ is defined in the same manner as in [2]. Again, the vector $\boldsymbol{d}_{R,m}[k]$ is defined as $\boldsymbol{d}_{R,m}[k] = [d_{R,m}[k + L_{b_2} + L_{\bar{g}_2}] \quad \cdots \quad d_{R,m}[k - L_{b_1} - L_{\bar{g}_1}]]^{\mathrm{T}}$, where $L_{\bar{g}_1}$ and $L_{\bar{g}_2}$ depend on the excess delay of the channel impulse response and the overlapping factor of the prototype filter [2]. The multi-tap equalizer at each subcarrier is designed such that the signal-to-interference-plus-noise ratio is maximized. Finally, a complete per-subband received data model is given by

$$y_{R,m} = h_{1,m}^{(e)} d_{1,m} + h_{2,m}^{(e)} d_{2,m} + Z_{R,m}, \tag{4-7}$$

$$y_{1,m} = \tilde{h}_{1,m}^{(e)} r_m + Z_{1,m}, \tag{4-8}$$

$$y_{2,m} = \tilde{h}_{2,m}^{(e)} r_m + Z_{2,m}, \tag{4-9}$$

where $h_{1,m}^{(e)}$, $h_{2,m}^{(e)}$, $\tilde{h}_{1,m}^{(e)}$, and $\tilde{h}_{2,m}^{(e)}$ are the equivalent channel coefficients on the m-th subband, which are defined in Section 3.1 of D7.1. Similarly, the interference plus noise terms $Z_{R,m}$, $Z_{1,m}$, and $Z_{2,m}$ are also defined in Section 3.1 of D7.1.

For practical implementation of a DF two-way relaying scheme, a physical layer network coding (PLNC) scheme at the relay is required. It will be used to decode the desired signal from the received signal at the HHTs, which is a mixture of the desired signal and the self-interference. In Section 3.1 of D7.1 we assume that an optimal PLNC scheme [17] is used and then an upper bound of the achievable rate of the system is derived using the information-theoretic analysis. The goal is then to develop optimal power allocation schemes such that the achievable rate is maximized. In practice, the perfect network coding scheme which maximizes the throughput of the system is unknown. Practical network coding schemes, such as the XOR code and the superposition code, are far from optimal. Therefore, the decoding and re-encoding strategy at the relay will has a strong impact on the throughput of the system. Given the XOR code is applied, our goal is to design practical decoding strategy at the relay.

4.3 *Decoding schemes at the relay*

Let $\boldsymbol{u}_i \in \mathrm{F}_2^L$ represent binary information words of length L from the i-th HHT. Both HHTs use the same linear channel code with code rate $R_c = L/N$ such that we can write the codeword of length N of the i-th HHT as $\boldsymbol{c}_i = \overline{\boldsymbol{G}}\boldsymbol{u}_i \in \mathrm{F}_2^N$, where $\overline{\boldsymbol{G}} \in \mathrm{F}_2^{N\times L}$ is the generator matrix. This formulation holds for any linear block code, e.g., the LDPC codes and the turbo codes. In our work, we consider the LDPC codes. In a multicarrier system, in our case the FBMC system, the source codewords are then interleaved, modulated, and then mapped to

different subbands of the system via serial to parallel operation [4]. That is saying, one codeword might be mapped to several FBMC symbols. In our case, the modulated symbols on the m-th subband at the k-th time slot of the i-th HHT is denoted by $d_{i,m}[k]$. After the signal is received at the relay, the relay should detect and demodulate the received symbols and then perform the channel decoding to estimate $\boldsymbol{u}_1$ and $\boldsymbol{u}_2$. Then an XOR coding is performed such that an XOR coded information is obtained as $\boldsymbol{u}_{\mathrm{R}} = \boldsymbol{u}_1 \oplus \boldsymbol{u}_2$. Then the information word $\boldsymbol{u}_{\mathrm{R}}$ is encoded using the same linear channel code and a codeword $\boldsymbol{c}_{\mathrm{R}}$ is obtained. Finally, the multicarrier modulation is performed and the re-encoded symbols are transmitted. During the BC phase, each HHT decodes the desired message using the property of the XOR code, i.e., by simple XOR the estimated binary information $\widehat{\boldsymbol{u}}_{\mathrm{R}}$ with its own transmitted information $\boldsymbol{u}_i$ as $\boldsymbol{u}_{3-\mathrm{i}} = \widehat{\boldsymbol{u}}_{\mathrm{R}} \oplus \boldsymbol{u}_i$. Before we discuss the possible decoding schemes for $\boldsymbol{y}_{\mathrm{R}} \rightarrow \boldsymbol{u}_{\mathrm{R}}$, it is worth pointing out that the sum of the two codewords is also a valid codeword $\boldsymbol{c}_{\mathrm{R}} = \boldsymbol{c}_1 \oplus \boldsymbol{c}_2 = \overline{\boldsymbol{G}}(\boldsymbol{u}_1 \oplus \boldsymbol{u}_2)$. This is the consequence of using the same linear code at both HHTs. If we drop the index for the number of FBMC symbols, the per-subband mapping rules for the code bits and modulated symbols are then given by the following table, where 2-PAM modulation is considered (corresponds to OQPSK).

j	$\boldsymbol{c}_{1,m}$	$\boldsymbol{c}_{2,m}$	$\boldsymbol{c}_{R,m}$	$\boldsymbol{d}_{1,m}$	$\boldsymbol{d}_{2,m}$	$\widehat{\boldsymbol{y}}_{R,m}$
1	0	0	0	-1	-1	$-h_{1,m}^{(e)} - h_{2,m}^{(e)}$
2	0	1	1	-1	1	$-h_{1,m}^{(e)} + h_{2,m}^{(e)}$
3	1	0	1	1	-1	$h_{1,m}^{(e)} - h_{2,m}^{(e)}$
4	1	1	0	1	1	$h_{1,m}^{(e)} + h_{2,m}^{(e)}$

Table 4-1: mapping rules for 2-PAM modulation, $\hat{y}_{R,m}$ is the noise free version of $y_{R,m}$

Moreover, the soft-in decoder, which makes use of the log-likelihood ratios (LLRs), and the sum product algorithm (SPA) is used for decoding the LDPC codes. To calculate the LLR, the the a-posteriori probability (APP) is required. Similarly as in [18], the a-priori probabilities of each realization of $c_{R,m}$ and $\hat{y}_{R,m}$ are assumed to be equal, which is thus ¼. The probability density function (PDF) of the received signal $y_{R,m}$, given that $Z_{R,m}$ is a real valued Gaussian random variable with variance $\frac{\sigma_R^2}{2} + I^2$, is then computed as

$$P\{y_{R,m} | \hat{y}_{R,m} = \hat{y}_{R,m}(j)\} = \frac{1}{\sqrt{\pi(\sigma_R^2 + 2I^2)}} e^{-\frac{|y_{R,m} - \hat{y}_{R,m}(j)|^2}{\sigma_R^2 + 2I^2}}. \quad (4\text{-}10)$$

where $j = 1, \cdots, 4$ and I^2 is the interference power. Then the a-posteriori probability (APP) that the signal $c_{R,m}$ was transmitted given the received signal $y_{R,m}$ is calculated by

$$P\{c_{R,m} = c_{R,m}(j) | y_{R,m}\} = P\{\hat{y}_{R,m} = \hat{y}_{R,m}(j) | y_{R,m}\} \quad (4\text{-}11)$$

$$= P\{y_{R,m}|\hat{y}_{R,m} = \hat{y}_{R,m}(j)\}\frac{P\{\hat{y}_{R,m} = \hat{y}_{R,m}(j)\}}{P\{y_{R,m}\}}$$
$$= P\{y_{R,m}|\hat{y}_{R,m} = \hat{y}_{R,m}(j)\}\frac{1}{4}.$$

4.3.1 **Separated channel decoding and physical layer network coding**

According to our previous discussion, a straightforward decoding strategy is to decode the messages from each HHT separately and then perform the XOR coding the channel coding.

Take HHT_1 as an example, we propose to calculate the LLRs per subband, i.e., the LLR $\lambda_{i,m}$ on the m-th subband of the relay is defined as

$$\lambda_{i,m} = \ln\frac{P\{c_{i,m} = 1|y_{R,m}\}}{P\{c_{i,m} = 0|y_{R,m}\}}. \quad (4\text{-}12)$$

According to the mapping table and (11), the APP $P\{c_{i,m} = 0|y_{R,m}\}$ is calculated by

$$P\{c_{i,m} = 0|y_{R,m}\} = P\{c_{R,m} = c_{R,m}(1)|y_{R,m}\} + P\{c_{R,m} = c_{R,m}(2)|y_{R,m}\}. \quad (4\text{-}13)$$

Similarly, the APP $P\{c_{i,m} = 1|y_{R,m}\}$ can be calculated. This procedure can be interpreted as the traditional multiple access problem and thus is a separate decoding scheme. Since only a single antenna is used, there is no additional spatial dimension available, which can be used to distinguish $c_{1,m}$ and $c_{2,m}$ from their sum. Finally, the LLR values will be fed into the SPA based channel decoder. The decoded information will be then XOR coded and re-encoded before the transmission.

4.3.2 **Joint channel decoding and physical layer network coding via binary decoding**

However, since the relay is only interested in the combined signal u_{R}, a more efficient approach is to derive the LLRs with respect to the combined codeword $c_{R,m}$, instead of decoding $c_{1,m}$ and $c_{2,m}$ independently [16]. Therefore, we calculate the APP $P\{c_{R,m} = 0|y_{R,m}\}$ as

$$\begin{aligned} P\{c_{R,m} = 0|y_{R,m}\} &= P\{c_{R,m} = c_{R,m}(1)|y_{R,m}\} + P\{c_{R,m} = c_{R,m}(4)|y_{R,m}\} \\ &= P\{y_{R,m}|\hat{y}_{R,m} = \hat{y}_{R,m}(1)\}\frac{1}{4} + P\{y_{R,m}|\hat{y}_{R,m} = \hat{y}_{R,m}(4)\}\frac{1}{4} \\ &= \frac{1}{4\sqrt{\pi(\sigma_R^2 + 2I^2)}}\left(e^{-\frac{|y_{R,m}-\hat{y}_{R,m}(1)|^2}{\sigma_R^2}} + e^{-\frac{|y_{R,m}-\hat{y}_{R,m}(1)|^2}{\sigma_R^2+2I^2}}\right) \end{aligned} \quad (4\text{-}14)$$

The similar approach can be applied to obtain the APP $P\{c_{R,m} = 1|y_{R,m}\}$. Afterwards, the final LLR values for each subband is decided by

$$\lambda_{R,m} = \ln \frac{P\{c_{R,m} = 1 | y_{R,m}\}}{P\{c_{R,m} = 0 | y_{R,m}\}}. \quad (4\text{-}15)$$

These LLR values are fed to the soft-in decoder, which finds an estimate for $\boldsymbol{u}_{\mathrm{R}}$. This method directly decodes the desired message $\boldsymbol{u}_{\mathrm{R}}$ without decoding the messages individually compared to the scheme. Therefore, it is a joint channel decoding and physical layer network coding method. It can be seen as the extension of the algorithm in [18] to a multicarrier system. Note that when compared to an OFDM extension the FBMC extension suffers also from the residual interference terms, which are simply treated as additional additive noise in our work.

In the case of OFDM the received signal at the relay is given by

$$y_{R,m} = H_{1,m} d_{1,m} + H_{2,m} d_{2,m} + n_{R,m}, \quad (4\text{-}16)$$

where $H_{i,m}$represents the channel gain in frequency domain, and $n_{R,m}$ denotes the additive noise at the relay. The PDF of $y_{R,m}$, given that $n_{R,m}$ is ZMCSCG with variance σ_R^2, can be written as

$$P\{y_{R,m} | \hat{y}_{R,m} = \hat{y}_{R,m}(j)\} = \frac{1}{\pi \sigma_R^2} e^{-\frac{|y_{R,m} - \hat{y}_{R,m}(j)|^2}{\sigma_R^2}}. \quad (4\text{-}17)$$

The following table summarizes the per-subband mapping for QPSK modulation, where the two bits represented by the QPSK symbols is written as $c_{i,m}^{(1)}\, c_{i,m}^{(2)}$ and the QPSK symbols are given by $s_l = e^{-j(\frac{2\pi l}{4} + \frac{\pi}{4})}, l = 0,1,2,3.$

j	$\boldsymbol{c_{1,m}^{(1)}\ c_{1,m}^{(2)}}$	$\boldsymbol{c_{2,m}^{(1)}\ c_{2,m}^{(2)}}$	$\boldsymbol{c_{R,m}^{(1)}\ c_{R,m}^{(2)}}$	$\boldsymbol{d_{1,m}}$	$\boldsymbol{d_{2,m}}$	$\boldsymbol{\hat{y}_{R,m}}$
1	1 1	1 1	0 0	s_0	s_0	$s_0 H_{1,m} + s_0 H_{2,m}$
2	1 1	0 1	1 0	s_0	s_1	$s_0 H_{1,m} + s_1 H_{2,m}$
3	1 1	0 0	1 1	s_0	s_2	$s_0 H_{1,m} + s_2 H_{2,m}$
4	1 1	1 0	0 1	s_0	s_3	$s_0 H_{1,m} + s_3 H_{2,m}$
5	0 1	1 1	1 0	s_1	s_0	$s_1 H_{1,m} + s_0 H_{2,m}$
6	0 1	0 1	0 0	s_1	s_1	$s_1 H_{1,m} + s_1 H_{2,m}$
7	0 1	0 0	0 1	s_1	s_2	$s_1 H_{1,m} + s_2 H_{2,m}$
8	0 1	1 0	1 1	s_1	s_3	$s_1 H_{1,m} + s_3 H_{2,m}$
9	0 0	1 1	1 1	s_2	s_0	$s_2 H_{1,m} + s_0 H_{2,m}$

10	0 0	0 1	0 1	s_2	s_1	$s_2H_{1,m} + s_1H_{2,m}$
11	0 0	0 0	0 0	s_2	s_2	$s_2H_{1,m} + s_2H_{2,m}$
12	0 0	1 0	1 0	s_2	s_3	$s_2H_{1,m} + s_3H_{2,m}$
13	1 0	1 1	0 1	s_3	s_0	$s_3H_{1,m} + s_0H_{2,m}$
14	1 0	0 1	1 1	s_3	s_1	$s_3H_{1,m} + s_1H_{2,m}$
15	1 0	0 0	1 0	s_3	s_2	$s_3H_{1,m} + s_2H_{2,m}$
16	1 0	1 0	0 0	s_3	s_3	$s_3H_{1,m} + s_3H_{2,m}$

Table 4-2: mapping rules for QPSK modulation,
$\hat{y}_{R,m}$ is the noise free version of $y_{R,m}$

$$P\left\{c_{R,m}^{(i)} = 0 \middle| y_{R,m}\right\} = \sum_{j \in \mu^{(i)}} P\left\{c_{R,m} = c_{R,m}(j) \middle| y_{R,m}\right\} = \frac{1}{16\,\pi\sigma_R^2} \sum_{j \in \mu^{(1)}} e^{-\frac{\left|y_{R,m} - \hat{y}_{R,m}(j)\right|^2}{\sigma_R^2}}, \quad (4\text{-}18)$$

where $\mu^{(1)} = \{1, 4, 6, 7, 10, 11, 14, 10\}$ and $\mu^{(2)} = \{1, 2, 5, 6, 11, 12, 15, 10\}$. $P\left\{c_{R,m}^{(i)} = 1 \middle| y_{R,m}\right\}$ can be calculated from the complement indexes. Then the LLR values of the bits are fed to the soft-in decoder.

4.4 *Simulation settings*

The data is generated according to the equivalent model which is defined in (7 - 9). In all the Monte-Carlo simulations, the number of subcarriers is fixed to 128 with sampling frequency $F_s = 1.92$ MHz. The ITU-Vehicular A and B channel models are considered, and the frequency domain channel gains for OFDM are generated using M-FFT. The equalizer (pre-equalizer) has $L_{a_1} = L_{a_2}$ $(L_{b_1} = L_{b_2})$ and the number of taps is fixed to $L_a = L_b = 7$. The nodes employ DVB-S2 LDPC channel coding of rate $\frac{1}{2}$ and a codeword length of 64800 bits. QPSK modulation scheme is employed for OFDM system, which is equivalent to using BPSK scheme for FBMC system. The maximum allowed power P_T is equal to 1W for all nodes and it is distributed uniformly. The noise variance is identical and equal to σ^2 at all nodes, and the average SNR is defined as $\frac{P_T/N}{\sigma^2}$.

Frame structure	
Sampling frequency	1.92 MHz
Subcarriers number	128
OFDM CP	6.67% Symbol period

FBMC filter	OFDM/OQAM PHYDYAS
Overlapping factor	4
Modulation scheme	QPSK/BPSK
Channel coding	LDPC for DVB-S2, ½ code rate, L = 32400 bits
Transmitter/Receiver	
Noise power spectral density	Various
Equalizer length	7
Pre-equalizer length	7
Transmission scheme	SISO
Propagation	
Fast fading channel models	ITU-Vehicular A, B
Channel estimation	Ideal

Table 4-3: Simulation settings for FBMC based two-way relaying strategies.

4.5 *Simulation results*

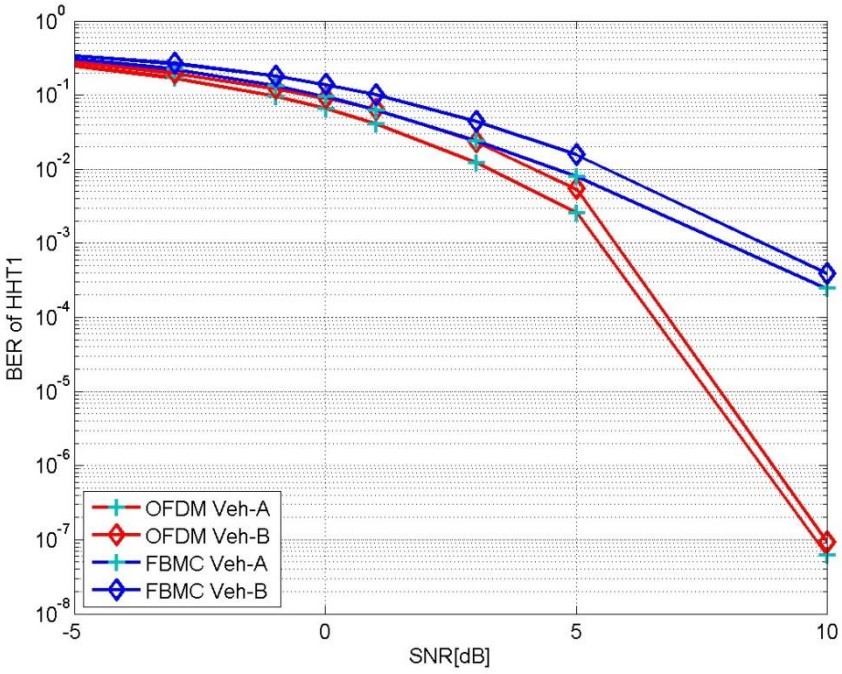

Figure 4-3: BER of HHT1. Joint decoding scheme in Section 3.3.1 is used.

Figure 4-3 and Figure 4-4 illustrate the BER of HHT1 and HHT2 in both OFDM and FBMC systems for ITU-Vehicular A and B channel models, respectively. As can be seen from the figures, in general the FBMC based system suffer from the residual interference. When the channel is less frequency selective, the FBMC based system is better than the OFDM based system.

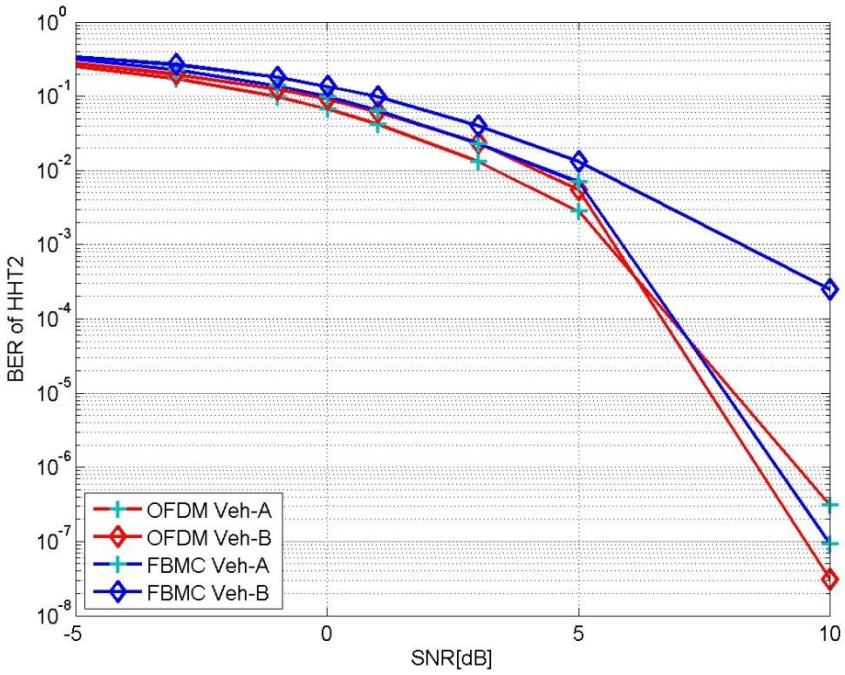

Figure 4-4: BER of HHT2. Joint decoding scheme in Section 3.3.2 is used.

4.6 *Final remarks*

We have evaluated the BER performance of OFDM and FBMC based two-way DF relaying systems. A joint channel decoding and XOR based PLNC scheme is developed. Simulation results show that the FBMC based system suffers from the residual interference in the system especially when the channel has a high frequency selectivity.

5. **Multi-hop relaying for FBMC using SONIR**

5.1 ***Description and motivation***

SONIR (Self-Organizing Network with Intelligent Relaying) it is a software platform for simulating and visualizing de-centralized and self-organized networks. It is built in MATLAB and its purpose is to implement an end-to-end multi-hop system capable for dealing with mobility of nodes. Different methods for clustering, mobility management, routing have been implemented in order to be able to visualize the multi-hop system and to investigate its end-to-end performance. SONIR was initially built to deal with the nodes in a Rayleigh fading environment, but within the scope of this project we provide an extension to frequency selective fading, and FBMC.

Moreover, a useful GUI [21] to go along with the software has been developed for a better visualisation and more practical usage of the platform even for uses that are not very familiar with MATLAB.

SONIR environment

The SONIR environment represents a field, for which the user can choose various values for its size. In general the field is three dimensional, and length, width, and height can be chosen. However the visualization is provided only for 2 dimensions. Also, different number of nodes could be chosen, as well as the distribution of the nodes. Currently, uniform and Poisson distribution of the nodes are supported.

In Figure 5-1 is presented the SONIR environment, with 200 m length, 200 m width and 350 uniformly distributed nodes.

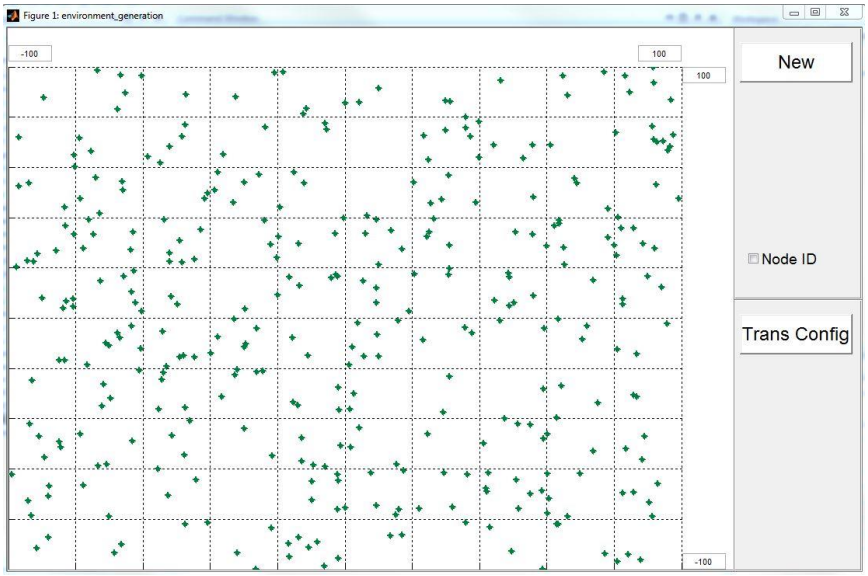

Figure 5-1: SONIR environment

Clustering

As a first step of the data transmission, clusters should be formed. The clustering of the nodes can be done based on two clustering schemes, RSSI (Received Signal Strength

Indicator) [19] and GPS based scheme [20]. When RSSI based clustering is used, the clusters are formed depending on the received power at each of the nodes. On the other hand, the main idea of GPS based clustering is to calculate the distances between the nodes from their GPS positions. Depending on the given thresholds the nodes that are fairly close to each other will belong in one cluster. Moreover, one of the nodes in the cluster is chosen as a cluster-head and it is responsible for routing the data through the cluster.

In our SONIR platform, for the RSSI clustering scheme a maximum BER can be chosen, and for the GPS clustering scheme different maximum distance can be chosen. These criteria represent also the thresholds for the clustering decisions.

In Figure 5-2 the clustered network is presented, where the clusters have been formed with the RSSI clustering scheme with maximum BER=10^{-6}.

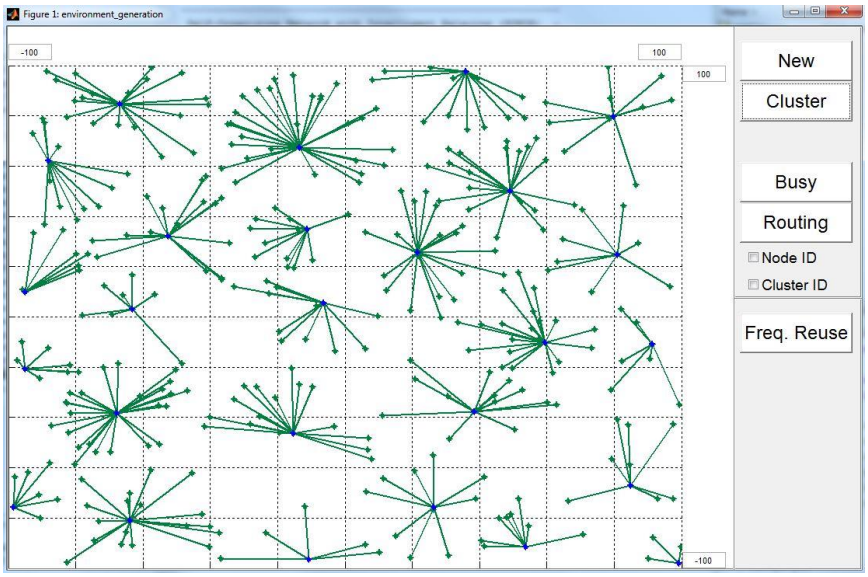

Figure 5-2 Clustered network

Routing

Moreover, the routing in the SONIR network should be performed, and for that reason a sender and a receiver node should be selected by the user. The routing is based on AODV (Ad-hoc On-demand Distance Vector). In our software the cluster-heads are responsible for most of the routing functions. The cluster-heads keep information for all the nodes in its cluster, as well as information for the neighboring clusters. The routing information is obtained via piloting mechanisms.

When a node tries to communicate with another node, it sends the receiver and sender node ID to its cluster head, which then looks first in its own set of nodes to find the receiver node. If successful it acts as a relay between the two, otherwise it asks its neighbouring cluster heads to find the receiving node. If not found there, these cluster heads in turn ask their neighbours and so on until we find the reception node and then the most optimal path back to the sender node is decided.

In Figure 5-3 an example of the calculated path is visualized, where the sender node is node 4, while the receiver node is node 7.

Mobility management

Furthermore the SONIR platform supports mobility of the nodes. The mobility is based on the random walk model, and the user can choose the speed of the nodes. The direction in which each of the nodes will move is chosen randomly.

With the mobility option in SONIR we can investigate how periodic re-clustering has to be performed. We can also monitor the required time the network to reach certain QoS (Quality of Service), for instance cumulative BER value.

In Figure 5-4 an example of the change in cluster formation before and after re-clustering along how the BER changes depending on the distance or RSSI parameters chosen in the clustering part, for GPS based and RSSI based clustering, respectively.

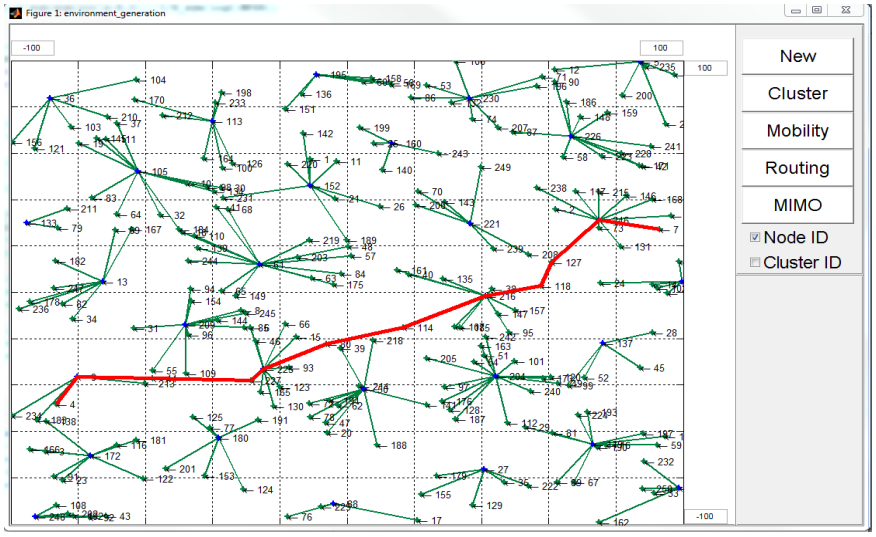

Figure 5-3 Routing

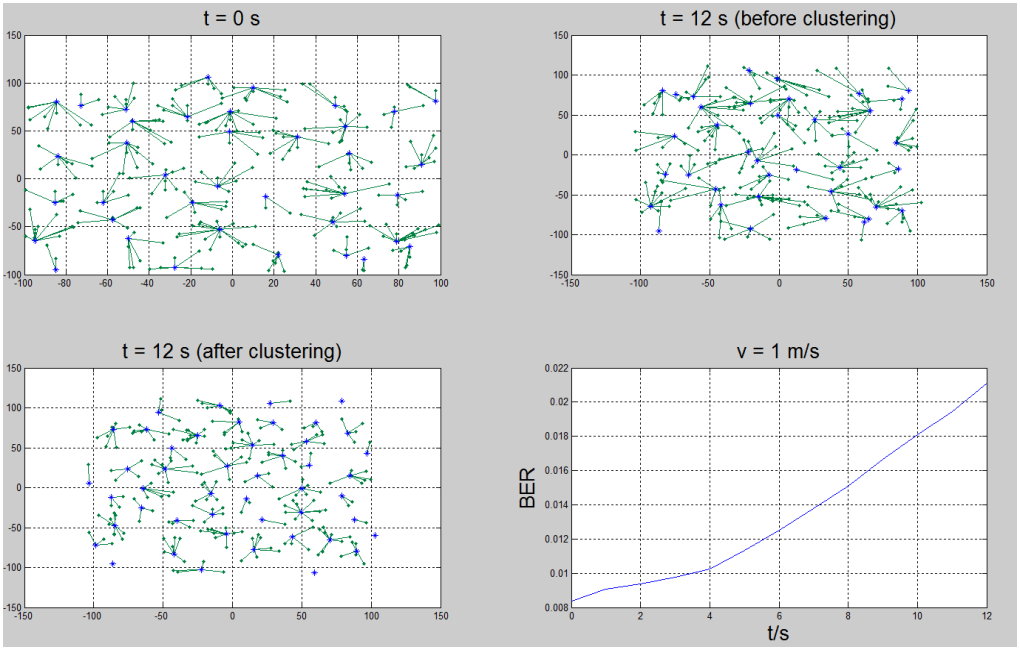

Figure 5-4 Optimal re-clustering time based on a chosen criteria

As previously mentioned our goal was to implement FBMC transmission technique into the SONIR platform, and for that we have modified the physical layer. For now, we have implemented FBMC only for the data transmission phase. This means that all piloting data which is used from clustering and routing has been transmitted. Therefore, the clustering and routing has already been performed. By this point we know the route through which data transmission between the sender and receiver node will be done.

For the transmission phase, that takes place between each of the nodes on the route we assume that we have multicarrier communication with *M* subcarriers, with overlapping factor *K*. Moreover, we assume that *N* symbols are transmitted, and they are modulated using OQAM as a modulation scheme. The parallel to serial convergence of the symbols is done with synthesis filter, FBMC filter with an impulse response designed as raised cosine. For the channel design we have taken into account several models, and for now we have implemented the Rayleigh flat, Rayleigh multi-tap channel, Pedestrian A channel and Vehicular A channel.

On the receiver side, accordingly analysis FBMC filter, which introduces a delay of 2K-1 symbol is used. After the filter bank for analysis the symbols are according demodulated.

Basically, we assume that each of the nodes performs the modulation and demodulation while forwarding the data to the next node, until it reaches the destination witch is the receiver node chosen by the user. This is equivalent to decode and forward relaying strategy.

In order to calculate the cumulative BER performance on the whole route, we obtain the BER performance for each hop, treating each hop as a point to point transmission. After witch we use the following formula to approximate the BER of the whole transmission:

$$BER = 1 - \prod_{i=1}^{N_{hop}} (1 - BER_i)$$

5.2 *Simulation settings*

We would like to investigate the cumulative BER performance in SONIR using FBMC. For that reason we have performed simulations with SONIR, using the following parameters. The size of the field was set to 200m of width and 200m of height in which 350 nodes are uniformly distributed. The clustering scheme used in the simulations is RSSI, and the routing was performed with node 21 as a sender, and node 232 as a receiver.

Moreover, 512 subcarriers were used with overlapping factor of 4. In the simulation results both, 4 OQAM and BPSK are used as a modulation schemes. Simulation results for Rayleigh flat channel and Pedestrian A channel are presented in the following subsection.

The simulation parameters are summarized in Table 5-1.

Frame structure	
Subcarriers number	512
Subcarrier spacing	15 kHz

FBMC filter	OFDM/OQAM PHYDYAS
Overlapping factor	4
Modulation schemes	4 OQAM, BPSK
Propagation	
Static fading channel models	Rayleigh, flat Rayleigh, multi-tap channel, Pedestrian A channel
Channel estimation	Preamble-based Least-Squares method
Path loss exponent	2
SONIR parameters	
Number of nodes and distribution	350, uniform
Clustering	RSSI
Routing	Note ID 21 to Note ID 232

Table 5-1 Simulation parameters

5.3 *Simulation results*

In this subsection we present the simulation results for cumulative BER performance, for multi-hop relaying using the SONIR platform.

In Figure 5-5 a comparison of FBMC and BPSK is illustrated, assuming data transmission over Rayleigh flat channel. From the figure can be concluded that both schemes perform fairly the same, although it is worth noting that in the FBMC scenario 4 OQAM is used as a modulation scheme.

Next the compare again the BSPK and FBMC cumulative BER performance, but this time using the Pedestrian A channel in the simulations. The simulation results are presented in Figure 5-6. According to the simulation results in this case the SISO- BPSK outperforms the SISO-FBMC.

5.4 *Final remarks*

Our goal within this project was to implement the FBMC in SONIR, in order to investigate the performance in multi-hop, de-centralized and self-organized network. Currently we have managed to implement FBMC on physical level, and to investigate the cumulative BER performance.

As a future work we would continue investigating the impact on overall throughput. Moreover, we will have to investigate the impact of using FBMC over clustering, routing and mobility schemes.

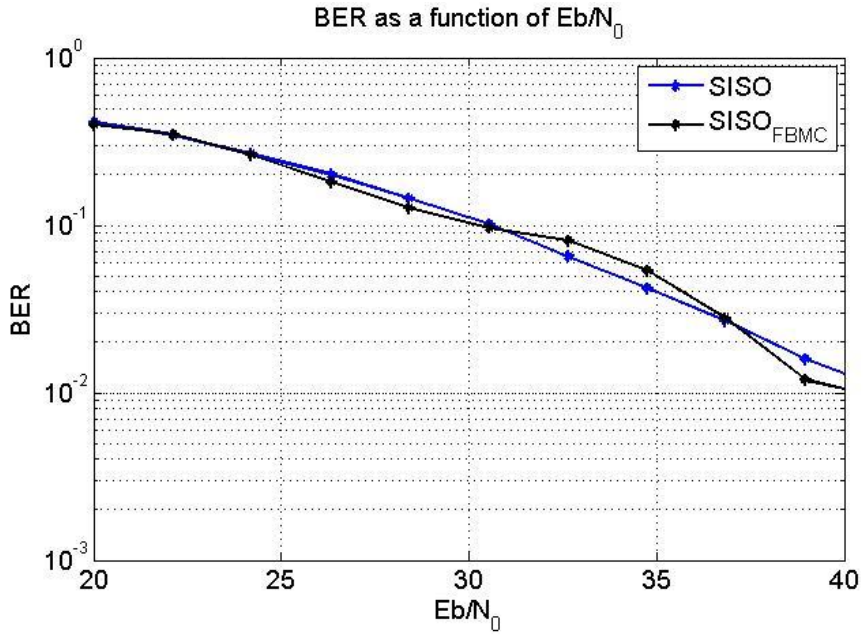

Figure 5-5 Cumulative BER performance, Rayleigh flat channel.

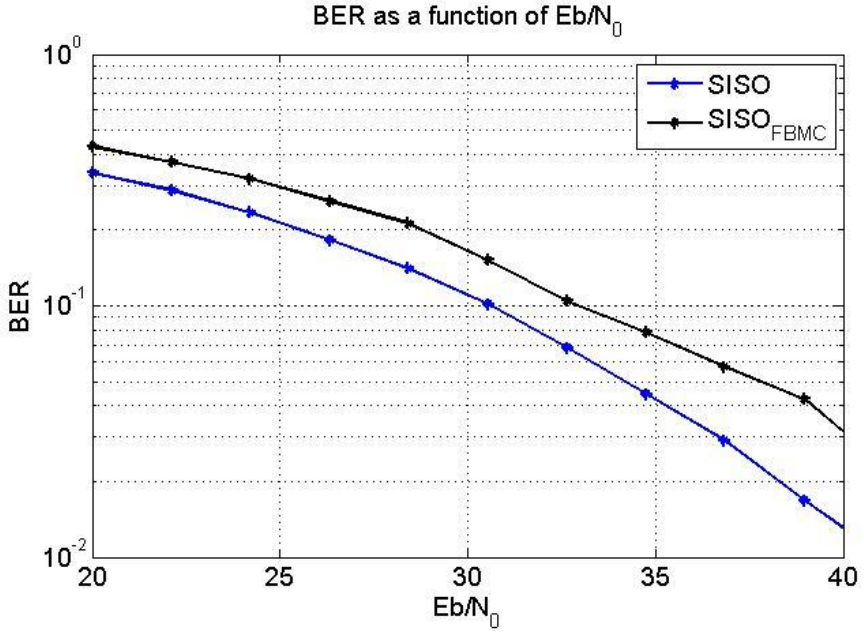

Figure 5-6 Cumulative BER performance, Pedestrian A channel.

6. **Assessment of two-way relaying for SC-FDMA using PHY layer abstraction**

6.1 ***General Description and motivation***

The goal of this section is to evaluate the end-to-end reliability and end-to-end total achievable throughput for different relaying schemes. A new adaptive relaying scheme employing Two-Way-Relaying (TWR) has been first proposed, and then, an abstraction method of the PHY Layer for SC-FDMA signals was presented.

There are quite a few results recently published which consider TWR and other relaying schemes, as well as different Key Performance Indicators (KPIs). We have first performed a selection among these relaying techniques, then we decided which the most relevant comparisons are and then which the most efficient KPIs are.

For example, in [50], a cross-layer resource allocation of TWR for statistical delay-QoS constraints is proposed. The objective of this paper is to maximize the weighted sum-rate of the TWR system while satisfying the individual delay requirement at each node.

In [51], a multi-user TWR using Alamouti space-time block code is proposed. In the first phase all users transmit their symbols simultaneously to the relay, and the relay uses minimum mean square error detection to estimate the transmitted symbols. Then, in a second phase, the relay uses XOR operation to combine the estimates of the symbols for each user pair and broadcasts them. Moreover, the relay and further each user are equipped with multi-antennas so that the relay is able to separate the signals coming from the nodes. For the system model the paper considers 2 pairs of nodes (i.e. 4 users) and evaluates the TWR maximum throughput when 2 pairs are communicating at the same time.

In [52], classic (half-duplex) Amplify-and-Forward is compared with TWR and full-duplex AF. MIMO relaying is considered with 4 antennas per each user. Finally, an adaptive scheme which combines the performance of full-duplex AF and TWR is evaluated in terms of end-to-end capacity and outage capacity. However, even if [52] evaluates the performance of such adaptive TWR and it clearly shows the interest of combining AF and TWR, details of how this scheme would function in practice are not provided.

In [53] the authors try to provide a low complexity algorithm for multiple relay selection in TWR with use for cognitive radio networks. Multiple Secondary Users (SUs) employing TWR and a Primary User (PU) are using the spectrum at the same time. The paper further studies the relay selection for SUs under the following interference constraints: 1) interference from SUs to PU has to be limited during the transmission phase; 2) interference from relay to PUs has to be limited during the broadcast phase. Then, simulation results are provided in terms of sum rate for different power quantization levels and different number of SU links.

In [54] it is presented for the first time an analytical study of average delay and throughput in a TWR network exploiting network coding to exchange user packets, where arrival and

departure of packets are considered to be stochastic. Because of the stochastic nature of packet arrivals, packets from both users are not available at the same time instants and the relay node cannot encode them at once. Three opportunistic networks coding schemes based on power-delay constraints are further proposed: power-efficient network coding, delay efficient network coding, and quasi-general network coding. Finally, the fundamental trade-off between packet delay and transmission power is addressed. Results revealed that for symmetric packet arrival rates, minimizing transmission power results in an infinite delay, a result which is somewhat expected. However, an important result is missing, which is a comparison with classical DF or AF schemes at least in terms of delay and packet error rates.

In [55] the authors provide the outage performance of cooperative protocols for the TWR model. If only one user is correctly decoded, then a successive interference cancelation (SIC) mechanism can be employed by the relay to correctly decode the data stream from the user which was not correctly decoded.

In [56] the authors applied an adaptive modulation and coding technique to enhance the performance of the TWR AF networks. The work from [56] also provides closed-form expressions of the average frame error probability and spectral efficiency.

In [57] the authors studied TWR scheme for the same system parameters as used in LTE networks, however the system architecture is now sufficiently well described nor how this scheme would be applicable to LTE networks. The paper also introduces key performance indicators and metrics such as energy consumption rate, energy reduction gain, information exchange rate, resource utilization and resource utilization gain.

With respect to all this prior work, this section focuses mainly on how to use DF techniques and how to exploit TWR when DF is used combined with XOR. We have decided not to use AF techniques because for AF there is no control over what is actually send through the channel and in certain settings noise amplification can degrade performance in particular if simple receivers are used. Moreover, with AF the complexity of the receiver processing is moved at the source/destination node side, while with DF this complexity is moved at the relay node side. The second solution is interesting when the relay node is part of the radio access network and is mounted for example on a vehicle - which has fewer constraints in terms of cost and energy budget than e.g. a user equipment. Then, after this pre-selection of the relaying techniques and after proposing an abstraction method, MAC Layer simulations were performed in order to compare these schemes. Finally, using the MAC Layer simulator, results expressed in terms of End-to-End Packet Error Rate (PER) and End-to-End Throughput were obtained. Again, compared with the above mentioned scientific papers, these selected KPIs seem to be the most adequate for the purpose of this study.

In order to evaluate the overall performances from the system point of view and MAC point of view respectively, we first describe the transmission chain from one user to another user via a relay, for two techniques: DF and TWR. These two schemes have been further detailed in Section 6.1.1. Then, Section 6.1.2 presents possible improvements of DF and TWR schemes from the data traffic point of view (see Subsection 6.1.2.1) and from the packet point of view which corresponds to MAC Layer design (see Subsection 6.1.2.2).

Further, Section 6.2 describes the selected scenarios together with the Key Performance Indicators (KPIs) and Section 6.3 describes the proposed PHY Layer abstraction method to be used further in Section 6.4 dedicated to simulation results. Moreover, Section 6.4 is divided in three important parts: Subsection 6.4.1 dedicated to simulation parameters, Subsection 6.4.2 dedicated to the validation of the PHY Layer proposed in Section 6.3, and Subsection 6.4.3 dedicated to MAC Layer simulations and results obtained with the help of the PHY Layer abstraction method. Finally, conclusions are provided in Section 6.5.

6.1.1 **Decode-and-Forward and Two-Way-Relaying**

As described on the left hand side of Figure 6-1, for Decode-and-Forward (DF) technique one slot is used by the first user to transmit towards the relay and then a second slot is used by the relay to transmit towards the second user. Between the two consecutive transmissions it is considered that the relay first decodes the information and then forwards it. In total, the first user needs 2 slots to transmit to the second user. Similarly, another two slots are used by the second user to transmit towards the first user via the same relay (see the right hand side of Figure 6-1). For this reason, DF technique uses in total 4 slots. As a result, the transmission from one user to the relay is not interfering with the transmission from the other user to the relay, or with the transmission of the relay to the other user.

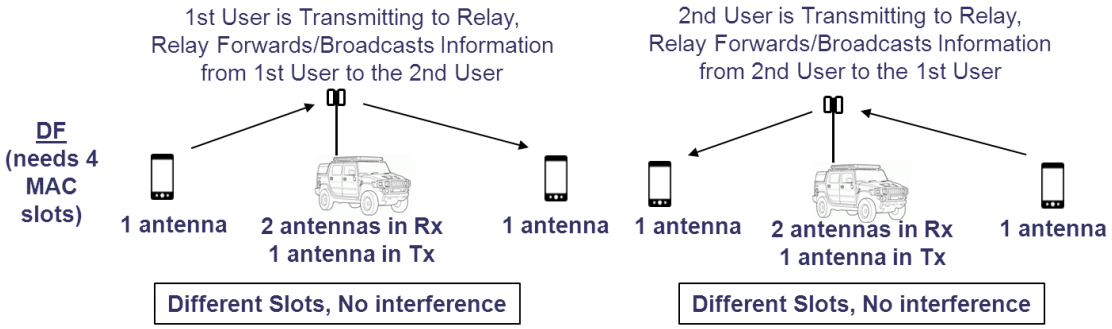

Figure 6-1. System Description of Decode-and-Forward Scheme

Moreover, as seen in Figure 6-1, it is considered that the relay uses 2 antennas in reception mode and that the users are using only a single antenna both in reception and transmission modes.

In order to increase the spectral efficiency, TWR scheme has been proposed. As described in Figure 6-2, TWR scheme uses only 2 slots instead of 4. This is possible through the use of multiple-antenna reception techniques at the relay level, in order to separate between the two users concomitantly transmitting: i.e. at the same time, on the same frequency band (e.g. using the same Resource Blocks or RBs). While the first slot is used by the users to transmit towards the relay, the second slot is used by the relay to broadcast the data to both users, after priory performing a XOR (eXclusive OR) operation on the decoded data. At the end, each end-user is able to decode information from the other user by subtracting own previously transmitted data from the information broadcasted by the relay.

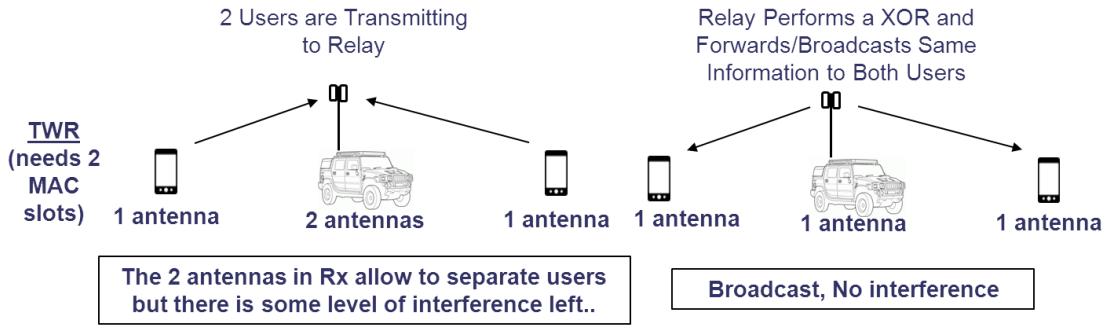

Figure 6-2. System Description of Two-Way-Relaying Scheme

If the two users are co-located, then the use of the 2 antennas in reception will not be sufficient to separate the information at the relay level. However, as described in Deliverable D7.1 by the scenario "clustered wireless ad hoc network with bridging relay", one use case of interest for EMPhAtiC project is inter-cell relaying which means that the 2 users to be relayed will always belong to different cells and therefore the data received by the relay on the two links will be separable through the use of 2 antennas is reception.
The role of the XOR operation is crucial for TWR technique since it allows retransmitting data to both users at the same time without the use of multiple antennas techniques. This would therefore simplify the transmitter since it does not need any prior channel estimation which may have been affected by user mobility, multi-user interference and fast time-variation of the channel. However, in situations when the Relay does not receive two packets at the same time on both links (e.g. because the channel of one link is in bad state, or because the packets are not synchronized, or because the delay between the received packets is too high), it cannot perform XOR operation and one of the packets or even the two packets are being dropped.

Another alternative for these two schemes provided in Figure 6-1 and Figure 6-2 would have been to consider a DF method allowing the two users to simultaneously transmit in the first slot towards the relay. Similarly to TWR technique, the relay would have been able to separate these two users using 2 antennas in reception mode. However this alternative has been neglected from our scenarios because it would have increased the interference in the first slot without any benefits in terms of spectral efficiency in the second slot. Therefore, this scheme would have been a compromise between classical DF and TWR schemes.

6.1.2 **Possible Improvements of Decode-and-Forward and Two-Way-Relaying**

This section presents possible improvements for the DF and TWR schemes described above, in order to alleviate secondary effects from the upper layer and lower layer design. For example, situations such as asymmetric traffic (i.e. the end-to-end traffic from one user to the other is not the same) may decrease the total achievable throughput for DF and TWR schemes. Similarly, as mentioned in the previous section, the low performance of the PHY Layer on one of the links may decrease the overall performance of the MAC Layer.

6.1.2.1 Description of Improvements from the Data Traffic Point of View

From the upper layer point of view, when the traffic is asymmetric, achievable throughput is limited for both DF and TWR schemes as represented in Figure 6-3. For fair comparison of

the schemes from Figure 6-3, we consider a transmission phase (Tx Phase) followed by a broadcast phase. During the transmission phase of the DF scheme only one user (U1 or U2) transmits data towards the relay (R), while for the transmission phase of the TWR scheme both users (U1 and U2) may transmit data towards the relay (R) at the same time.
However, in some situations the users may not transmit both at full rate (e.g. their buffers are not both of the same size or the service type is not the same for both users) or in other situations only one user may need to transmit data to the other user (e.g. one of the buffers is empty). In these situations (represented by white boxes in Figure 6-3), DF scheme will not optimally use the available bandwidth while for TWR scheme the relay broadcasts only the amount of traffic which is common to both users and drops the extra traffic send by the user with higher transmitted traffic.

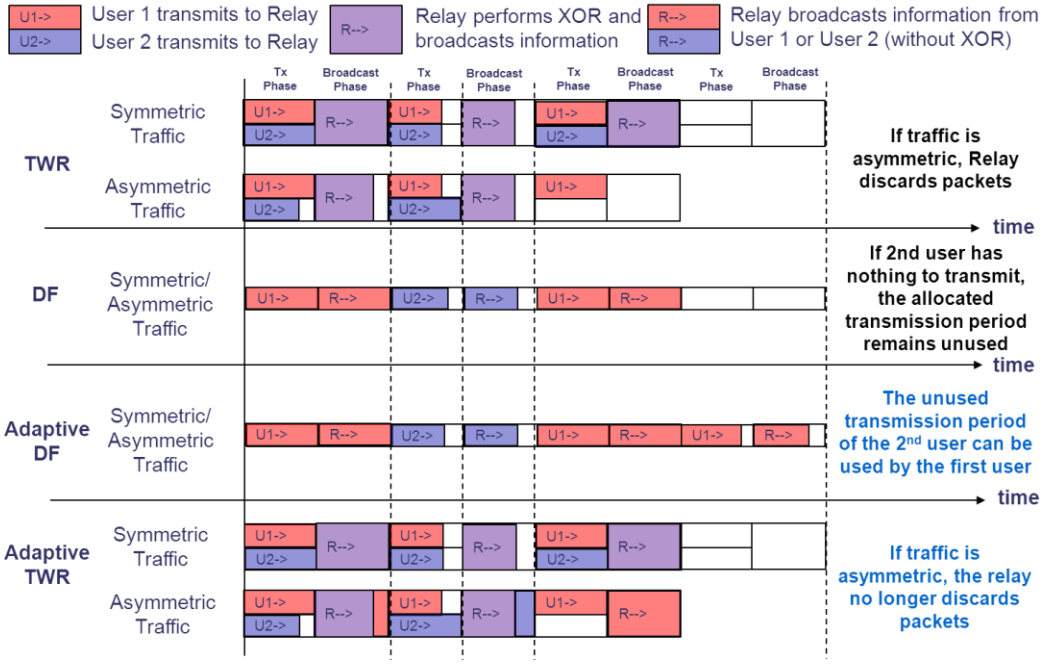

Figure 6-3. Description of Asymmetric and Symmetric Traffic Situations for Different Relaying Schemes – each coloured box represents traffic values expressed in bps.

To resolve all these inconveniences, one can imagine improved versions of DF and TWR schemes from the traffic point of view. For example, instead of using the available resources to send data from User2 to User1 via the relay, the adaptive DF can use these resources to send data from User1 to User2 if User1 has something to transmit. In such a situation the scheme increases the total send traffic on the link from User1 to User2 while decreasing the total send traffic on the link from User2 to User1. Another example represented in Figure 6-3 is another variant of TWR scheme named “adaptive” TWR which before broadcasting information to both users performs XOR operation on *min(traffic from User1, traffic from User2)* and performs DF operation on the difference *max(traffic from User1, traffic from User2)-min(traffic from User1, traffic from User2)*.
In order to better explain the implications of the ideas previously mentioned, we have graphically represented in Figure 6-4 the achievable throughput for DF and TWR schemes (and their variants) while varying transmitted traffic of both User1 and User2. Please note that the four subfigures from Figure 6-4 represent rotations of the same graphical result. Each of these subfigures shows that when using QPSK modulation, adaptive TWR technique can achieve the maximum throughput for a 1.4MHz LTE system only when both users

transmit at a transmission rate of 1.728 Mbps. Figure 6-4 also shows that adaptive TWR outperforms simple TWR in terms of transmitted traffic, but also that simple TWR has the same performance as adaptive TWR when the traffic is symmetric (i.e. when both users are exchanging the same amount of traffic through the relay). Another interesting result can be seen when comparing adaptive DF with simple DF. Adaptive DF outperforms simple DF only in the region where one user is transmitting at full rate (1.728 Mbps) and the other user has nothing to transmit: in this situation adaptive DF reacts to the exchanged traffic values in the two directions and allocates more resources to the user which transmits at full traffic. However, since the frame is divided into distinct time slots corresponding to a transmission phase and a broadcast phase, the total achievable throughput for DF scheme is only 0.864 Mbps.

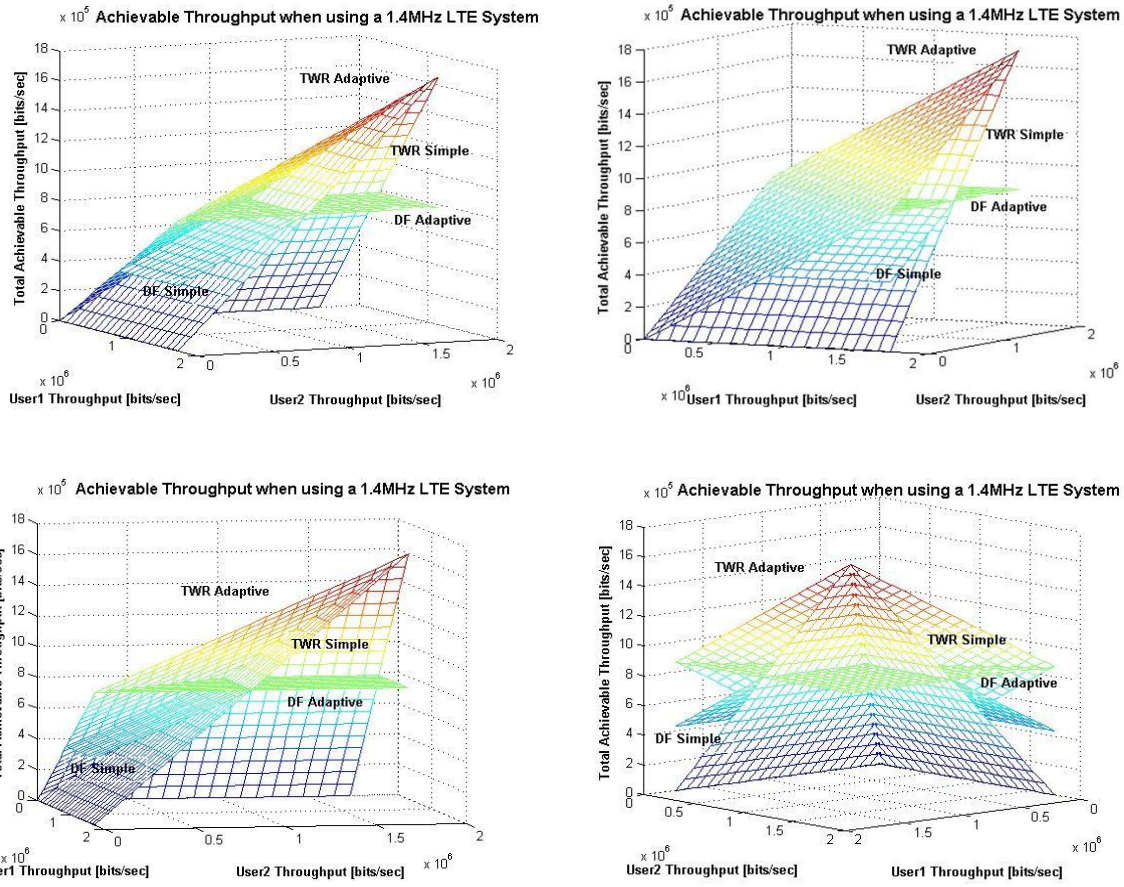

Figure 6-4. Achievable Throughput [bps] for Different Relaying Schemes for Asymmetric Traffic when using a 1.4MHz LTE System

6.1.2.2 Description of Improvements from the Packet Point of View

The main difference between the previous section and this section is that in Section 6.1.2.1 we have considered a traffic situation (and therefore each coloured box from Figure 6-3 was related to a traffic value) while in Section 6.1.2.2 we have considered a MAC layer situation, and therefore each coloured box from Figure 6-5 corresponds herein to a packet.

As seen on top of Figure 6-5, due to channel impairments on the link from User1 to relay (here denoted by "U1->") during the Tx Phase, classic TWR cannot perform XOR operation and just before the Broadcast Phase drops the packet from User2 to relay (here denoted by "U2->") . For this reason, in this section it is proposed a novel relaying technique which consists in combining the TWR and DF:

- When XOR operation is possible (i.e. successful reception from User1 and successful reception from User2 at the same time), the relay uses classic TWR;
- When XOR operation is not possible (e.g. unsuccessful reception from User1 or unsuccessful reception from User2), the relay uses DF.

As previously described, this novel technique adapts to the real-time channel impairments. For this reason it is further called “adaptive” TWR and the classic TWR it is further referred as “simple” TWR.

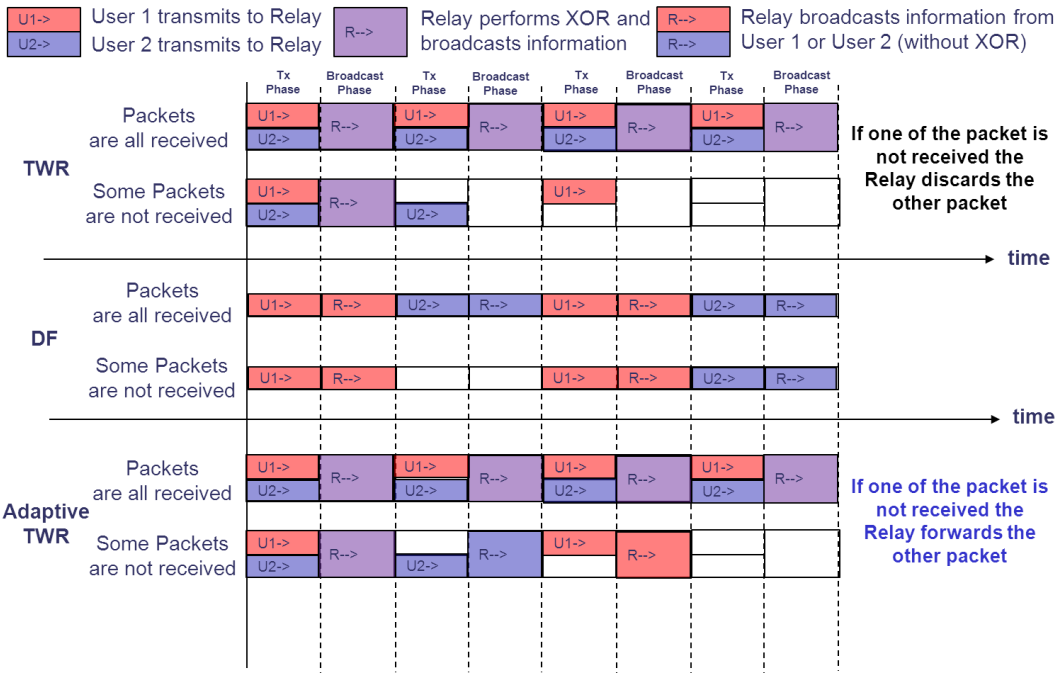

Figure 6-5. Impact of Channel Impairments for Different Relaying Schemes – each coloured box represents a packet

Please also note that TWR, DF and adaptive TWR schemes from Figure 6-5 have been further used for comparison purposes in Section 6.4.3 where MAC Layer simulations have been provided. As further showed also in Section 6.4.3, adaptive TWR scheme provides better results in terms of achievable throughput, proving the importance of a good design of the MAC scheme.

6.2 *Scenarios of Interest and Description of Key Performance Indicators (KPIs)*

As represented in Figure 6-6, the goal of this study is to evaluate the communication performance between User1 and User2 via the relay as a function of the SNR of the first link (i.e. between User1 and the relay) for different power loads between User2 and User1 (mainly impacting the quality of the second link, i.e. between the relay and User2). The performances are evaluated in the 2 possible directions resulting in a total of 3 use cases: unidirectional communication 1) from User1 to User2 and 2) from User2 to User1 and for 3) bidirectional communication involving both User1 and User2 transmissions over the relay.
For each of the use cases different KPIs such as throughput and Packet Error Rate (PER) have been considered, resulting in 3x2 simulation scenarios. Then, for each scenario, different relaying schemes from Figure 6-5 have been considered: 1) classic TWR (here called TWR Simple of TWR1) which drops the packets when XOR operation is not possible, 2) adaptive

TWR (or TWR2) which performs DF when XOR operation is not possible, and finally 3) classic DF. Then, for each of these schemes, simulations for 1) 3GPP ETU (Extended Typical Urban) Channel Model and 2) 3GPP EPA (Extended Pedestrian A Model) Channel Model have been considered, resulting in a total of 3x2x3x2=**36** possible simulations scenarios. From all these scenarios only a few have been selected for representation in Section 6.4.

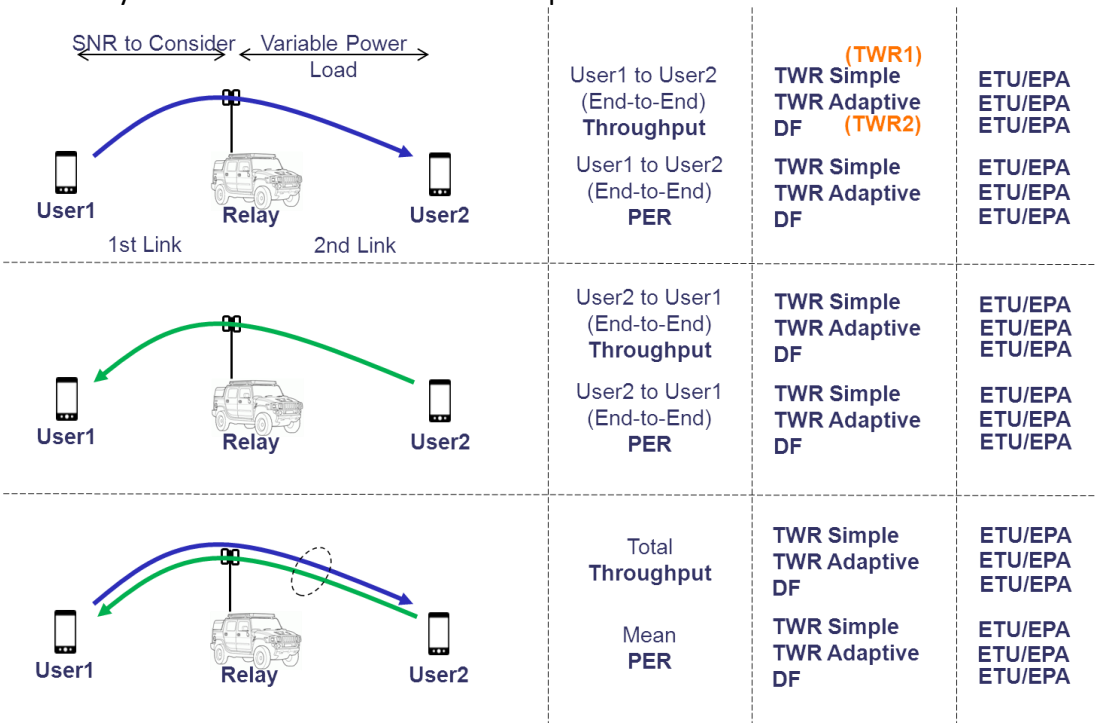

Figure 6-6. Considered Scenarios and Evaluation KPIs

As explained in Figure 6-6, the KPIs to be used in the simulations from Section 6.4 are:

- End-to-End PER (User to User) e.g.:
  - User1 to User2 End-to-End PER
  - User2 to User1 End-to-End PER
- Mean PER computed such as (User1 to User2 End-to-End PER + User2 to User1 End-to-End PER)/2 e.g.:
  - Mean End-to-End PER or
  - 1 – Mean End-to-End PER
- XOR Occurrences [%] for TWR, a statistic representing the number of times expressed in percentage of when the TWR technique is able to perform XOR operations (i.e. both packets from both links have been received in good conditions by the relay);
- End-to-End Throughput [packets/second], e.g.:
  - Throughput from User1 to User2
  - Throughput from User2 to User1
- Total Throughput [packets/second], i.e.:
  - Throughput User1 to User2 + Throughput User2 to User1

6.3 *Proposed PHY Layer Abstraction Method*

The proposed PHY Layer abstraction method is presented in Figure 6-7. For each packet, for each transmitting user we set the power loads for each user, the number of antennas and the channel type. Then, for a given noise level, we compute the estimated SNR after the

equalization. Then, using the mutual information function and the modulation type it is possible to compute an average value of the estimated SNR over multiple realizations or over multiple Resource Blocks (RBs) being used. This value is expressed as a mean estimated SNR, and serves to obtain an instantaneous Packet Error Rate using the direct PHY Layer simulation results described in Figure 6-8 which have been obtained in AWGN case for a limited set of points. However, the estimated SNR obtained after equalization can vary in a very large range, and since the curve from Figure 6-8 contains only a small set of points (SNR, PER) and therefore a limited number of possible realizations, in order to obtain the (intermediate) instantaneous PER value corresponding to the estimated SNR we further use an interpolation block. As further seen in Section 6.4.2, the interpolation block can be set to perform linear or cubic interpolation and provides an instantaneous PER directly extracted from the AWGN curve for the previously provided SNR estimated value. After computing the instantaneous PER and after a comparison of this obtained value with a threshold T from a random number generator, the PHY Layer abstraction provides information on whether the transmitted packet has been correctly received or not.

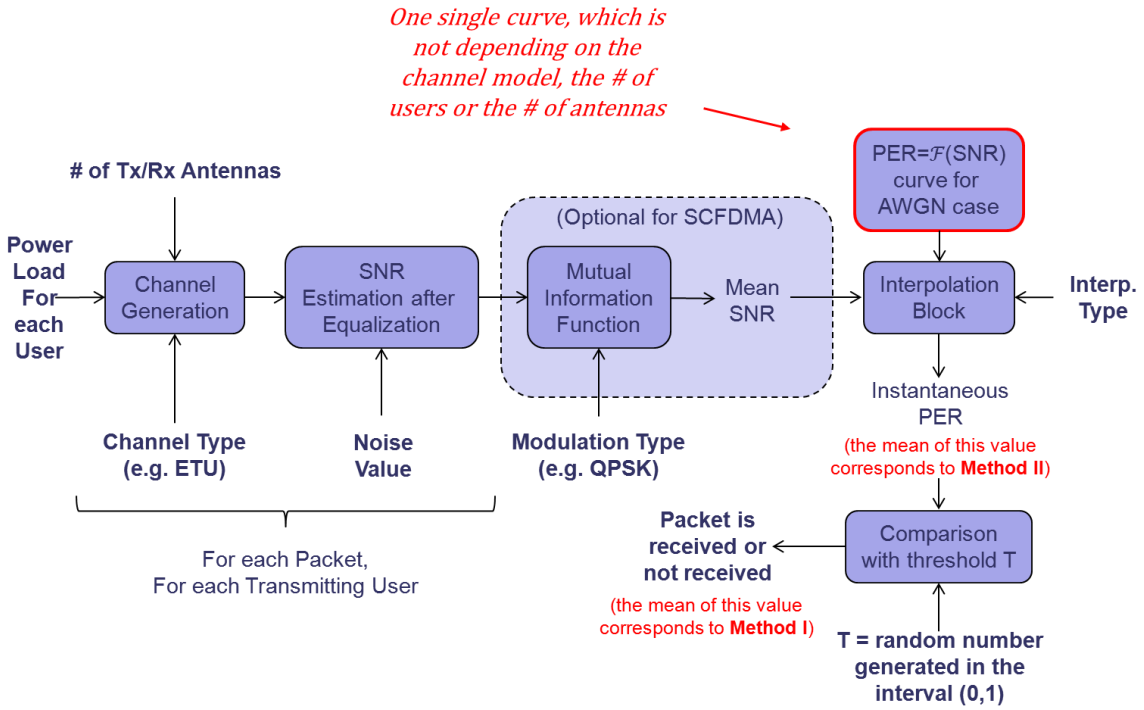

Figure 6-7. PHY Layer Abstraction Method

Moreover, the PHY Layer abstraction from Figure 6-7 proposes 2 methods to evaluate the mean PER obtained for any given number of realizations, per one SNR value. Method II computes the mean PER from all the instantaneous PER values (i.e. values between 0 and 1), while Method I computes the mean PER from the discrete PER information (i.e. packet is received or not received, corresponding to 1 or 0 values). The main differences between the Method II and Method I are therefore related to the random number generator from Figure 6-7.

6.4 *Simulation Results*

This section is dedicated to the description of the simulation parameters and simulation results. Section 6.4.1 describes the simulation parameters used for both PHY Layer

abstraction model described in Section 6.4.2 and MAC Layer simulations described in Section 6.4.3.

6.4.1 **Simulation Parameters**

The choice of these simulation parameters has been performed with respect to LTE-compliant PMR applications such as Push-To-Talk (PTT) applications. However, these parameters can be easily adapted for other applications by e.g. changing packet size (which in the case described below was obtained from the vocoder characteristics). The parameters which have been taken into account at PHY Layer are further described in Table 6-1. It can be easily computed that for a 1.4 MHz bandwidth the system can support up to 60 concomitant PTT transmissions. Moreover, SC-FDMA technique has been considered for user to relay and relay to user links. This choice can be justified easily for flexible architectures where a user can take the place of a relay. These situations where SC-FDMA is being used in both directions (from and to the relay) will benefit of low PAPR (Peak-to-Average Power Ratio), translating thus into a better energy efficiency.

Parameter	**Value**
Frame Duration	10 ms
Slot Duration	0.5 ms
PMR Transmission Period	20 ms (vocoder parameter)
Bandwidth	1.4 MHz or 5 MHz
Subcarrier Spacing	15 KHz
Number of Subcarriers	72 or 300
Number of Subcarriers per RB	12
Number of Symbols per Slot	6 (Extended Cyclic Prefix)
Coding Scheme	Convolutional Code with Rate 1/3
PMR Necessary Bits per Packet	480 bits
Number of Bits per Symbol	2 bits/symbol (QPSK modulation)
Total Throughput (including pilots)	1.728 Mbps or 7.2 Mbps
Total Throughput (excluding pilots)	1.440 Mbps or 6 Mbps
Maximum Number of Concomitant PMR PTT Links (after excluding pilot signals)	60 or 250
Multiple Access Technique	Single-Carrier Frequency Division Multiple Access (SC-FDMA)

Table 6-1. Simulation Parameters

Using the LTE-compliant parameters provided in Table 6-1, we have simulated a PMR transmission using packets of 480 bits length over the AWGN channel. We have further evaluated the PER in terms of Signal to Noise Ratio (SNR). In Figure 6-8 two different curves were represented: one corresponds to a simulation on 9 points, with lower precision (i.e. 10^5 Monte-Carlo simulations/point) and the other to a simulation on 15 points, with higher precision (i.e. $5x10^6$ Monte-Carlo simulations/point). For the PHY Layer abstraction method we have used the second curve since it has been observed that it gives the optimal amount of precision for both linear and cubic interpolation techniques in a reasonable SNR range further used for MAC Layer simulation.

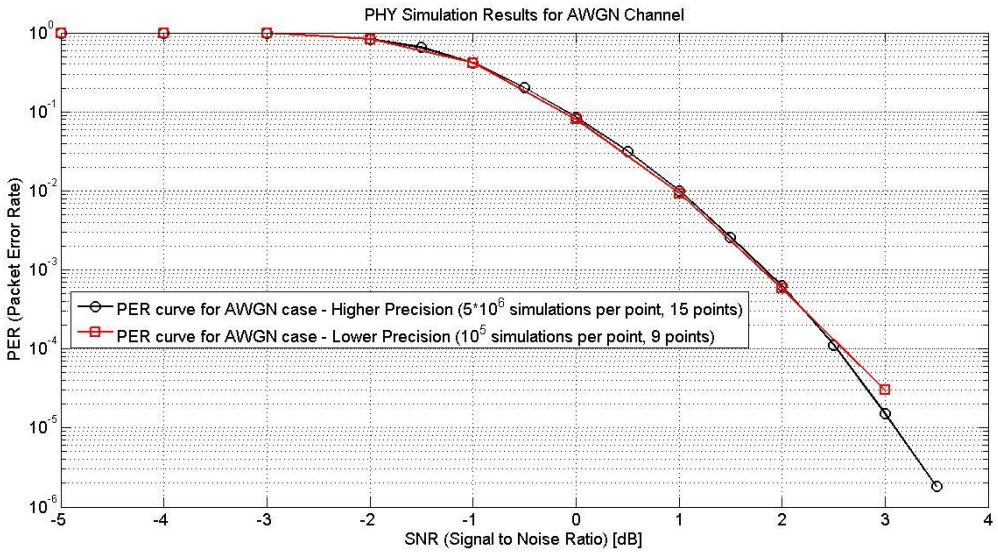

Figure 6-8. PHY Layer Simulation Results for AWGN Channel

6.4.2 **Validation of PHY Layer Abstraction Model by Comparison with PHY Layer Simulations**

The purpose of this section is to validate the PHY Layer abstraction model for both low number of realizations (see Section 6.4.2.2) and high number of realizations (see Section 6.4.2.3). These evaluations have been performed for both 3GPP ETU and EPA channel models in order to identify which is the most convenient parameterisation of the abstraction scheme provided in Section 6.3.

6.4.2.1 Tested Scenarios

In order to validate the PHY Layer abstraction model, 10 scenarios have been selected for testing purposes, scenarios which have been used throughout the Sections 6.4.2.2 and 6.4.2.3. All these scenarios are resumed in Table 6-2 for different number of users, different power loads (if 2 users are involved), different number of antennas. While scenario 1 applies to both DF and TWR schemes, scenarios from 2 to 9 apply to TWR only and scenario 10 applies to DF only.

Scenario #	UL: User(s)->Relay or	# of Tx Users	Power Load Between Users	# Tx Antennas	# Rx Antennas	Relevant Transmission

	DL: Relay->User(s)					**Scheme**
1	DL	1	-	1	1	DF, TWR
2	UL	2	0 dB; -30 dB	1	2	TWR
3	UL	2	0 dB; -15 dB	1	2	TWR
4	UL	2	0 dB; -10 dB	1	2	TWR
5	UL	2	0 dB; -5 dB	1	2	TWR
6	UL	2	0 dB; 0 dB	1	2	TWR
7	UL	2	0 dB; 5 dB	1	2	TWR
8	UL	2	0 dB; 15 dB	1	2	TWR
9	UL	2	0 dB; 30 dB	1	2	TWR
10	UL	1	-	1	2	DF

Table 6-2. Tested Scenarios

Moreover, as presented in Section 6.3, there are two methods are being used to evaluate the mean PER. The main differences between the Method II and Method I are related to the random number generator from Figure 6-7. Please also note that in situations where Method I provided zero PER, Method II was used for comparison throughout the following sections, i.e. Section 6.4.2.2 and Section 6.4.2.3.

6.4.2.2 Prediction Results for Low Number of Realizations

In the case of low number of realizations, the abstraction of the PHY Layer uses only 10^4 realizations. The results obtained through the abstraction of the PHY Layer have been further compared with those obtained from direct PHY Layer simulation (using 10^6 realizations) for two scenarios: scenario 10 and scenario 1 (as seen later on, these two scenarios are the most representative of all 10 scenarios, since they represent bounds for maximum and minimum PER). ETU and EPA channels are further tested below.

ETU Channel

Simulations using ETU channel have been performed for a normal interpolation limit (AWGN curve from Figure 6-8 limited at 3.5dB value) and for a higher interpolation limit (i.e. 4dB value which is beyond AWGN curve values provided by Figure 6-8 which provides results only till 3.5dB value). ETU channel has been also tested for linear (see the first two subfigures of Figure 6-9) and cubic interpolations (see the first two subfigures of Figure 6-9). Results show that cubic interpolation is always better for low number of realizations.

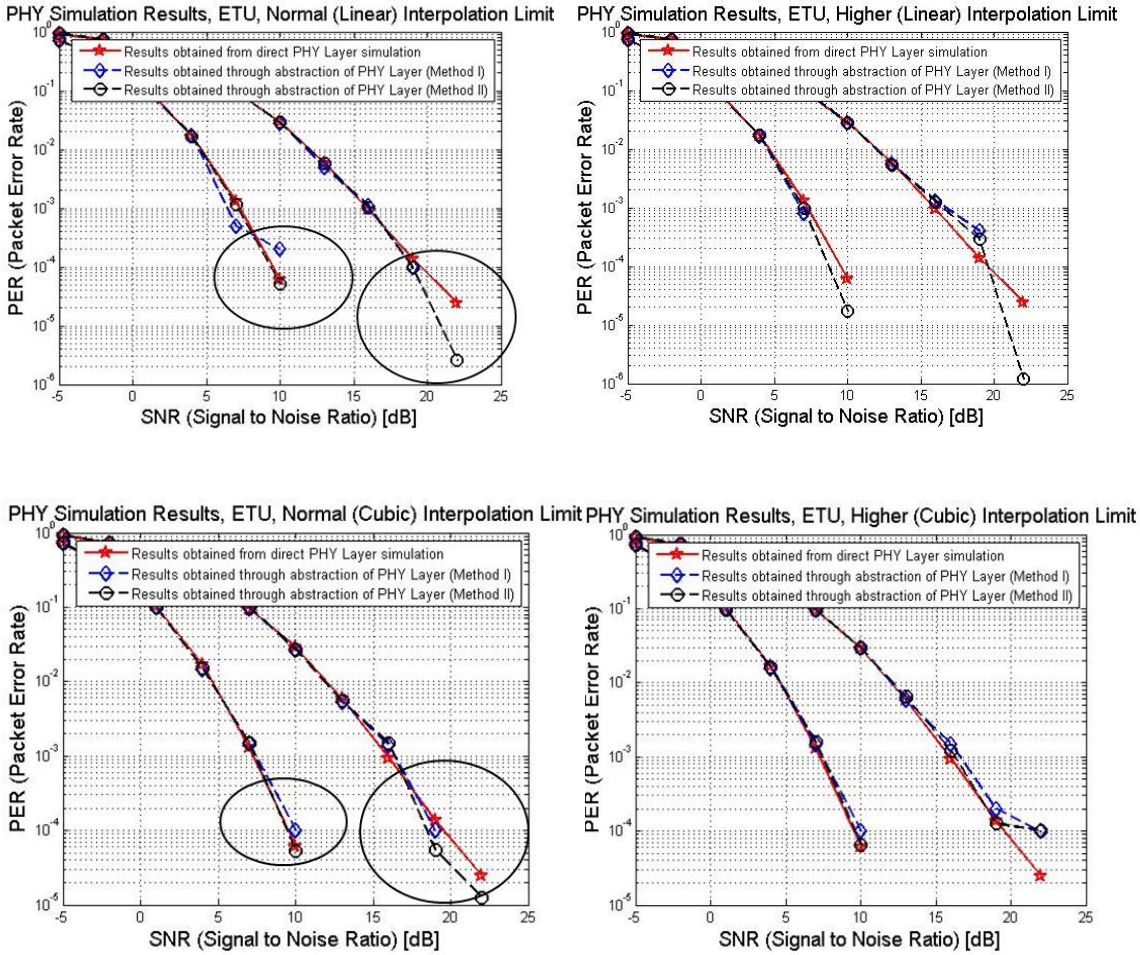

Figure 6-9. PHY Layer Abstraction Method on Lower Number of Realizations, for ETU Channel Model, for Scenarios 10 and 1 (from left hand side to right hand side of each sub-figure)

EPA Channel

Similar as for previous section, simulations using EPA channel have been performed for a normal interpolation limit (AWGN curve from Figure 6-8 limited at 3.5dB value) and for a higher interpolation limit (4dB value which is outside the interval provided by Figure 6-8). ETU channel has been also tested for linear (see the first two subfigures of Figure 6-10) and cubic interpolations (see the first two subfigures of Figure 6-10). Results show that cubic interpolation is always better for low number of realizations. Figure 6-10 also shows that for a better approximation it is preferable to use the same interval provided by Figure 6-8.

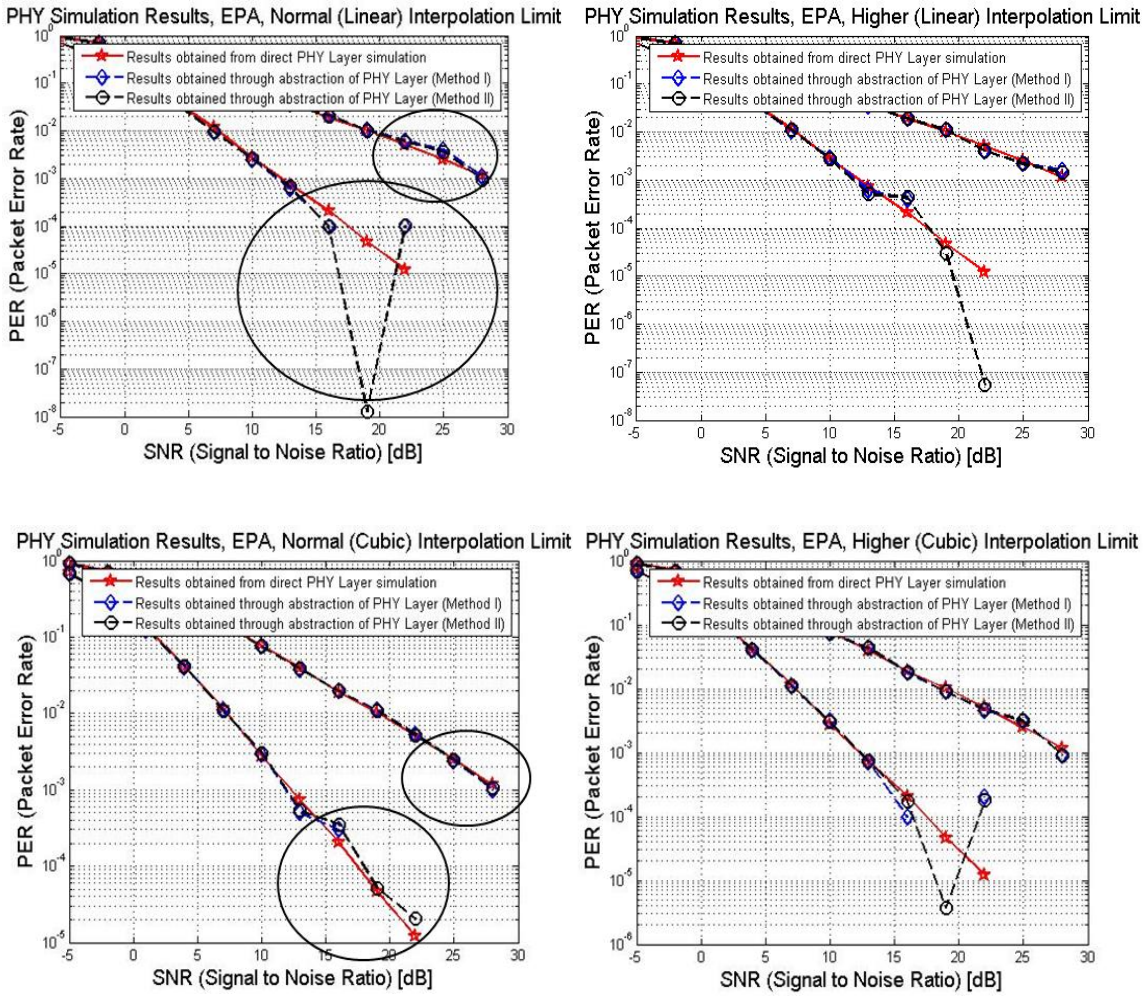

Figure 6-10. PHY Layer Abstraction Method on Lower Number of Realizations, for EPA Channel Model, for Scenarios 10 and 1 (from left hand side to right hand side of each sub-figure)

In this section we showed that cubic interpolation is a better choice than linear interpolation for both ETU and EPA scenarios with lower number of realizations. A very good approximation of PHY Layer was therefore obtained when using cubic interpolation. However, a very precise AWGN PER curve is still required (e.g. 15 points, and for each point at least $5x10^6$ PHY Layer simulations).

Section 6.4.2.2 showed that for all the simulations is better to use interpolation only for SNR values inside the AWGN curve interval provided by Figure 6-8 (i.e. [-5dB 3.5dB]). For this reason, this conclusion will be also used in the next sections.

6.4.2.3 Prediction Results for High Number of Realizations

In the case of high number of realizations, the abstraction of the PHY Layer uses 10^5 realizations. The results obtained through the abstraction of the PHY Layer have been further compared with those obtained from direct PHY Layer simulation (using 10^6 realizations) for 1) scenario 10 and scenario 1 (see Figure 6-11 and Figure 6-13) and 2) scenarios 2 to 9 (see Figure 6-12 and Figure 6-14). ETU and EPA channels are further tested below.

ETU Channel

Figure 6-11 presents results obtained for scenario 10 and 1 for 3GPP ETU channel model with 10^5 realizations for PHY abstraction. Results have been compared with results obtained from direct PHY Layer simulations for 10^6 realizations. A comparison between cubic and linear interpolation method was also provided.

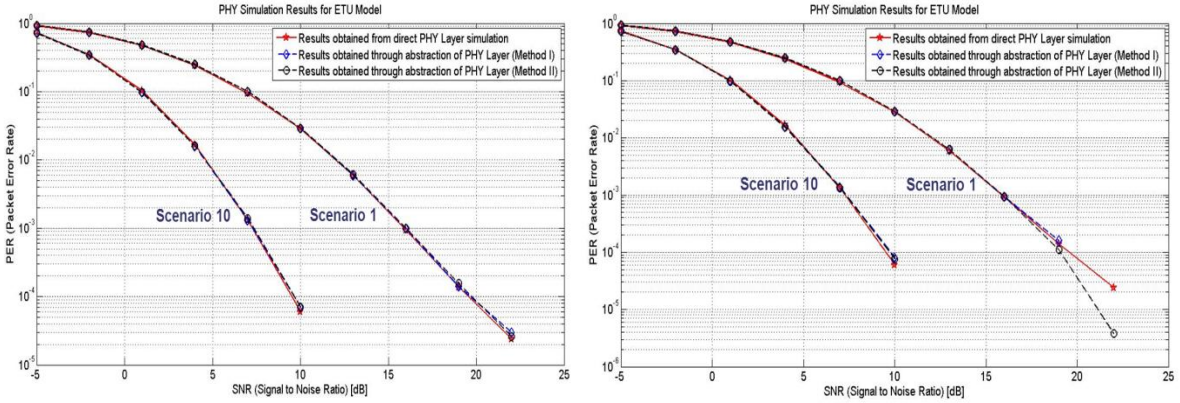

Figure 6-11. PHY Layer Abstraction Method on Higher Number of Realizations, for ETU Channel Model, for Scenarios 10 and 1 (from left to right), results obtained from a) cubic interpolation of AWGN curve (left hand side) and b) linear interpolation of AWGN curve (right hand side) for Method I and Method II.

Figure 6-12 presents results obtained for scenarios 2 to 9, for cubic and linear interpolation methods, for 3GPP ETU channel model with 10^5 realizations for PHY abstraction. Results have been compared with results obtained from direct PHY Layer simulations for 10^6 realizations.

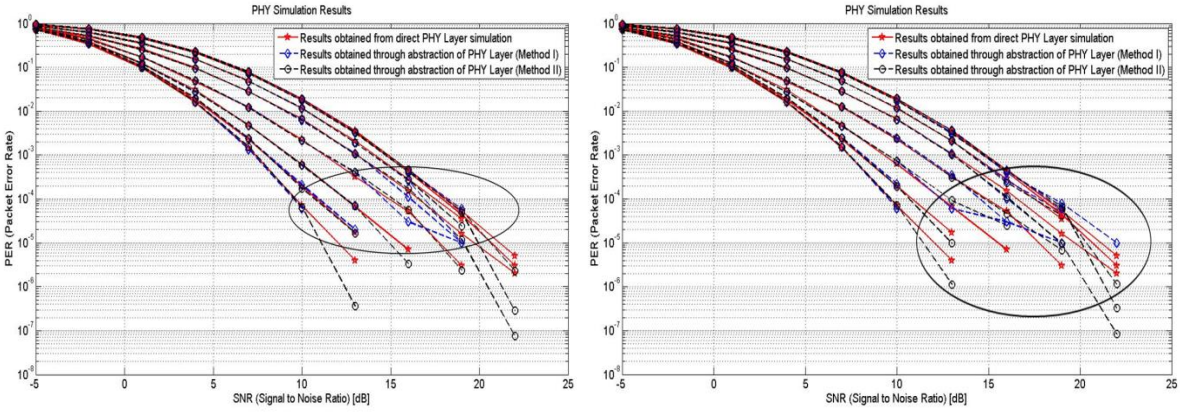

Figure 6-12. PHY Layer Abstraction Method on Higher Number of Realizations, for ETU Channel Model, for Scenarios 2-9 (from left to right), results obtained from a) cubic interpolation of AWGN curve (left hand side) and b) linear interpolation of AWGN curve (right hand side) for Method I and Method II.

Results provided in Figure 6-11 and Figure 6-12 show that for ETU channel models with higher number of realizations, cubic interpolation (left hand side) provides better approximation results than linear interpolation (right hand side). In situations when Method I provided zero PER, Method II was used for comparison. Please also note that the comparison has been performed for PER higher than 10^{-5} (since the number of realizations is normally not sufficient for obtaining PERs below that value).

EPA Channel

Same reasoning as the one provided in the previous paragraph dedicated to ETU channel has been applied. Figure 6-13 therefore presents results obtained for scenario 10 and 1 for 3GPP EPA channel model with 10^5 realizations for PHY abstraction. Results obtained from abstraction of PHY Layer Method I and Method II have been further compared with results obtained from direct PHY Layer simulations for 10^6 realizations. A comparison between cubic and linear interpolation method was also provided.

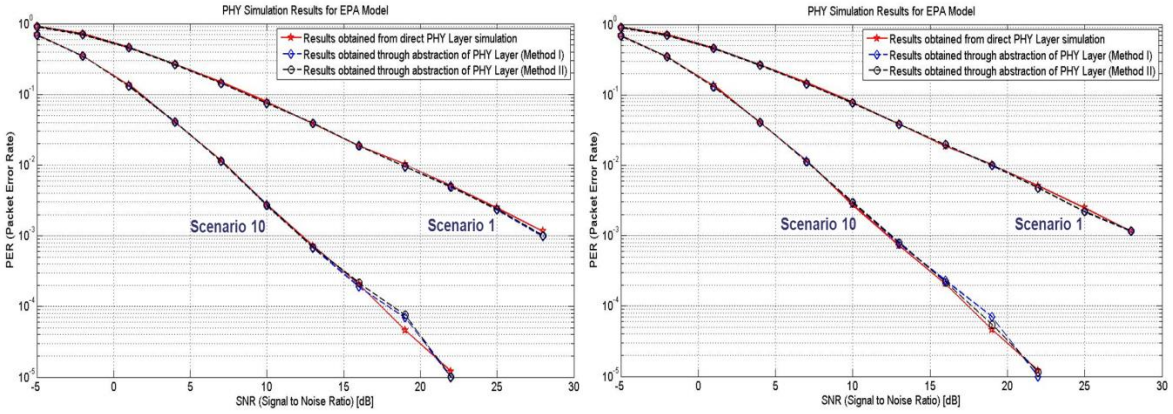

Figure 6-13. PHY Layer Abstraction Method on Higher Number of Realizations, for EPA Channel Model, for Scenarios 10 and 1 (from left to right), results obtained from a) cubic interpolation of AWGN curve (left hand side) and b) linear interpolation of AWGN curve (right hand side) for Method I and Method II.

Figure 6-14 presents results obtained for scenarios 2 to 9, for cubic and linear interpolation methods, for 3GPP EPA channel model with 10^5 realizations for PHY abstraction. Results have been compared with results obtained from direct PHY Layer simulations for 10^6 realizations.

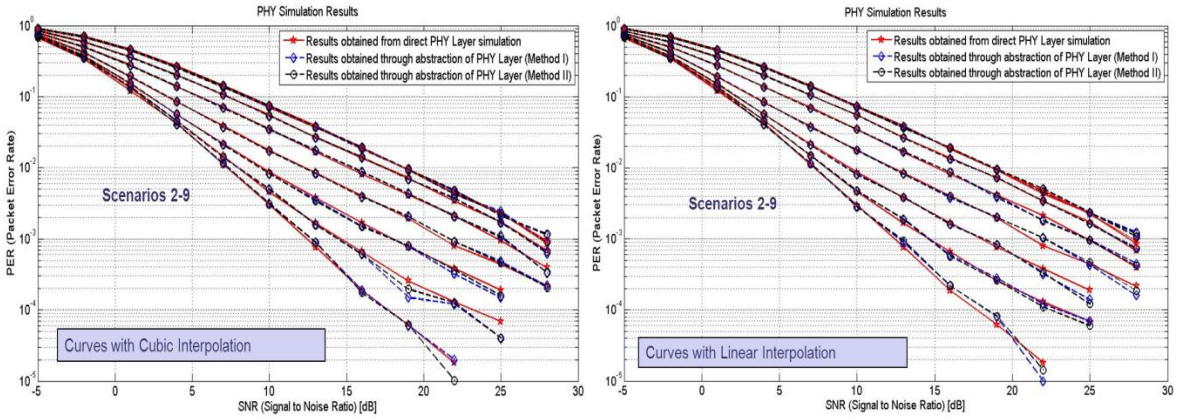

Figure 6-14. PHY Layer Abstraction Method on Higher Number of Realizations, for EPA Channel Model, for Scenarios 2-9 (from left to right), results obtained from a) cubic interpolation of AWGN curve (left hand side) and b) linear interpolation of AWGN curve (right hand side) for Method I and Method II.

Results provided in Figure 6-13 and Figure 6-14 show that for EPA channel models with higher number of realizations, linear interpolation (right hand side) provides better approximation results than cubic interpolation (left hand side). These results are therefore different than the one obtained for ETU channel models.
In Section 6.4.2.3 we therefore showed that cubic interpolation is a better choice than linear interpolation only for ETU scenarios with higher number of realizations. Same simulations have been performed for EPA scenarios and for higher number of points it seems that linear interpolation gives a better approximation of PHY Layer than cubic interpolation.

6.4.2.4 Advantages of the new Proposed PHY Layer Abstraction Method

Firstly, the new proposed PHY Layer abstraction method provides a reliable approximation of the PHY Layer, for both low and high number of realizations. Therefore, abstraction model can be used for any number of realizations (i.e. even a lower number of realizations), without affecting the results. Secondly, the new proposed PHY Layer abstraction method allows a faster simulation at MAC Layer level since only the channels are generated (and the PHY Layer simulation chain is not employed anymore).

The method provides low complexity and can be easily upgraded since it does not require a family of predefined curves for the data base, it requires only one curve: PER=$\mathcal{F}$(SNR) for AWGN. Moreover, it is possible to define more PER=$\mathcal{F}$(SNR) curves for different packet sizes, different coding schemes, any number of retransmissions to be implemented for e.g. HARQ, any modulation type.

At last, the method provides adaptability – since the model can be used for any number of users, any number of antennas, any channel model type, and any power load between the users.

6.4.3 **MAC Layer Simulations and Main Results**

Using the PHY Layer abstraction method provided in Section 6.4.2, in Section 6.4.3 we provide MAC Layer simulation results for the relaying schemes described in Figure 6-5. The

KPIs used in this section are the KPIs described in Section 6.2 and the considered simulation parameters are the parameters provided in Section 6.4.1 for a 1.4 MHz LTE system, and for a 3GPP EPA channel model. Please also note that on all figures described below, all KPIs are represented as a function of the SNR of the link between the first user and the relay.
For the following figures and results, please note that the notation "User1 to User2 [0dB -30dB]" refers to the indirect transmission link (i.e. with the help of a relay) between User1 and User2 when the power of User2 is below the power User1 with 30dB. Similarly, please also note that the notation "User2 to User1 [0dB -30dB]" refers to the indirect transmission link (i.e. with the help of a relay) between User2 and User1 when the power of User2 is below the power User1 with 30dB. These use cases therefore correspond to the ones from Figure 6-6 previously presented in Section 6.2.
In Figure 6-15 we have represented End-to-End PERs for simple TWR relaying scheme. When the SNR of one user is low compared to the SNR of the other user, the simple TWR relaying scheme does not perform any transmission during the broadcast phase. For this reason, End-to-End reliability is not assured even if the SNR of one link is sufficiently good.
However, in Figure 6-16 we have represented End-to-End PERs for adaptive TWR relaying scheme. Comparing Figure 6-16 with Figure 6-15, one can see that adaptive TWR relaying scheme assures a better End-to-End reliability when the SNR of one link is low.
Moreover, one can easily notice that in Figure 6-15 the links [User1 to User2] and [User2 to User1] are not symmetrical. The reason for which these links are not symmetrical is because the relay uses 2 antennas in reception, as being explained in Section 6.
Another interesting result for both Figure 6-15 and Figure 6-16 is e.g. when the power of User2 is much higher than the power of User1: this would correspond to a high level of interference that even 2 antennas (at the relay side) will not be able to separate. For this reason, the results from both figures seem to be somewhat bounded when the power of the second user increases with 20-30 dBs above the power of the first user.

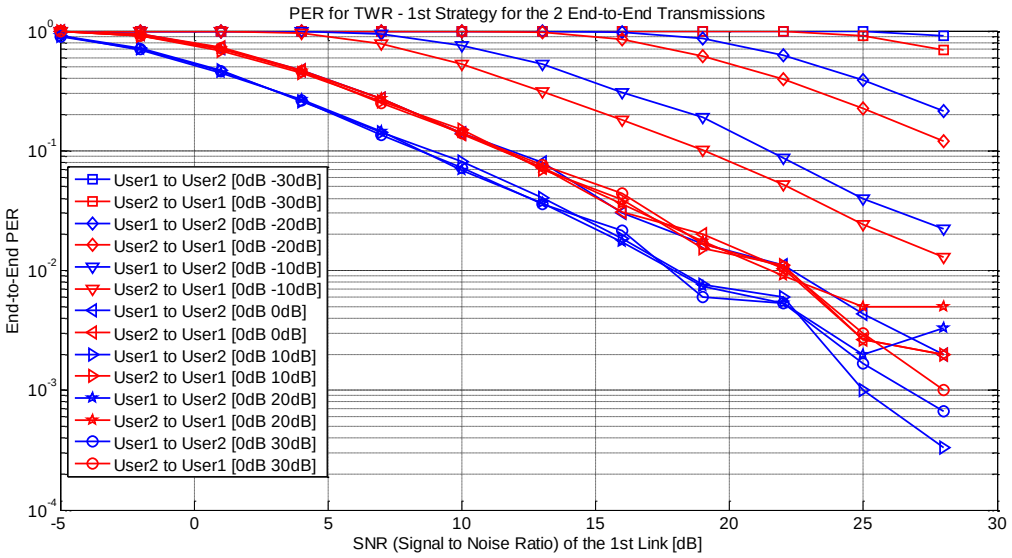

Figure 6-15. End-to-End PER - Comparison between different transmissions for different power loads (for simple TWR)

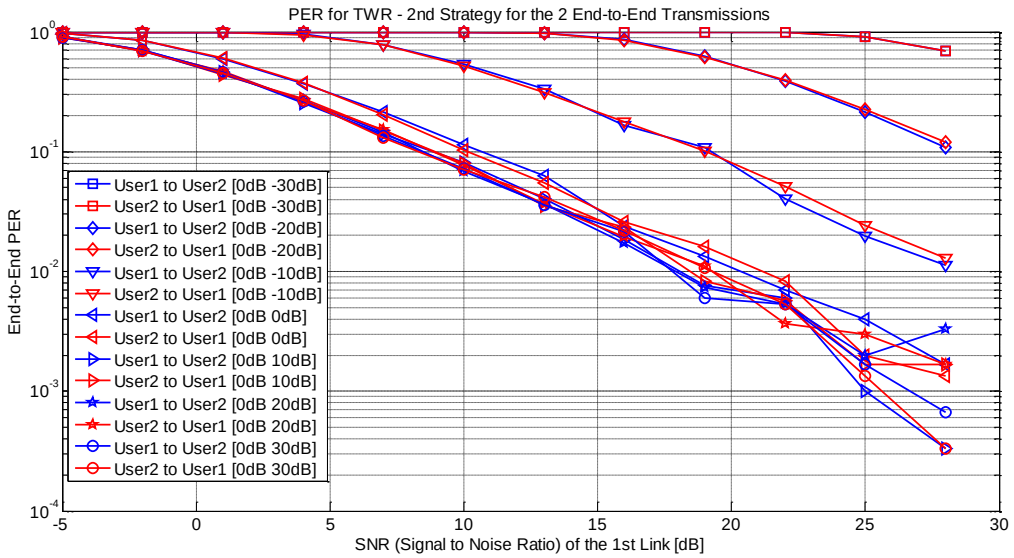

Figure 6-16. End-to-End PER - Comparison between different transmissions for different power loads (for adaptive TWR)

In terms of mean PER between the two End-to-End transmissions, Figure 6-17 clearly shows that adaptive TWR is better than simple TWR. Also, for the results represented in Figure 6-17 the notations e.g. “[0dB -30dB]” and “[0dB 30dB]” refers to the power load between User1 and User2: in the first case the power of User2 is 30dB smaller than the power of User1, while in the second case the power of User2 is 30dB higher than the power of User1.

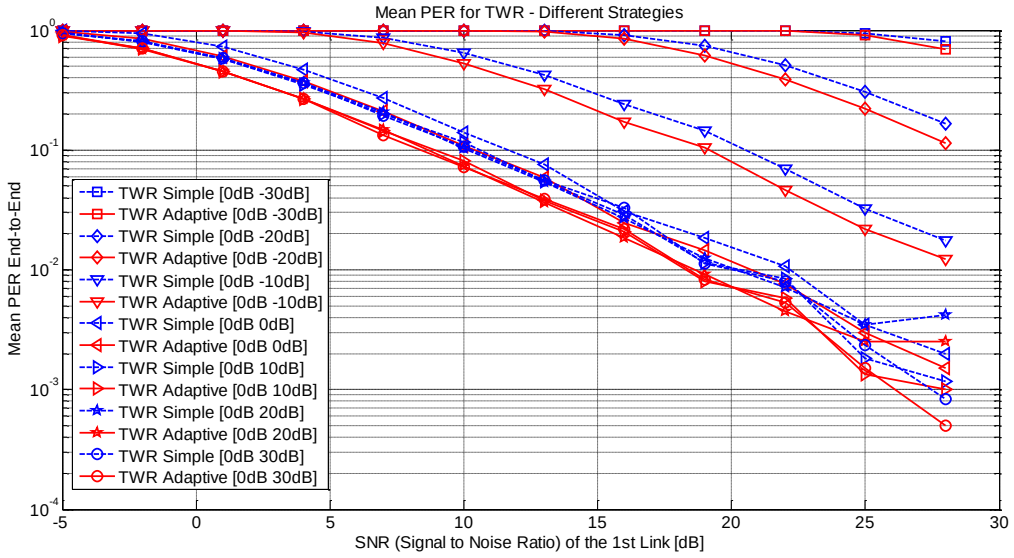

Figure 6-17. Mean PER - Comparison between different transmissions for different power loads (for simple TWR and adaptive TWR)

Following the same reasoning as the one provided in Figure 6-15, Figure 6-16 and Figure 6-17, in the following figures i.e. Figure 6-18, Figure 6-19 and Figure 6-20 we have represented User1 to User2 End-to-End PER, User2 to User1 End-to-End PER and mean PER respectively, but for adaptive TWR and DF schemes. All these figures clearly show that for all considered scenarios, DF has a clear advantage over TWR in terms of End-to-End reliability:

DF PER is better than adaptive TWR PER for both User1 to User2 (see Figure 6-18) and User2 to User1 (see Figure 6-19) links. Moreover, even when computing the mean PER (see Figure 6-20) between the two End-to-End links, one can clearly notice a maximum of 3dB of gain between DF and adaptive TWR schemes. As a matter of fact, simple TWR and adaptive TWR are more sensitive to PERs than DF when the power of one user is much higher with respect to the power of the other user, and that is because the 2 antennas used in reception at relay side are not able to entirely separate the two users, resulting in extra interference.

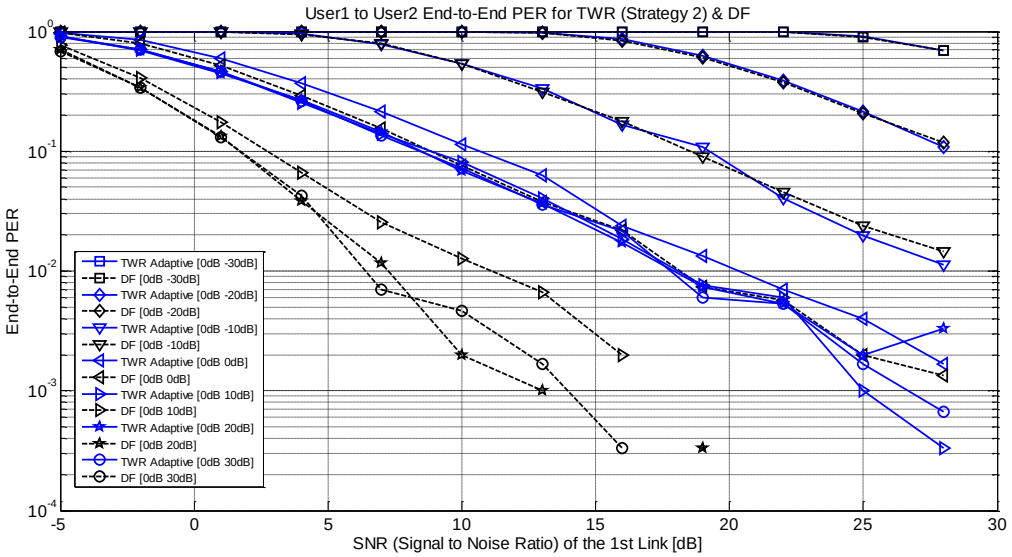

Figure 6-18. End-to-End PER - Comparison between adaptive TWR and DF for different power loads (for User1 to User2 transmissions)

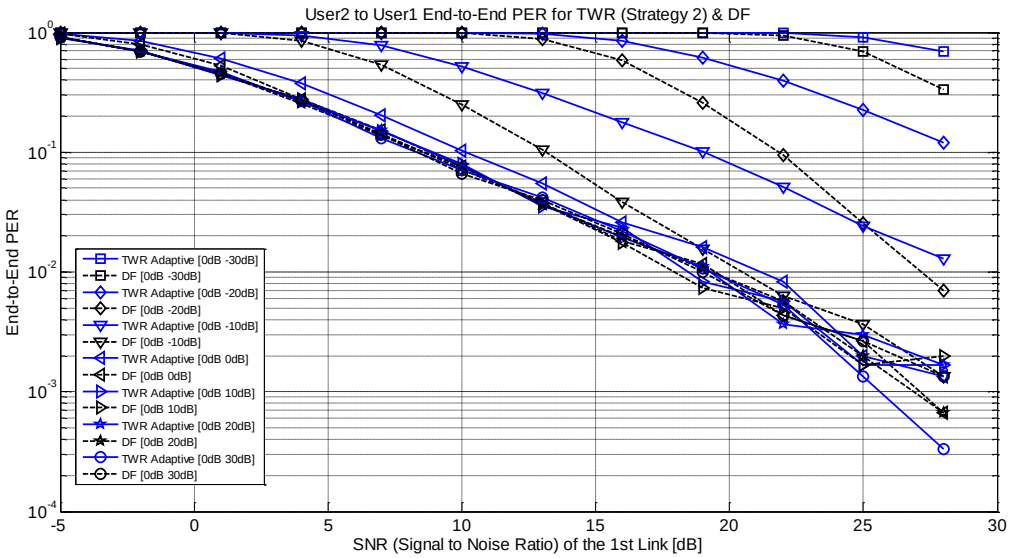

Figure 6-19. End-to-End PER - Comparison between adaptive TWR and DF for different power loads (for User2 to User1 transmissions)

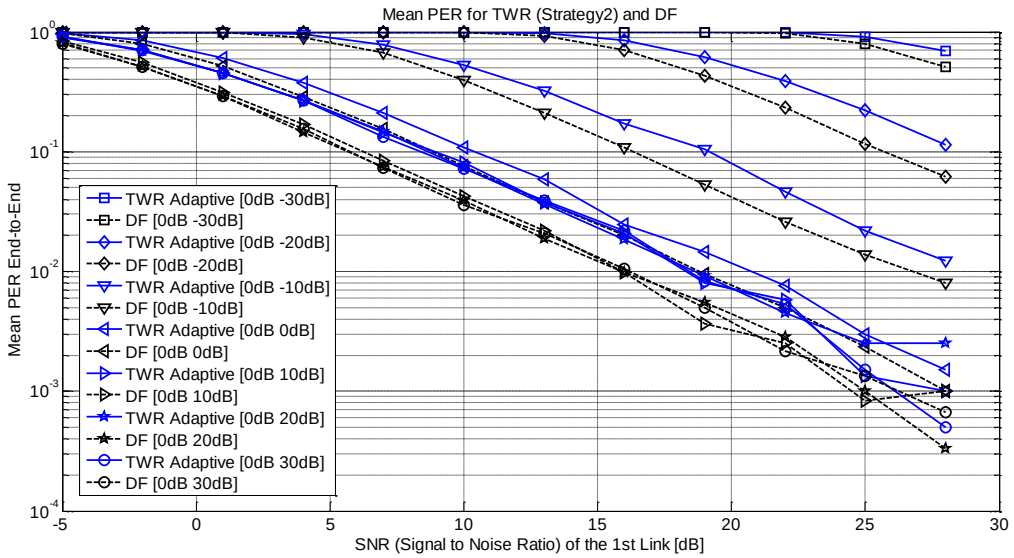

Figure 6-20. Mean PER - Comparison between adaptive TWR and DF for different power loads

Further results from Figure 6-21, Figure 6-22 and Figure 6-23 show End-to-End throughput values between User1 and User2, between User2 and User1, and total throughput values respectively. While in Figure 6-21 and Figure 6-22 we show results only for adaptive TWR and DF schemes, in Figure 6-23 we show results for simple TWR scheme as well.

In Figure 6-21, for User1 to User2 communication, sometimes DF technique is better than adaptive TWR technique in terms of throughput, but only at very low SNR. However, even in those situations (e.g. for SNR= -5dB, at [0dB 30dB] and [0dB 20dB] power load values), the gain is very small and cannot be easily exploited. Overall, except those few situations, the adaptive TWR scheme throughput is almost double than the DF scheme throughput (e.g. for SNR values above 15dBs and the power of the second user above -10dBs with respect to the power of the first user).

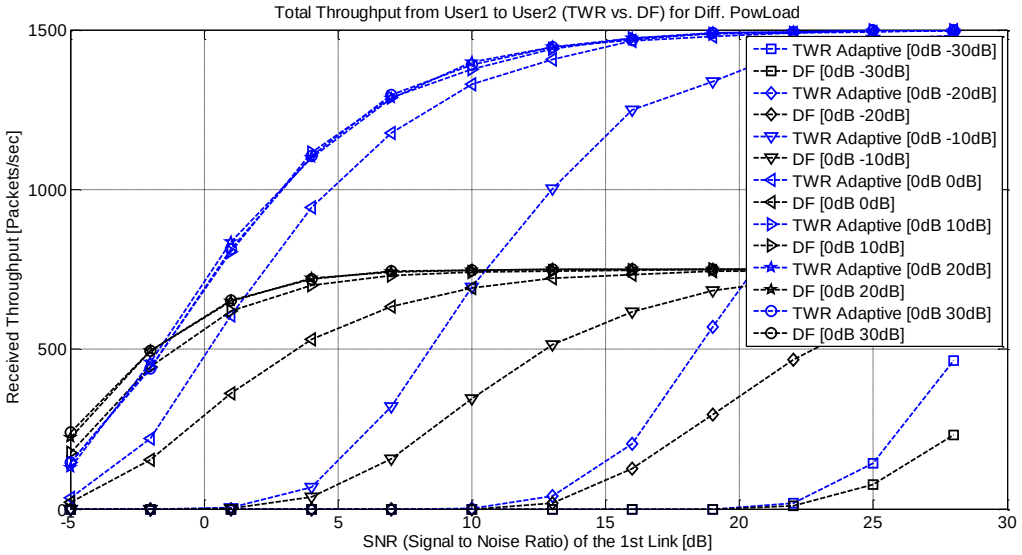

Figure 6-21. End-to-End Throughput - Comparison between adaptive TWR and DF for different power loads (for User1 to User2 transmissions)

Similarly, in Figure 6-22 (for User2 to User1 communication), DF technique may be better than TWR in terms of throughput, but only at very small power loads (please note again that the representation is in terms of SNR of the 1st link). Except those few situations, for adaptive TWR scheme the throughput achieves even 1500 packets per second while for DF scheme the throughput achieves only a maximum of 750 packets per second, which is only half.

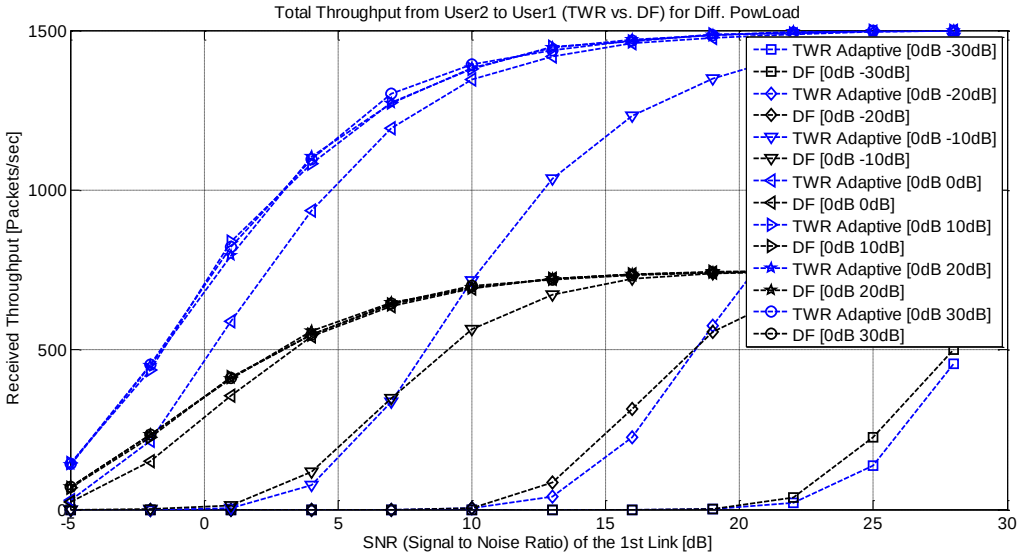

Figure 6-22. End-to-End Throughput - Comparison between adaptive TWR and DF for different power loads (for User2 to User1 transmissions)

Finally, in Figure 6-23, where it is represented the total throughput as a function of SNR, adaptive TWR is better than both simple TWR and DF scheme. Adaptive TWR therefore shows a clear benefit in terms of total achievable End-to-End throughput.

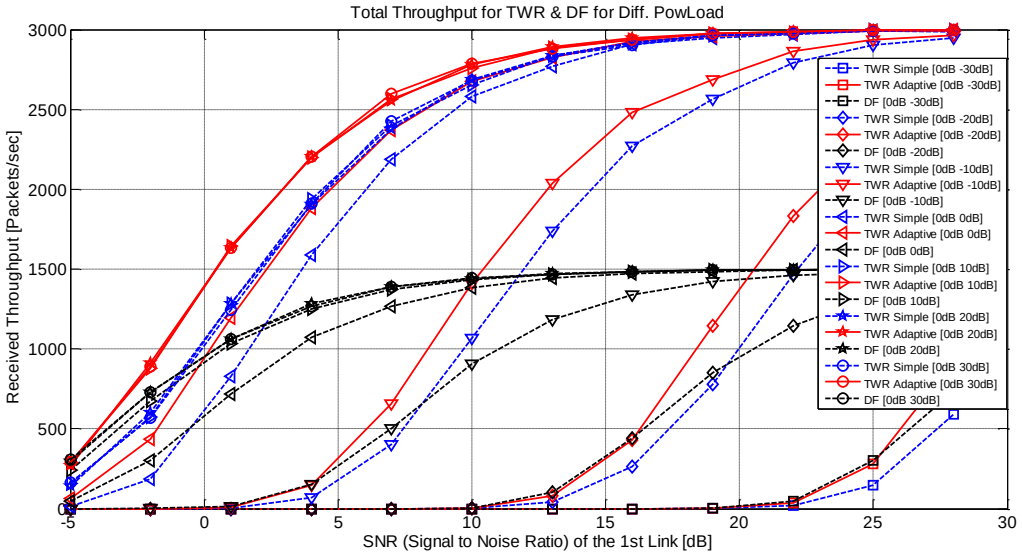

Figure 6-23. Total Throughput - Comparison between simple TWR, adaptive TWR and DF for different power loads

After comparing TWR schemes (2 strategies) with DF, we have shown that PER of DF is slightly better than PER of TWR in many scenarios. However, as also seen in Table 6-3, TWR is better than DF in terms of achievable throughput.

	PMR using an LTE 1.4 MHz System			**PMR using an LTE 5 MHz System**		
	User1 to User2	**User2 to User1**	**Total Max Achievable Throughput**	**User1 to User2**	**User2 to User1**	**Total Max Achievable Throughput**
TWR	1500 packets/sec	1500 packets/sec	**3000** packets/sec	6250 packets/sec	6250 packets/sec	**12500** packets/sec
DF	750 packets/sec	750 packets/sec	1500 packets/sec	3125 packets/sec	3125 packets/sec	6250 packets/sec

Table 6-3. Achievable Throughput [packets/sec] for a PMR system using LTE technology

6.5 *Conclusions*

This work introduced a simulation method using abstraction of PHY Layer for SC-FDMA transmissions. The method can employ cubic interpolation or linear interpolation and simulations show that cubic interpolation is a better choice than linear interpolation for ETU scenarios with higher number of realizations, and for ETU and EPA scenarios with low number of realizations. However, for EPA scenarios with low number of realizations, linear interpolation is better than cubic interpolation. The explanation for this result is the linearity of the PER curve for the considered use cases. Results also confirm that a very precise AWGN PER curve is necessary, and that 15 points with $5x10^6$ simulations per point are sufficient to have a reliable abstraction.

After firstly introducing a new TWR scheme which adapts with respect to the channel impairments, the PHY Layer abstraction has been further used to create a MAC Layer simulator and to compare TWR with DF in terms of PER and throughput. In total, 3 relaying schemes have been considered: classic TWR, adaptive TWR and DF. Simulations provide results expressed in terms of Mean PER, End-to-End PER, mean throughput and End-to-End throughput for all these relaying schemes. While it is clearly showed that PER of DF scheme is better than PER of TWR scheme for many scenarios, adaptive TWR is better than DF in terms of achievable throughput providing thus a good and convenient relaying scheme in terms of total transmitted packets.

7. Sum-rate optimization for asynchronous OFDM/FBMC based DF-relay transmission under sum power constraint

In this Section, we investigate the issue of resource allocation for FBMC-based DF relaying. In the literature, a lot of attention has been focused on OFDM-based relaying e.g. [61]-[64]. Actually, many of the existing techniques could be applied almost directly in a synchronized FBMC scenario as long as the interference between nodes remains low. However, one of the advantages of FBMC is its robustness to timing asynchronism by using frequency well-localized prototype filters [65]-[68]. We therefore consider a non-synchronized scenario and investigate the optimization of the sum rate in an OFDM or FBMC based DF-relay transmission system under sum power constraint, taking into account the potential interference between adjacent subcarriers. The impact of interference and the efficiency of the proposed algorithm are investigated through simulation results.

7.1 *System Model*

We consider the system depicted in Figure 1, where a source communicates with two destinations with the help of a half-duplex Decode-and-Forward relay node in two time slots. All links are assumed to be frequency selective motivating thus the use of multicarrier modulation techniques. Two multicarrier schemes are considered: Cyclic Prefix based Orthogonal Frequency Division Multiplexing (CP-OFDM) and Filter Bank based MultiCarrier (FBMC).

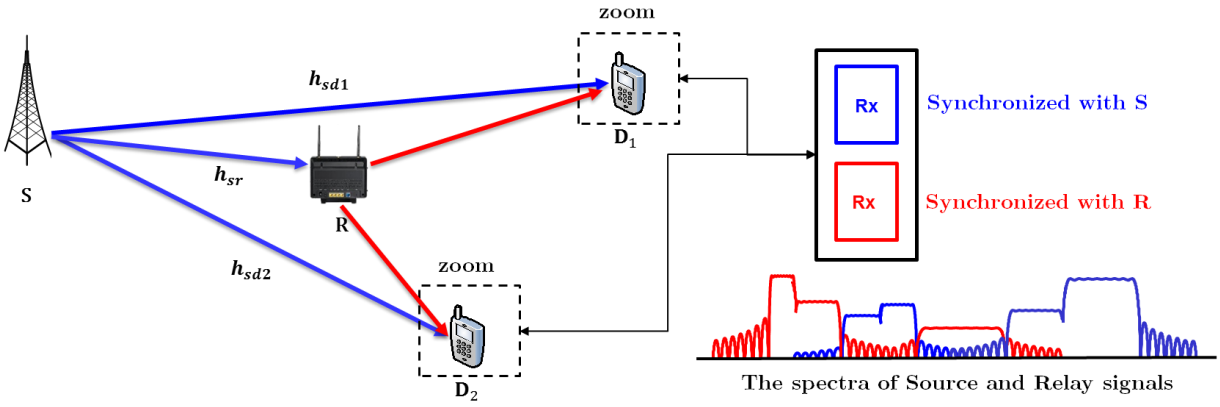

Figure 7-1: Structure of the DF-relayed system

During the first time slot, the source sends one modulated symbol on each carrier. The relay selects a subset of the modulated symbols that it decodes, and forwards them to corresponding destinations, during the second time slot. For each relayed symbol, the relay is constrained to use the same carrier as that used by the source for the same symbol. Based on the two signalling periods, each destination implements maximum ratio combining (MRC) for the relayed subcarriers.

Each destination is equipped with two receivers. The first receiver and the second one are assumed to be perfectly synchronized with the source and the relay, respectively.
In this work, we consider the case where a new independent modulated symbol is sent by the source in the second time slot each non-relayed subcarrier. Such a protocol has been proposed in [57].

Let $A_s(m)$ and $A_r(m)$ be the amplitude of the symbol sent respectively by the source and the relay on the m-th subcarrier. Moreover, $H_{sdi}(m)$ (resp. $H_{rdi}(m)$) denotes the complex channel gain for the m-th subcarrier between the source (resp. relay) and the i-th destination. After a proper maximum ratio combining at the i-th destination, the m-th demodulated output is given by,

$$y_{sri}(m) = A_s^2(m)|H_{sdi}(m)|^2 a_m + A_r^2(m)|H_{rdi}(m)|^2 a_m + A_s(m)H_{sdi}^*(m)n_s(m) + A_r(m)H_{rdi}^*(m)n_r(m) \quad (7\text{-}1)$$

Where, a_m denotes the symbol transmitted on the m-th subcarrier and $n_s(m)$ and $n_r(m)$ stand for two noise samples that are zero-mean circular Gaussian, white and uncorrelated with a variance σ_n^2.

The resulting Signal-to-Noise-Ratio (SNR) can thus be written as follows,

$$\gamma_{sri}(m) = \frac{P_s(m)|H_{sdi}(m)|^2 + P_r(m)|H_{rdi}(m)|^2}{\sigma_n^2} \quad (7\text{-}2)$$

Where, $P_s(m) = A_s^2(m)$ and $P_r(m) = A_r^2(m)$.

It is worth noticing that the SNR expression given in (7-2) is valid only when signals of source and relay arrive synchronously at the destination, in the second time slot. In the presence of a timing misalignment between both signals, the orthogonality between both signals may be loosed (e.g. when the timing offset exceeds the cyclic prefix duration). In such a case, the loss of orthogonality leads to a mutual asynchronous interference between both signals. This interference can be computed using the so-called “interference power tables” that gives the interference weights as a function of the spectral distance and the timing offset between the both signals [69]. The average interference weights of CP-OFDM and PHYDYAS [70]-FBMC are given in Table 7-1.

Spectral distance (*l*)	CP-OFDM	PHYDYAS-FBMC
l	7.05×10^{-1}	8.23×10^{-1}
$l \pm 1$	8.94×10^{-2}	8.81×10^{-2}
$l \pm 2$	2.23×10^{-2}	0
$l \pm 3$	9.95×10^{-3}	0
$l \pm 4$	5.60×10^{-3}	0
$l \pm 5$	3.59×10^{-3}	0
$l \pm 6$	2.50×10^{-3}	0
$l \pm 7$	1.84×10^{-3}	0
$l \pm 8$	1.12×10^{-3}	0

Table 7-1: OFDM and FBMC Interference power weights

It is worth to point out that the interference weights below 1×10^{-3} have been neglected.

We denote by S_{Si} the set of subcarriers assigned to the i-th destination and receiving power at the source only, S_{Ri} the set of subcarriers assigned also to the destination i and receiving power at both source and relay. These sets are not known in advance and must be optimally characterized. It is worth noticing that these sets are complementary, i.e.

$$S_{Si} \cap S_{Ri} = S_{Si} \cap S_{Rj} = S_{Si} \cap S_{Sj} = S_{Ri} \cap S_{Rj} = \emptyset, \qquad i \neq j \tag{7-3}$$

Considering the mutual asynchronous interference between both source and relay signal, the SNR of a given relayed subcarrier (i.e. $m \in S_R$) becomes,

$$\gamma_{sri}(m) = \frac{P_s^{(1)}(m)|H_{sdi}(m)|^2}{\sigma_n^2} + \frac{P_r(m)|H_{rdi}(m)|^2}{\sigma_n^2 + \sum_{m' \in \{S_{S1}, S_{S2}\}} P_s^{(2)}(m')|H_{sdi}(m')|^2 I(|m-m'|)} \tag{7-4}$$

Here, $I(|m-m'|)$ stands for the interference weight corresponding to a spectral distance $|m-m'|$.

Moreover, the SNR of a non-relayed subcarrier can be written as,

$$\gamma_{si}^{(2)}(m) = \frac{P_s^{(2)}(m)|H_{sdi}(m)|^2}{\sigma_n^2 + \sum_{m' \in \{S_{R1}, S_{R2}\}} P_r(m')|H_{rdi}(m')|^2 I(|m-m'|)} \tag{7-5}$$

The superscripts (1) and (2) stand respectively for the first and second time slots. We note that during the first time slot, the SNRs at both relay and destination are not affected by interference since only the source is the unique transmitter during this period.

7.2 *Optimization problem with a sum power constraint*

In this section, we investigate the case of a sum power constraint. The channel gains of all links are assumed to be perfectly known to both source and relay.

Following the protocol previously described where the source sends new independent modulated symbols on non-relayed subcarriers, the achieved rate during two OFDM symbols is given by [71],

$$R = \frac{1}{2}\sum_{i=1}^{2}\sum_{m \in S_{Si}} \log\left(1+\gamma_{si}^{(1)}(m)\right) + \log\left(1+\gamma_{si}^{(2)}(m)\right) + \frac{1}{2}\sum_{i=1}^{2}\sum_{m \in S_{Ri}} \min\left\{\log\left(1+\gamma_{sr}(m)\right), \log\left(1+\gamma_{sri}(m)\right)\right\} \tag{7-6}$$

For a relayed subcarrier, assuming a decode-and-forward mode, the rate is the minimum between the rate on source-destination link and source-relay one.

Let $\mathrm{a}_{ij}[m]$ be the subcarrier allocation indicator taking values 1 if m is a subcarrier assigned to the destination $i \in \{1,2\}$ and 0, otherwise. The index j is 1 (resp. 2) if m is a non-relayed (resp. relayed) subcarrier. Hence, for any subcarrier $m = 1, \ldots, M$, we have,

$$\sum_{i=1}^{2}\sum_{j=1}^{2} \mathrm{a}_{ij}[m] = 1 \tag{7-7}$$

Substituting each SNR by its corresponding expression, the sum rate R becomes,

$$\begin{aligned} R = \frac{1}{2}\sum_{i=1}^{2}\sum_{m=1}^{M} \mathrm{a}_{i1}[m]\Bigg\{&\log\left(1+\frac{P_s^{(1)}(m)|H_{sdi}(m)|^2}{\sigma_n^2}\right) \\ &+\log\left(1+\frac{P_s^{(2)}(m)|H_{sdi}(m)|^2}{\sigma_n^2+\sum_{m'\in\{S_{R1},S_{R2}\}}P_r(m')|H_{rdi}(m')|^2 I(|m-m'|)}\right)\Bigg\} \\ +\mathrm{a}_{i2}[m]\min\Bigg\{&\log\left(1+\frac{P_s^{(1)}(m)|H_{sr}(m)|^2}{\sigma_n^2}\right), \\ &\log\left(1+\frac{P_s^{(1)}(m)|H_{sdi}(m)|^2}{\sigma_n^2} \right. \\ &\left.\left. +\frac{P_r(m)|H_{rdi}(m)|^2}{\sigma_n^2+\sum_{m'\in\{S_{S1},S_{S2}\}}P_s^{(2)}(m')|H_{sdi}(m')|^2 I(|m-m'|)}\right)\right\} \end{aligned} \tag{7-8}$$

As aforementioned, the power allocation maximizing (7-8) is investigated for a sum power constraint,

$$\sum_{i=1}^{2}\sum_{m=1}^{M} \mathrm{a}_{i1}[m]\left(P_s^{(1)}(m)+P_s^{(2)}(m)\right) + \mathrm{a}_{i2}[m]\left(\underbrace{P_s^{(1)}(m)+P_r(m)}_{P(m)}\right) \le P_{tot} \tag{7-9}$$

Where is P_{tot} the total power available for both source and relay and M is the total number of subcarriers.

The objective function given in (7-8) is defined as a mixed integer problem since it incorporates both integer ($\mathrm{a}_{ij}[m] \in \{0,1\}$) and continuous variables. Moreover, it is nonlinear and non-convex since it involves ratios of powers $P_s^{(2)}(m)$ and $P_r(m)$.

Hence, the problem is non-convex nonlinear which means that it might have multiple local optima and it is hard to find the global optima. In the next section, we propose an algorithm providing a solution with a reasonable computational complexity.

For simplicity sake, let us denote by V_R and V_S the interference terms caused, during the second period, by the relay and the source, respectively.

$$\begin{aligned} V_R(m) &= \sum_{m'\in\{S_{R1},S_{R2}\}} P_r(m')|H_{rdi}(m')|^2 I(|m-m'|) \\ V_S(m) &= \sum_{m'\in\{S_{S1},S_{S2}\}} P_s^{(2)}(m')|H_{sdi}(m')|^2 I(|m-m'|) \end{aligned} \tag{7-10}$$

It is worth mentioning that the victim subcarrier m belongs to $\{S_{S1}, S_{S2}\}$ when the interfering belong to $\{S_{R1}, S_{R2}\}$ and vice versa.

7.3 *Sum-Rate maximization algorithm*

In order to maximize the sum-rate, we propose a joint algorithm where we allocate simultaneously both resources (powers and subcarriers). Based on the algorithm solution, the interference terms are updated V_R and V_S. This process is repeated until convergence (i.e. no further improvements of the sum rate).

Let us denote by $R^{(t)}$ the value of the sum-rate at some iteration t. To maximize R given by (7-8) iteratively, we develop the following algorithm,

Proposed algorithm for maximization of R as given by (7-8)
1: Initialization: set $\boldsymbol{t = 1}$ and $\mathbf{V}_{\boldsymbol{R}}^{(\mathbf{0})} = \mathbf{V}_{\boldsymbol{S}}^{(\mathbf{0})} = \mathbf{0}$
2: Set $\mathbf{V}_{\boldsymbol{R}} = \mathbf{V}_{\boldsymbol{R}}^{(\boldsymbol{t-1})}$, $\mathbf{V}_{\boldsymbol{S}} = \mathbf{V}_{\boldsymbol{S}}^{(\boldsymbol{t-1})}$
3: Solve the joint subcarrier and power allocation: $\mathbf{P}^{(\boldsymbol{t})}$and $\mathbf{A}^{(\boldsymbol{t})}$
4: Update: $\boldsymbol{R}^{(\boldsymbol{t})}$, $\mathbf{V}_{\boldsymbol{R}}^{(\boldsymbol{t})}$ and $\mathbf{V}_{\boldsymbol{S}}^{(\boldsymbol{t})}$
6: Increment the iteration index $\boldsymbol{t = t + 1}$, Go back to Step 2
7: Terminate if $\left\|\boldsymbol{R}^{(\boldsymbol{t})} - \boldsymbol{R}^{(\boldsymbol{t-1})}\right\| \leq \boldsymbol{\varepsilon}$ and set $\boldsymbol{R = R}^{(\boldsymbol{t})}$

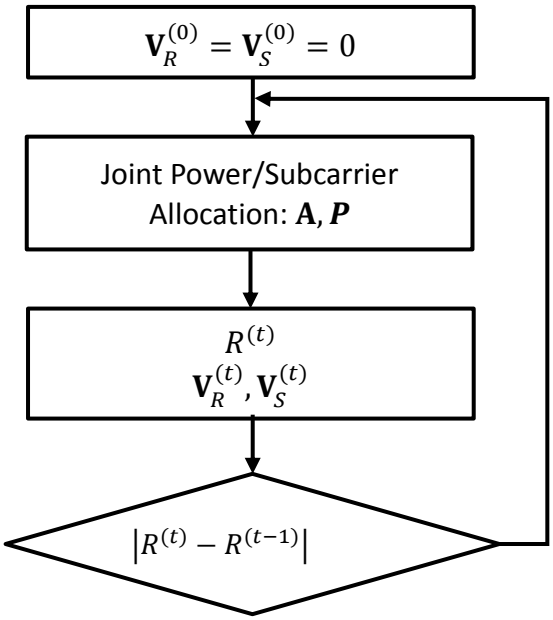

Figure 7-2: Flowchart of the proposed rate maximization algorithm

Where, $\mathbf{P}$ and $\mathbf{A}$ are matrices standing for the power allocation solution and the subcarrier allocation one, respectively. $\mathbf{V}_{\boldsymbol{R}}$ and $\mathbf{V}_{\boldsymbol{S}}$ are $(M \times 1)$ vectors denoting relay and source interference vectors, respectively.

As described in the algorithm and shown in the flowchart, we allocate the resources and compute the interference terms, alternately. More specifically, at iteration $t \geq 1$, the algorithm jointly allocates powers and subcarriers that correspond to a maximum of (7-8) computed with the choice of the interference terms set to their values obtained from the previous iteration , i.e. $\mathbf{V}_R = \mathbf{V}_R^{(t-1)}$, $\mathbf{V}_S = \mathbf{V}_S^{(t-1)}$. For the initialization, set $\mathbf{V}_R^{(0)} = \mathbf{V}_S^{(0)} = 0$

which correspond to the case where a perfect synchronization between the source and the relay signals is assumed.

In order to solve this sub-problem, we propose a joint algorithm allocating powers and subcarriers, simultaneously. According to the system model described in the previous section, we can distinguish 4 links or cases:

- Link 1: indirect (through the relay) with destination 1.
- Link 2: indirect with destination 2.
- Link 3: direct with destination 1.
- Link 4: direct with destination 2.

Using these notations, we give the pseudo-code of the proposed joint subcarrier/power allocation algorithm,

Joint CA/PA for a given $\mathbf{V}_R, \mathbf{V}_S$
Repeat
for all subcarriers $m = 1:M$ do
for all links $n = 1:4$ do
move subcarrier m to link n
power allocation maximizing the rate
calculate the resulting rate
end for
assign subcarrier m to link n with the highest sum rate R
end for
until no further improvements of the sum rate $\boldsymbol{R}$
return CA,PA

For the allocated powers and subcarriers, the algorithm computes the values of V_S and V_R using (7-10) based on the obtained solution of the joint CA/PA. Finally, the global iterative process terminates when $|R(t) - R(t-1)| \leq \varepsilon$.

Accordingly, the Lagrangian for this optimization, considering the total power constraint, the decode-and-forward constraints and fixed values of $\mathbf{V}_R$ and $\mathbf{V}_S$, can be defined as,

$$\mathcal{L} = \frac{1}{2}\sum_{i=1}^{2}\sum_{m=1}^{M} \mathrm{a}_{i1}[m]\left\{\log\left(1+\frac{P_s^{(1)}(m)|H_{sdi}(m)|^2}{\sigma_n^2}\right)+\log\left(1+\frac{P_s^{(2)}(m)|H_{sdi}(m)|^2}{\sigma_n^2+V_R(m)}\right)\right\}$$
$$+\frac{1}{2}\sum_{i=1}^{2}\sum_{m=1}^{M} \mathrm{a}_{i2}[m]\log\left(1+\frac{P_s^{(1)}(m)|H_{sdi}(m)|^2}{\sigma_n^2}+\frac{P_r(m)|H_{rdi}(m)|^2}{\sigma_n^2+V_S(m)}\right)$$
$$-\mu\left\{\sum_{i=1}^{2}\sum_{m=1}^{M} \mathrm{a}_{i1}[m]\left(P_s^{(1)}(m)+P_s^{(2)}(m)\right)+\mathrm{a}_{i2}[m]\left(\underbrace{P_s^{(1)}(m)+P_r(m)}_{P(m)}\right)-P_{tot}\right\}$$
$$-\sum_{i=1}^{2}\sum_{m=1}^{M}\rho_m \mathrm{a}_{i2}[m]\left\{P_s^{(1)}(m)|H_{sdi}(m)|^2+\frac{P_r(m)|H_{rdi}(m)|^2}{1+\frac{V_S(m)}{\sigma_n^2}}-P_s^{(1)}(m)|H_{sr}(m)|^2\right\}$$

$$-\sum_{m=1}^{M}\beta_m\left(\sum_{i=1}^{2}\sum_{j=1}^{2}\mathrm{a}_{ij}[m]-1\right) \quad (7\text{-}11)$$

Where, μ denotes the Lagrange multiplier associated with the global power constraint and ρ_m stands for the Lagrange multiplier associated with the decodability constraint on the m–th subcarrier. Moreover, β_m is the Lagrange multiplier associated with the subcarrier assignment indicator $\mathrm{a}_{ij}[m]$.

Let us first investigate the saturation of the decodability constraints for relayed subcarriers. For the i–th destination, let us assume that the decodability constraint related to relayed subcarrier k is not saturated (i.e. $\mathrm{a}_{i1}[k]=0$ and $\rho_k=0$). Taking the derivative of the Lagrangian with respect to the powers for this subcarrier k, we obtain,

$$\frac{\partial\mathcal{L}}{\partial P_s^{(1)}(k)}=\frac{1}{2}\frac{|H_{sdi}(k)|^2}{\sigma_n^2}\left(1+\frac{P_s^{(1)}(k)|H_{sdi}(k)|^2}{\sigma_n^2}+\frac{P_r(k)|H_{rdi}(k)|^2}{\sigma_n^2+V_S(k)}\right)^{-1}-\mu=0$$

$$\frac{\partial\mathcal{L}}{\partial P_r(k)}=\frac{1}{2}\frac{|H_{rdi}(k)|^2}{\sigma_n^2+V_S}\left(1+\frac{P_s^{(1)}(k)|H_{sdi}(k)|^2}{\sigma_n^2}+\frac{P_r(k)|H_{rdi}(k)|^2}{\sigma_n^2+V_S(k)}\right)^{-1}-\mu=0 \quad (7\text{-}12)$$

This implies that assuming the non-saturation of the decodability constraint leads to

$$\frac{|H_{sdi}(k)|^2}{\sigma_n^2}=\frac{|H_{rdi}(k)|^2}{\sigma_n^2+V_S(k)} \quad (7\text{-}13)$$

Substituting $V_S(k)$ by its expression (7-10) in (7-13), we get,

$$\frac{|H_{sdi}(k)|^2}{\sigma_n^2}=\frac{|H_{rdi}(k)|^2}{\sigma_n^2+\sum_{m'\in\{S_{S1},S_{S2}\}}P_s^{(2)}(m')|H_{sdi}(m')|^2I(|k-m'|)} \quad (7\text{-}14)$$

Therefore, the non-saturation of the decode-and-forward constraint imposes a constraint on the current channel state, which is almost unlikely to happen. Accordingly, the decodability constraint has to be saturated except in very marginal cases. We write then,

$$\frac{P_s^{(1)}(m)|H_{sr}(m)|^2}{\sigma_n^2}=\frac{P_s^{(1)}(m)|H_{sdi}(m)|^2}{\sigma_n^2}+\frac{P_r(m)|H_{rdi}(m)|^2}{\sigma_n^2+V_S(m)} \quad (7\text{-}15)$$

Let $\alpha_i(m)$ be coefficient defined by,

$$\alpha_i(m)=\frac{\sigma_n^2}{\sigma_n^2+V_S(m)}\times\frac{|H_{rdi}(m)|^2}{|H_{sr}(m)|^2-|H_{sdi}(m)|^2} \quad (7\text{-}16)$$

From (7-15) and (7-16), we can write,

$$P_s^{(1)}(m)=\alpha_i(m)P_r(m) \quad (7\text{-}17)$$

Following the notation given in (7-9), that for any relayed subcarrier $m\in S_{Ri}$

$$P(m) = P_s^{(1)}(m) + P_r(m) \tag{7-18}$$

According to (7-17) and (7-18), we have,

$$P_s^{(1)}(m) = \frac{\alpha_i(m)}{1+\alpha_i(m)} P(m) \tag{7-19}$$

$$P_r(m) = \frac{1}{1+\alpha_i(m)} P(m) \tag{7-20}$$

Therefore, the Lagrangian can be rewritten as,

$$\begin{aligned}\mathcal{L} = &\frac{1}{2}\sum_{i=1}^{2}\sum_{m=1}^{M-1} \mathrm{a}_{i1}[m]\left\{\log\left(1+\frac{P_s^{(1)}(m)|H_{sdi}(m)|^2}{\sigma_n^2}\right)+\log\left(1+\frac{P_s^{(2)}(m)|H_{sdi}(m)|^2}{\sigma_n^2+V_R(m)}\right)\right\}\\ &+\frac{1}{2}\sum_{i=1}^{2}\sum_{m=1}^{M-1} \mathrm{a}_{i2}[m]\log\left(1+\frac{\alpha_i(m)}{1+\alpha_i(m)}\frac{|H_{sr}(m)|^2}{\sigma_n^2}P(m)\right)\\ &-\mu\left\{\sum_{i=1}^{2}\sum_{m=1}^{M-1}\mathrm{a}_{i1}[m]\left(P_s^{(1)}(m)+P_s^{(2)}(m)\right)+\mathrm{a}_{i2}[m]\left(\underbrace{P_s^{(1)}(m)+P_r(m)}_{P(m)}\right)-P_{tot}\right\}\\ &-\sum_{m=1}^{M-1}\beta_m\left(\sum_{i=1}^{2}\sum_{j=1}^{2}\mathrm{a}_{ij}[m]-1\right)\end{aligned} \tag{7-21}$$

The solution for the power allocation can be found by applying and solving the KKT conditions [35]. This leads to a waterfilling solution which can be determined by taking the derivatives with respect to the powers: $P_s^{(1)}(m)$, $P_s^{(2)}(m)$ and $P(m)$. We have then,

$$\begin{aligned}&\frac{\partial\mathcal{L}}{\partial P_s^{(1)}(m)} = 0 \xrightarrow{yields} \frac{1}{2}\frac{|H_{sdi}(m)|^2}{\sigma_n^2}\left(1+\frac{P_s^{(1)}(m)|H_{sdi}(m)|^2}{\sigma_n^2}\right)^{-1}-\mu=0\\ &\xrightarrow{yields} P_s^{(1)}(m) = \left[\frac{1}{2\mu}-\frac{\sigma_n^2}{|H_{sdi}(m)|^2}\right]^+\\ &\frac{\partial\mathcal{L}}{\partial P_s^{(2)}(m)} = 0 \xrightarrow{yields} P_s^{(2)}(m) = \left[\frac{1}{2\mu}-\frac{\sigma_n^2+V_R(m)}{|H_{sdi}(m)|^2}\right]^+\\ &\frac{\partial\mathcal{L}}{\partial P(m)} = 0 \xrightarrow{yields} P(m) = \left[\frac{1}{2\mu}-\frac{1+\alpha_i(m)}{\alpha_i(m)}\frac{\sigma_n^2}{|H_{sr}(m)|^2}\right]^+\end{aligned} \tag{7-22}$$

It is wise mentioning that the proposed algorithm does not make any control on the interference levels of $\mathbf{V}_R$ and $\mathbf{V}_S$. The variation of the latter terms may lead to a non-optimal solution. Such behavior can be explained by the fact that each iteration is completely independent from the previous one due to the variation of $\mathbf{V}_R$ and $\mathbf{V}_S$.

7.4 *Improved algorithm considering an additional interference constraint*

In order to ensure the optimality of the obtained solution, the variation of the interference terms $\mathbf{V}_R$ and $\mathbf{V}_S$ should be controlled during the algorithm process. To ensure this, the optimization problem should consider a constraint related to the total interference power which can be written as,

$$\begin{aligned} V_{tot} &= \sum_{m\in\{S_{S1},S_{S2}\}} V_R(m) + \sum_{m\in\{S_{R1},S_{R2}\}} V_s(m) \\ &= \sum_{m=1}^{M} \mathrm{a}_{i1}[m]V_R(m) + \mathrm{a}_{i2}[m]V_s(m) \end{aligned} \tag{7-23}$$

Substituting (7-10) in (7-23), the constraint becomes,

$$\begin{aligned} V_{tot} = &\sum_{m\in\{S_{S1},S_{S2}\}} \sum_{m'\in\{S_{R1},S_{R2}\}} P_r(m')|H_{rdi}(m')|^2 I(|m-m'|) \\ &+ \sum_{m\in\{S_{R1},S_{R2}\}} \sum_{m'\in\{S_{S1},S_{S2}\}} P_s^{(2)}(m')|H_{sdi}(m')|^2 I(|m-m'|) \end{aligned} \tag{7-24}$$

Using the subcarrier assignment indicator a_{ij} and substituting P_r by (7-20), we obtain the final expression of the interference constraint,

$$\begin{aligned} V_{tot} = &\sum_{i=1}^{2}\sum_{m=1}^{M}\sum_{m\prime=1}^{M} \mathrm{a}_{i1}[m]\mathrm{a}_{i2}[m']\frac{1}{1+\alpha_i(m')}P(m')|H_{rdi}(m')|^2 I(|m-m'|) \\ &+ \mathrm{a}_{i2}[m]\mathrm{a}_{i1}[m']P_s^{(2)}(m')|H_{sdi}(m')|^2 I(|m-m'|) \end{aligned} \tag{7-25}$$

Considering this additional constraint, the Lagrangian becomes,

$$\begin{aligned} \mathcal{L} = &\frac{1}{2}\sum_{i=1}^{2}\sum_{m=1}^{M} \mathrm{a}_{i1}[m]\left\{\log\left(1+\frac{P_s^{(1)}(m)|H_{sdi}(m)|^2}{\sigma_n^2}\right)+\log\left(1+\frac{P_s^{(2)}(m)|H_{sdi}(m)|^2}{\sigma_n^2+\mathrm{V}_R(m)}\right)\right\} \\ &+\frac{1}{2}\sum_{i=1}^{2}\sum_{m=1}^{M}\mathrm{a}_{i2}[m]\log\left(1+\frac{\alpha_i(m)}{1+\alpha_i(m)}\frac{|H_{sr}(m)|^2}{\sigma_n^2}P(m)\right) \\ &-\mu\left\{\sum_{i=1}^{2}\sum_{m=1}^{M}\mathrm{a}_{i1}[m]\left(P_s^{(1)}(m)+P_s^{(2)}(m)\right)+\mathrm{a}_{i2}[m]\left(\underbrace{P_s^{(1)}(m)+P_r(m)}_{P(m)}\right)-P_{tot}\right\} \\ &-\sum_{m=1}^{M}\beta_m\left(\sum_{i=1}^{2}\sum_{j=1}^{2}\mathrm{a}_{ij}[m]-1\right) \end{aligned}$$

$$-\theta\left\{\sum_{i=1}^{2}\sum_{m=1}^{M}\sum_{m'=1}^{M}\mathrm{a}_{i1}[m]\mathrm{a}_{i2}[m']\frac{1}{1+\alpha_i(m')}P(m')|H_{rdi}(m')|^2 I(|m-m'|)\right.$$
$$\left.+\,\mathrm{a}_{i2}[m]\mathrm{a}_{i1}[m']P_s^{(2)}(m')|H_{sdi}(m')|^2 I(|m-m'|)\right\} \quad (7\text{-}26)$$

where θ stands for the Lagrange multiplier associated with the interference constraint.

Similarly to the previous section, the derivatives with respect to the powers: $P_s^{(1)}(m)$, $P_s^{(2)}(m)$ and $P(m)$ lead to,

$$\frac{\partial\mathcal{L}}{\partial P_s^{(1)}(m)}=0\xrightarrow{yields}\frac{1}{2}\frac{|H_{sdi}(m)|^2}{\sigma_n^2}\left(1+\frac{P_s^{(1)}(m)|H_{sdi}(m)|^2}{\sigma_n^2}\right)^{-1}-\mu=0$$

$$\xrightarrow{yields}P_s^{(1)}(m)=\left[\frac{1}{2\mu}-\frac{\sigma_n^2}{|H_{sdi}(m)|^2}\right]^+$$

$$\frac{\partial\mathcal{L}}{\partial P_s^{(2)}(m)}=0\xrightarrow{yields}$$

$$P_s^{(2)}(m)=\left[\frac{1}{2}\frac{1}{\mu+\theta\sum_{i=1}^{2}\sum_{m'=1}^{M}\mathrm{a}_{i1}[m]\mathrm{a}_{i2}[m']|H_{sdi}(m)|^2 I(|m-m'|)}-\frac{\sigma_n^2+V_R(m)}{|H_{sdi}(m)|^2}\right]^+$$

$$\frac{\partial\mathcal{L}}{\partial P(m)}=0\xrightarrow{yields}$$

$$P(m)=\left[\frac{1}{2}\frac{1}{\mu+\theta\sum_{i=1}^{2}\sum_{m'=1}^{M}\frac{1}{1+\alpha_i(m)}\mathrm{a}_{i1}[m']\mathrm{a}_{i2}[m]|H_{\mathrm{r}di}(m)|^2 I(|m-m'|)}\right.$$
$$\left.-\frac{1+\alpha_i(m)}{\alpha_i(m)}\frac{\sigma_n^2}{|H_{sr}(m)|^2}\right]^+ \quad (7\text{-}27)$$

Now, the Lagrange multiplier associated with the interference constraint θ maximizing the final sum rate ($\hat{\theta}=\max_\theta R$) can be determined using the duality based resource allocation algorithm [72]. The latter is summarized in the following pseudo-code,

The duality based RA algorithm [72]
$\boldsymbol{q=1,\theta=1}$
Repeat
$\theta=\left[\theta-\frac{1+Q}{q+Q}\left(V_{tot}^{(0)}-V_{tot}(\mu,\theta)\right)\right]^+$ $q=q+1;$ Find μ with Joint CA/PA
until $\boldsymbol{\theta\left(V_{tot}^{(0)}-V_{tot}(\mu,\theta)\right)<\varepsilon}$

7.5 *Simulation settings*

In order to analyse the performances of the proposed algorithm, we have used the following parameters:

Parameter description	**Parameter value**
Frame structure	
Bandwidth	1.4 MHz,
Sample frequency	1.92 MHz
Subcarriers number	128 subcarriers
Subcarrier spacing	15 kHz
FBMC filter	OFDM/OQAM PHYDYAS [70]
FBMC symbol duration	66.67 µs
Overlapping factor	4
Transmitter/Receiver	
BS number of antenna	1
HH number of antenna	1
MS/RS number of antenna	1
Transmission scheme	SISO
HH antenna model	Isotropic
Propagation	
Carrier frequency	422.5 MHz (Downlink), 412.5 MHz (Uplink)
Channel estimation	Ideal

Table 7-2: Simulation parameters

Moreover, the channel state information (CSI) is assumed to be perfectly known as described in Table 7-2. We note that the following results are compared to the optimal case considering a perfect synchronization between both source and relay signals. In other words, the optimal case corresponds to the interference-free scenario.

In this performance evaluation, the following scenarios have also been envisaged for both OFDM (blue curves) and FBMC (red curves):

- **Interference ignorance:** In this case, the optimization is performed with unknown mutual interference terms $\mathbf{V}_R$ and $\mathbf{V}_S$. Obviously, the latter terms are used in the final sum rate computation. The corresponding sum rates are plotted with solid lines.
- **Interference awareness:** As its name indicates, the algorithm maximizing the sum rate has the updates of $\mathbf{V}_R$ and $\mathbf{V}_S$ over the entire process period. The sum rates in this case are plotted with dash-dot curves.

Besides, depending on the selected destination (1,2) and the transmission mode (direct, indirect), we have 4 possible links in the considered system model. In this section, we consider it appropriate to select specific configurations where both source and relay are transmitting during the second time slot. The coexistence between both signals in such configurations lead to the appearance of mutual interferences allowing then a meaningful evaluation of the proposed algorithm.

7.6 *Simulation results*

Figure 7-3 illustrates the OFDM/FBMC achieved rate averaged over 1000 channel realizations. The average channel power gains are $\sigma_{s-d}{}^2 = 0.1, \sigma_{s-r}{}^2 = 10, \sigma_{r-d}{}^2 = 2$.

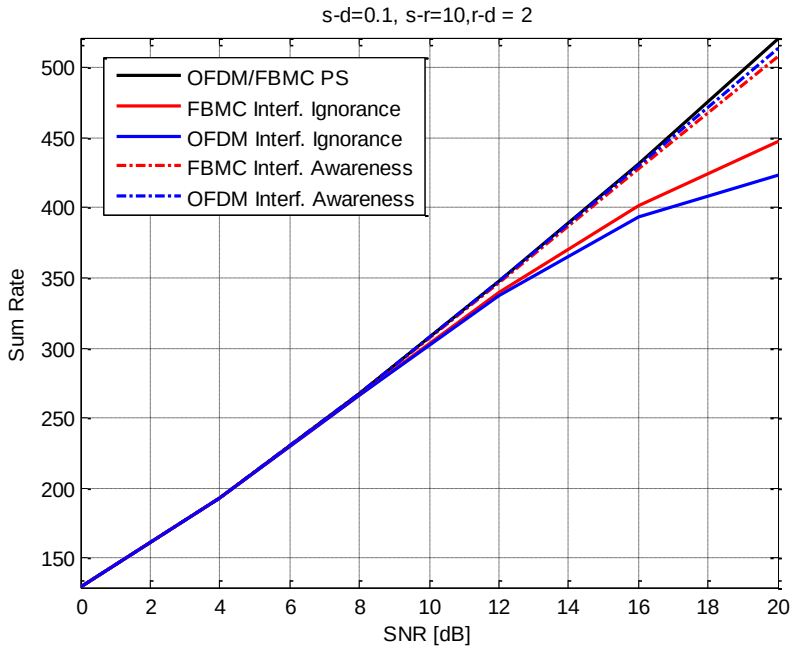

Figure 7-3: Synchronous and asynchronous OFDM/FBMC achieved sum rate as function of SNR, $\sigma_{s-d}{}^2 = 0.1, \sigma_{s-r}{}^2 = 10, \sigma_{r-d}{}^2 = 2$

In the interference ignorance scenario, we can observe that FBMC outperforms OFDM from SNR=12 dB. This advantage can be explained by the fact that a given interfering subcarrier can affect two subcarriers in the worst case (both adjacent subcarriers belong to the other link). However, higher number of victim subcarriers (up to 16 as illustrated in

Table 7-1) can be affected by a single interfering subcarrier in the OFDM case.

Moreover, the proposed algorithm is less-efficient when the mutual interference terms are unknown. In fact, there is gap with respect to the interference-free case which becomes larger when increasing the SNR level. Such a behaviour demonstrates the significant impact of the asynchronous interference on the algorithm performance.

Therefore, the algorithm needs to know the effective asynchronous interference caused mutually by both source and relay signals, in order to enhance the achievable sum rate for both modulations. Indeed, the algorithm the interference awareness scenario becomes more efficient providing practically the optimal sum rate.

Moreover, the algorithm achieves more significant improvement in OFDM (more than 21% at SNR=20 dB) allowing it to reach FBMC. It is worth noticing that OFDM outperforms FBMC with a negligible gap in high SNR regime.

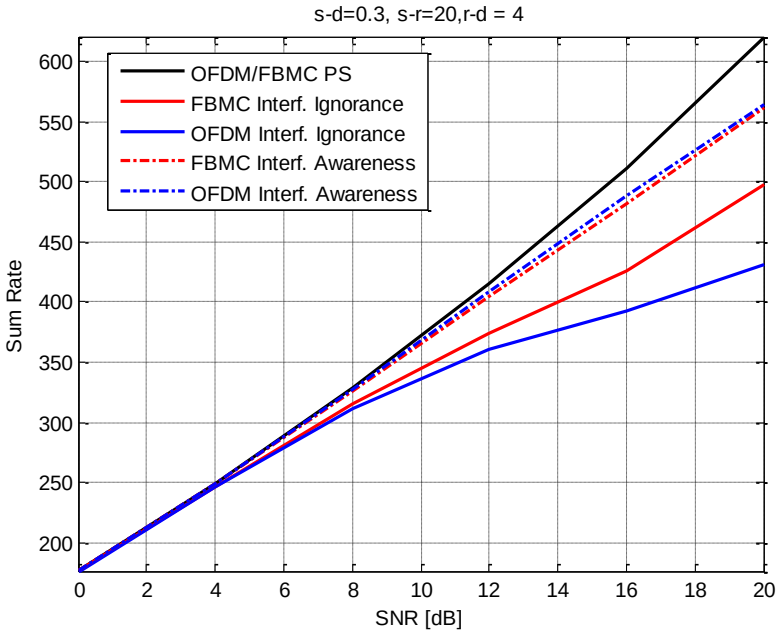

Figure 7-4: Synchronous and asynchronous OFDM/FBMC achieved sum rate as function of SNR, ${\sigma_{s-d}}^2 = 0.3, {\sigma_{s-r}}^2 = 20, {\sigma_{r-d}}^2 = 4$

Similarly to Figure 7-3, OFDM and FBMC average sum rates are plotted against the SNR in Figure 7-4 with the following average channel power gains ${\sigma_{s-d}}^2 = 0.3, {\sigma_{s-r}}^2 = 20, {\sigma_{r-d}}^2 = 4$. Also, the sum rates have been averaged over 1000 channel realizations.

The obtained results are in agreement with the previous analysis. In fact, when the interference is unknown, the FBMC provides a sum rate gain of more than 15% at SNR=20 dB compared to OFDM. Moreover, the gain achieved in the interference awareness case is more than 30% at SNR=20 dB compared to the interference ignorance scenario.

In contrast to Figure 7-3 and despite this significant enhancement, there is still gap with respect to the optimal case. Such a behaviour can be explained by the significant degradation (a relative loss of more than 30% at SNR=20 dB) caused by the interference compared to compared to the previous configuration (a relative loss of less than 19% at SNR=20 dB).

Finally, note that the useful OFDM sum rate is lower than what is depicted in Figure 7-3 and Figure 7-4 due to the redundancy introduced by the cyclic prefix (CP).

7.7 *Final remarks*

In this section, we have investigated the sum rate optimization in OFDM/FBMC based DF-relay transmission under sum power constraint. Both synchronous and asynchronous scenarios have been analysed. OFDM and FBMC interference power tables have been used in asynchronous interference modelling. Based on the resulting mutual interference, a joint subcarrier and power allocation algorithm has been proposed. Further, the latter has been

improved by introducing an additional constraint controlling the variation of the mutual interference. Finally, the impact of interference and the efficiency of the proposed algorithm have been investigated through simulation results. To this end, two scenarios have been proposed with respect to the interference ignorance or awareness. In the first scenario, OFDM suffers from a severe degradation because of the large number of interference-polluted subcarriers. In contrast to OFDM, FBMC provides a higher sum rate thanks to the well-localized interference. The efficiency of the proposed algorithm has been improved in the interference awareness scenario leading thus to substantial gains in the sum rate of both OFDM and FBMC.

8. **Conclusions**

This deliverable summarized the final contributions on relaying and coverage extension. Several sections have presented extension of results from D7.1 to the frequency selective scenario. Detailed performance evaluations have been provided and the issue of resource allocation for unsynchronized FBMC/OQAM relaying has been investigated. More specifically:

In section 2, multi-tap equalization has been investigated to cope with channel frequency selectivity in FBMC/OQAM based multi-hop relaying networks. The DF (decode-and-forward) strategy has been selected in order to avoid the amplification of noise and interferences at each hop. Similarly, efficient pre-equalizers have been considered at each transmission node to mitigate both the inter-symbol interference and the inter-carrier interference and therefore avoid as much as possible the issue of error propagation. The investigation has been performed using a linear multi-hop relaying network model and the overall network operation procedure has been explained in detail. Finally, the performance of FBMC/OQAM based multi-hop relaying networks with multi-tap equalization has been assessed. The various numerical results have provided insights into the impact of the number of hops on the performance as well as the choice of appropriate transmit and receive processing for each hop.

In section 3, an extension of the two-way relaying protocol to frequency selective channels has been proposed based on multicarrier modulations. The work has focused on a XOR combination using non binary codes (Galois-field LDPC) with higher-order modulations. Complete and functional decoding methods have been investigated and the achievable mutual information has been computed in both cases. Evaluation results have shown that functional decoding outperforms complete decoding (in terms of mutual information) for a sufficiently high SNR. The link-level simulation results indicate quite significant gains for joint decoding in all considered scenarios. The proposed coding scheme has also been implemented in a more realistic scenario with FBMC modulation and frequency selective channel models following LTE specifications. The same considerations about functional decoding outperforming complete decoding hold true in this case. Finally, future research lines have been presented which aim at improving the performance by mean of smart resource (i.e. power, modulation order, subcarrier) allocation.

In section 4, a practical decode and forward two-way relaying system has been analysed also based on XOR combination, but with binary coding and taking into account the frequency selectivity inside each subcarrier. Multi-tap pre-equalizer at the source and equalizers at the destination have been developed to cope with this frequency selectivity. Joint channel and physical layer network decoding have been studied and the BER performance has then been analysed in a practical scenario. OFDM and FBMC versions have been compared and it has been shown that FBMC can suffer from interference when the channel selectivity is high.

Section 5 explains how the FBMC transmission technique has been implemented into the SONIR platform. The focus has been on implementing the data transmission phase. So it has been assumed that the clustering and routing operations have already been performed prior to the considered data transmission. Simulations have been performed for multi-hop

relaying in a 200mx200m field with 350 nodes and the cumulative BER performance has been investigated. As a future work the impact on the overall throughput still needs further investigation. Moreover, the impact of using FBMC for clustering, routing and mobility schemes also needs to be investigated.

Section 6 focuses on the performance evaluation and comparison of two SC-FDMA transmission schemes using either DF relaying or two-way (XOR) relaying. The simulation method is based on an abstraction of the PHY Layer for SC-FDMA transmissions. The method can employ cubic interpolation or linear interpolation and simulations have shown in which situation to choose one over the other. Results also have confirmed that a very precise AWGN PER curve is necessary, and that 15 points with 5x106 simulations per point are sufficient to have a reliable abstraction. This abstraction has then been used to create a MAC layer simulator and to compare TWR with DF in terms of PER and throughput. The results have shown that, although the PER is not as good as DF for many scenarios, adaptive TWR is better than DF in terms of achievable throughput.

In section 7, the resource allocation issue has been investigated for relaying with multicarrier transmission, taking into account imperfect synchronization between nodes. The possibility to relax synchronization requirements is one of the advantages of FBMC transmission with respect to OFDM. However the imperfect synchronization can generate some interference between subcarriers which then has to be taken into account if subcarrier and power allocation is performed. Section 7 has focused on the optimization of the sum rate in a one source, one DF relay and two destinations scenario using either OFDM or FBMC and with limited synchronization between the source and relay nodes. Interference power tables have been used to model the asynchronous interference. A joint subcarrier and power allocation algorithm has been proposed. The impact of interference and the efficiency of the proposed algorithm have been investigated through simulation results. In particular, it has been shown that interference awareness leads to substantial gains in the sum rate of both OFDM and FBMC.

9. **References**

[1] Y. Cheng, P. Li, and M. Haardt, “Coordinated beamforming in MIMO FBMC/OQAM systems,'' in Proc. IEEE Int. Conference on Acoustics, Speech, and Signal Processing (ICASSP), (Florence, Italy), pp. 484 - 488, May 2014.

[2] M. Caus and A. Perez-Neira, “Transmitter-receiver designs for highly frequency selective channels in MIMO FBMC systems,” IEEE Trans. on Signal Processing, vol. 60, no. 12, pp. 6519 – 6532, Dec. 2012.

[3] P. Siohan, C. Siclet, and N. Lacaille, “Analysis and design of OFDM/OQAM systems based on filterbank theory,” IEEE Transactions on Signal Processing, vol. 50, no. 5, pp. 1170 – 1183, May 2002.

[4] M. G. Bellanger, “FBMC physical layer: a primer,” June 2010.

[5] R. Zakaria, D. Le Ruyet, and M. Bellanger, “Maximum Likelihood Detection in spatial multiplexing with FBMC,” in Proc. European Wireless 2010, June 2010.

[6] Y. Cheng and M. Haardt, “Widely Linear Processing in MIMO FBMC/OQAM Systems,” in Proc. ISWCS 2013, Aug. 2013.

[7] M. Caus and A. I. Perez-Neira, “Comparison of linear and widely linear processing in MIMO-FBMC systems,” in Proc. ISWCS 2013, Aug. 2013.

[8] M. Caus and A. I. Perez-Neira, “Multi-stream transmission in MIMO-FBMC systems,” in Proc. ICASSP 2013, May 2013.

[9] D. S. Waldhauser, L. G. Baltar, and J. A. Nossek, “MMSE Subcarrier Equalization for Filter Bank based Multicarrier Systems,” in Proc. IEEE 9th Workshop on Signal Processing Advances in Wireless Communications, pp. 525 – 529, Jul. 2008.

[10] D. S. Waldhauser, L. G. Baltar, and J. A. Nossek, “Adaptive Decision Feedback Equalization for Filter Bank based Multicarrier Systems,” in Proc. IEEE International Symposium on Circuits and Systems, pp. 2794 – 2797, May 2009.

[11] F. Khan, “Capacity and Range Analysis of Multi-Hop Relay Wireless Networks," in Proc. IEEE Vehicular Technology Conference 2006, Sept. 2006.

[12] C. Rao and B. Hassibi, “Diversity-multiplexing gain trade-off of a MIMO system with relays," in Proc. IEEE Inf. Theory Workshop, July 2007.

[13] ITU-R Recommendation M.1225, “Guidelines for evaluation of radio transmission technologies for IMT-2000,” 1997.

[14] FP7-ICT Project PHYDYAS Physical Layer for Dynamic Spectrum Access and Cognitive Radio. http://www.ictphydyas.org.

[15] B. Zafar, S. Gherekhloo, and M. Haardt, “Analysis of multihop relaying networks,'' in IEEE Vehicular Technology Magazine, vol. 7, No.3, pp. 40-47, Sept. 2012.

[16] B. Nazer and M. Gastpar, "Reliable Physical Layer Network Coding", Proceedings of the IEEE, vol. 99, no. 3, pp. 438-460, March 2011.

[17] T. J. Oechtering, E. A. Jorswieck, R. F. Wyrembelski, and H. Boche, “On the optimal transmit strategy for the MIMO bidirectional broadcast channel,” IEEE Transactions on Communications, Dec. 2009.

[18] D. Wübben and Y. Lang, “Generalized sum-product algorithm for joint channel decoding and physical-layer network coding in two-way relay systems,” in Proc. IEEE Globecom, Dec. 2010.

[19] A. L. R. Fazackerley and S. Paeth, “Cluster head selection using RF signal strength”, Canadian Conference on Electrical and Computer Engineering, pp. 334-338, 2009.

[20] B. An and Papavassiliou, “A mobility- based clustering approach to support mobility management and multicast routing in mobile ad-hoc wireless networks,” Int. J. Netw. Manag., Nov. 2001.

[21] B. Zafar, S. Cherekhloo, A. Asgharzadeh, M. T. Garrosi and M. Haardt “Self-Organizing Network with Intelligent Relaying (SONIR)”, in Proc. IEEE 7th International Conference on Mobile Adhoc and Sensor Systems, pp. 765-767, Nov. 2010.

[22] J. N. AL-Karaki and A. E. Kamal, “Routing Techniques in wireless sensor networks: A Survey”, IEEE Wireless Communications, vol.11, no.6, pp. 6-28, Dec. 2004.

[23] P. Popovski and H. Yomo, “The anti-packets can increase the achievable throughput of a wireless multi-hop network,” in *IEEE International Conference on Communication (ICC),* Istanbul, Turkey, Jun. 2006.

[24] S. Zhang, S. C. Liew, and P. P. Lam, “Hot topic: Physical Layer network coding,” in *ACM MobiCom,* Los Angeles, California, USA, Sep. 2006.

[25] B. Farhang-Boroujeny, “OFDM versus filter bank multicarrier,” *IEEE Signal Process. Mag.*, vol. 28, no. 3, pp. 92–112, May 2011.

[26] X. Mestre, M. Majoral, and S. Pfletschinger, “An asymptotic approach to parallel equalization of filter bank based multicarrier signals,” *IEEE Trans. Signal Process.*, vol. 61, no. 14, pp. 3592–3606, Jul. 2013.

[27] R. Ahlswede, N. Cai, S.-Y. R. Li, R. W. Yeung, “Network information flow”, *IEEE Transactions on Information Theory*, vol. 46, no. 4, pp. 1204-1216, July 2000.

[28] T. Koike-Akino, P. Popovski, V. Tarokh, “Adaptive Modulation and Network Coding with Optimized Precoding in Two-Way Relaying”, *IEEE Globecom*, Honululu, Hawaii, USA, Nov. 2009.

[29] P. Larsson, N. Johansson, K.-E. Sunell, “Coded Bi-directional Relaying”, *IEEE VTC Spring*, Melbourne, 7-10 May 2006.

[30] K. Narayanan, M. P. Wilson, A. Sprintson, “Joint Physical Layer Coding and Network Coding for Bi-Directional Relaying”, *Allerton Conference on Communication, Control and Computing*, Monticello, 2007.

[31] S. Katti, D. Katabi, W. Hu, H. Rahul, M. Médard, “The Importance of Being Opportunistic: Practical Network Coding for Wireless Environments”, *43rd Annual Allerton Conference on Communication, Control and Computing*, 2007.

[32] S. Katti, H. Rahul, W. Hu, D. Katabi, M. Medard, J. Crowcroft, “XORs in the Air: Practical Wireless Network Coding”, *SIGCOMM*, Pisa, Italy, 11-15 Sept. 2006.

[33] L. Ong, C. M. Kellett, S. J. Johnson, “Capacity Theorems for the AWGN Multi-Way Relay Channel”, *IEEE International Symposium on Information Theory (ISIT)*, Austin, Texas, USA, 13-18 June 2010.

[34] S. C. Liew, S. Zhang, L. Lu, “Physical-Layer Network Coding: Tutorial, Survey, and Beyond”, *Physical Communication*, Volume 6, Pages 1-164 (March 2013).

[35] S. Pfletschinger, D. Declercq, “Non-binary coding for vector channels”, *IEEE International Workshop on Signal Processing Advances in Wireless Communications (SPAWC)*, San Francisco, 26-29 June 2011.

[36] N. J. A. Sloane, “Tables of Sphere Packings and Spherical Codes”, *IEEE Transactions on Information Theory*, vol. 27, no 3, pp. 327-338, May 1981.

[37] G. Caire, G. Taricco, E. Biglieri, “Bit-Interleaved Coded Modulation”, *IEEE Transactions on Information Theory*, vol. 44, no. 3, pp. 927-946, May 1998.

[38] U. Wachsmann, R. F. H. Fischer, J. B. Huber, “Multilevel Codes: Theoretical Concepts and Practical Design Rules”, *IEEE Transactions on Information Theory*, vol. 45, no. 5, pp. 1361-1391, July 1999.

[39] D. Tse, P. Viswanath, *Fundamentals of Wireless Communication.* Cambrigde: Cambridge University Press 2005.

[40] S. ten Brink, *Design of concatenated coding schemes based on iterative decoding convergence*. PhD thesis, Institut für Nachrichtenübertragung, University of Stuttgart, April 2001.

[41] M. Hekrdla, J. Sykora, “Design of Uniformly Most Powerful Alphabets for HDF 2-Way Relaying Employing Non-Linear Frequency Modulations”, *EURASIP Journal on Wireless Communications and Networking* 2011, 2011:128, doi:10.1186/1687-1499-2011-128.

[42] S. Pfletschinger, “Joint decoding of multiple non-binary codewords”, *IEEE ICC Workshop on Massive Uncoordinated Access Protocols (MASSAP)*, Sydney (Australia), 10-14 June 2014.

[43] J. L. Massey, “Do Communication Engineers Need Information Theory?”, *Presentation at FTW*, Viena, 1 March 2004.

[44] P. Fertl, J. Jaldén, G. Matz, “Performance Assessment of MIMO-BICM Demodulators Based on Mutual Information”, *IEEE Transactions on Signal Processing*, vol. 60, no. 3, pp. 1366-1382, March 2002.

[45] K. Brüninghaus, D. Astély, T. Sälzer, S. Visuri, A. Alexiou, S. Karger, G.-A. Seraji, “Link Performance Models for System Level Simulations of Broadband Radio Access Systems”, *IEEE PIMRC*, Berlin, Sep. 2005.

[46] T. M. Cover, J. A. Thomas, *Elements of Information Theory*, New York: Wiley 1991.

[47] W. Yu, W. Rhee, S. Boyd, J. M. Cioffi, “Iterative Water-filling for Gaussian Vector Multiple Access Channels”, *IEEE Transactions on Information Theory*, vol. 50, no. 1, pp. 145-152, Jan 2004.

[48] S. Pfletschinger, “A practical physical-layer network coding scheme for the uplink of the two-way relay channel”, *Asilomar Conference on Signals, Systems, and Computers*, 6-9 Nov. 2011.

[49] W. Yu, J. M. Cioffi, “Constant-Power Waterfilling: Performance Bound and Low-Complexity Implementation”, *IEEE Transactions on Communications*, vol. 54, no. 1, pp. 23-28, Jan. 2006.

[50] Cen Lin, Yuan Liu, and Meixia Tao, “Cross-Layer Resource Allocation of Two-Way Relaying for Statistical Delay-QoS Guarantees”, IEEE ICC 2012.

[51] Rajab M. Legnain, Roshdy H.M. Hafez, and Ian D. Marsland, “Multiuser XOR-and-forward relaying using Alamouti STBC”, CCECE 2012.

[52] Sho Mukai, Fumie Ono, Hideki Ochiai and Ryu Miura, “Adaptive One-Way and Two-Way Relaying for MIMO Relay Networks”, WPMC 2012.

[53] Ahmad Alsharoa, Hakim Ghazzai, and Mohamed-Slim Alouini, “A Low Complexity Algorithm for Multiple Relay Selection in Two-Way Relaying Cognitive Radio Networks”, ICC 2013.

[54] Mohammad H. Amerimehr and Farid Ashtiani, “Delay and Throughput Analysis of a Two-Way Opportunistic Network Coding-Based Relay Network”, IEEE Transactions on Wireless Communications, 2014.

[55] Qiang Li, See Ho Ting, Ashish Pandharipande, and Yang Han “Adaptive Two-Way Relaying and Outage Analysis”, IEEE Transactions on Wireless Communications, 2009.

[56] Shaohui Sun, Kun Yang, Jianjun Wu, Dalin Zhu, and Ming Lei “Adaptive modulation and coding for two-way relaying with amplify-and-forward protocols”, IET Communications, 2013.

[57] Hassan Hamdoun, Pavel Loskot, Timothy O’Farrell and Jianhua He, “Practical Network Coding for Two Way Relay Channels in LTE Networks”, VTC Spring 2011.

[58] “Definition and Specification of Requirements for the Physical Layer Implementation and Channel Model,” Milestone MS4, ICT EMPhAtiC, 2013.

[59] “Prototype Filter and Structure Optimization,” Deliverable D5.1, ICT PHYDYAS, 2009.

[60] A. Lozano, A. M. Tulino, and S. Verdú, “Optimum Power Allocation for Parallel Gaussian Channels with Arbitrary Input Distributions,” IEEE Trans. Inf. Theory, vol. 52, no. 7, pp. 3033–3051, Jul. 2006.

[61] L. Vandendorpe, J. Louveaux, O. Oguz and A. Zaidi, "Rate-Optimized Power Allocation for DF-Relayed OFDM Transmission under Sum and Individual Power Constraints," *EURASIP Journal on Wireless Communications and Networking,* vol. 2009, p. 11, 2009.

[62] L. Vandendorpe, J. Louveaux, O. Oguz and A. Zaidi,” Rate-optimized power allocation for OFDM transmission with multiple DF/regenerative relays and an improved protocol,” in IEEE Wireless Communications and Networking Conference, 2009, pp. 1–6.

[63] L. Vandendorpe R. Duran, J. Louveaux et al., " Power Allocation for OFDM transmission with DF relaying," *in IEEE International Conference on Communication (ICC), Jun. 2008.*

[64] T. Wang and L. Vandendorpe, “WSR maximized resource allocation in multiple DF relays aided OFDMA downlink transmission,” *IEEE Trans. Sig. Proc., vol. 59, no. 8, pp. 3964–3976, Aug. 2011.*

[65] Y. Medjahdi, M. Terré, D. Le Ruyet, D. Roviras, A. Dziri, “Performance analysis in the downlink of asynchronous OFDM/FBMC based multi-cellular networks,” *IEEE Trans.* Wireless Commun., *vol. 10, no. 8,* pp. 2630-2639, *Aug. 2011.*

[66] Y. Medjahdi, M. Terré, D. Le Ruyet, D. Roviras, A. Dziri, “Performance analysis in the downlink of asynchronous OFDM/FBMC based multi-cellular networks,” *IEEE ICC*, *Kyoto, Jun. 2011.*

[67] Y. Medjahdi, M. Terré, D. Le Ruyet and D. Roviras, “On spectral efficiency of asynchronous OFDM/FBMC based cellular networks,” ”, *IEEE PIMRC*, Toronto, Sep. 2011.

[68] Y. Medjahdi, M. Terré, D. Le Ruyet, D. Roviras, H. Shaiek, R. Zakaria, “On the impact of the prototype filter on fbmc sensitivity to time asynchronism,” in Proc. ISWCS 2012, Aug. 2012.

[69] Y. Medjahdi, M. Terré, D. Le Ruyet and D. Roviras, “Interference tables: a useful model for interference analysis in asynchronous multicarrier transmission,” *EURASIP Journal on Advances in Signal Processing,* vol. 1, p. 17, 2014.

[70] M.G. Bellanger, “Specification and design of a prototype filter for filter bank based multicarrier transmission,” in *IEEE International Conference on in Acoustics, Speech, and Signal Processing*, 2001.

[71] J. N. Laneman, D. N. C. Tse, and G.W.Wornell, "Cooperative diversity in wireless networks: efficient protocols and outage behaviour," *IEEE Transactions on Information Theory,* vol. 50, pp. 3062-3080, 2004.

[72] T. Wang and L. Vandendorpe, “Sum Rate Maximized Resource Allocation in Multiple DF Relays Aided OFDM Transmission,” *IEEE Journal on Selected Areas in Communications,* vol. 29, no. 8, pp. 1559-1571, September 2011.

Glossary and Definitions

Acronym	Meaning
AF	Amplify-and-Forward
AFB	Analysis FilterBank
AODV	Ad-hoc On-demand Distance Vector
APP	A Posteriori Probability
AWGN	Additive White Gaussian Noise
BC	BroadCast
BER	Bit Error Rate
BICM	Bit-Interleaved Coded Modulation
BPSK	Binary Phase Shift Keying
BS	Base Station
CA	Carrier Allocation
CDF	Complete Decode Forward
CIR	Channel Impulse Response
CP	Cyclic Prefix
CP-OFDM	Cyclic Prefix-Orthogonal Frequency Division Multiplexing
CSI	Channel State Information
DF	Decode-and-Forward
DFT	Discrete Fourier Transform
DL	DownLink
EPA	Extended Pedestrian-A [channel]
ETU	Extended Typical Urban [channel]
EVA	Extended Vehicular-A [channel]
FBMC	Filter-Bank Multi Carrier
FDF	Functional Decode Forward
FFT	Fast Fourier Transform
HHT	Hand Held Terminals
IFFT	Inverse Fast Fourier Transform
ISI	Inter-Symbol Interference
ITU	International Telecommunication Union
KKT	Karush-Kühn-Tucker
KPI	Key Performance Indicator
LLR	Log-Likelyhood Ratio
LTE	Long Term Evolution
LTE-A	Long Term Evolution-Advanced

MAC	Medium Access Control
MIMO	Multiple Input Multiple Output
ML	Maximum Likelihood
MMSE	Minimum Mean Square Error
MRC	Maximum Ratio Combining
OFDM	Orthogonal Frequency Division Multiplexing
OQAM	Offset Quadrature Amplitude Modulation
OQPSK	Offset Quadrature Phase Shift Keying
PA	Power Allocation
PAM	Pulse Amplitude Modulation
PDF	Probability Density Function
Ped-A	Pedestrian-A [channel model]
PER	Packet Error Rate
PHY	PHYsical [Layer]
PLNC	Physical Layer Network coding
PMR	Private Mobile Radio
PPDR	Public Protection and Disaster Relief
PTT	Push-to-Talk
QAM	Quadrature Amplitude Modulation
QoS	Quality of Service
QPSK	Quadrature Phase Shift Keying
RB	Resource Block
RSSI	Received Signal Strength Indicator
SC-FDMA	Single-Carrier Frequency Division Multiple Access
SFB	Synthesis Filter Bank
SIC	Successive Interference Cancellation
SISO	Single Input Single Output
SLNR	Signal to Leakage plus Noise Ratio
SNR	Signal to Noise Ratio
SONIR	Self-Organizing Network with Intelligent Relaying
SPA	Sum Product Algorithm
TDMA	Time Division Multiple Access
TETRA	TErrestrial Trunked RAdio
TWR	Two-way Relaying
TWRC	Two-way Relay Channel
UL	UpLink
Veh-A	Vehicular-A [channel model]

XOR	eXclusive OR
ZF	Zero Forcing
ZMCSCG	Zero-Mean Circularly Symmetric Complex Gaussian